ABSTRACT

AYERS, MARTIN WILLIAM PAUL. Lithium-Oxygen Batteries – A Comprehensive Finite Element Model. (Under the direction of Dr. Hsiao-Ying Shadow Huang.)

The development of improved energy storage technologies with greater specific energies is critical to the success and development of electric vehicles and renewable energy products. Among the different energy storage technologies under study, lithium-oxygen batteries are one of the most promising due to their great gravimetric energies and capacities 6-10 times greater than other technologies such as conventional lithium-ion cells. Lithium-oxygen batteries still pose several challenges before they can be commercialized. Some of the most prominent and important issues that require investigating with lithium-oxygen batteries are the formation of dendrites on the anode surface as well as the buildup of precipitate (Li_2O_2) within the cathode. The objective of this research is to develop a comprehensive understanding of how the anodic and cathodic designs and parameters affect the discharge characteristics of lithium-oxygen cells through the use of the finite element method and computational fluid dynamics software ANSYS Fluent. Using these programs, three lithium-oxygen battery models were constructed with varying anode surface homogeneities and dendrite structures. The discharge characteristics were collected and compared to assess the overall performance of the cells. The finite element models consider each of these previously mentioned issues to gain an understanding of their collective effect on the performance of a lithium-oxygen cell. This comprehensive understanding will aid in the design of a cyclable and commercially viable lithium-oxygen battery that could be used for a wide range of energy storage applications.

Lithium-Oxygen Batteries – A Comprehensive Finite Element Model

by
Martin William Paul Ayers

A thesis submitted to the Graduate Faculty of
North Carolina State University
in partial fulfillment of the
requirements for the degree of
Master of Science

Mechanical Engineering

Raleigh, North Carolina

2015

APPROVED BY:

Dr. Hsiao-Ying Shadow Huang Committee Chair	Dr. Kara Peters
Dr. Alexei V. Saveliev	

DEDICATION

To my parents, David and Beth Ayers, for their support throughout my academic career and forever encouraging me to pursue excellence.

My brother and sister, Danny and Jaci.

And the NYE group

For the continued inspiration and support.

BIOGRAPHY

Martin William Paul Ayers was born in Ottawa, Canada on July 27th, 1990. His family moved throughout the United States, from the East Coast to the Midwest, before settling in Raleigh, North Carolina when Martin was 13 years old. He attended Athens Drive High School before pursuing an undergraduate degree at the University of North Carolina at Charlotte. While attending UNC Charlotte, Martin discovered his passion for learning which led him to pursue dual Bachelor of Science degrees in Mechanical Engineering and Physics with a minor in Economics. His undergraduate concentration was in Energy Engineering in which his final engineering project and technical elective courses focused on energy production and energy policy in the United States. Upon completing his undergraduate degree in May of 2013, Martin moved back to Raleigh, North Carolina to work as an intern at Highwoods Properties to work on the Energy Engineering team. Martin began to pursue his Master of Science degree in Mechanical Engineering at North Carolina State University the following August to further sharpen his technical skills expand his knowledge on energy related technologies. Throughout his graduate career, Martin did research on lithium-oxygen batteries while continuing to work at Highwoods Properties as an Energy Engineering Intern.

ACKNOWLEDGEMENTS

I would like to thank North Carolina State University for giving me the opportunity to pursue my graduate degree in a world-class school of Engineering. It has been an honor and a privilege to attend classes and pursue my research with the diverse faculty and students of the University. My experiences at the University have shaped me as an engineer and provided me with the technical acumen and confidence to go forth and pursue my career and professional goals.

I would like to thank my family and friends for their ongoing support and encouraging me to challenge myself each and every day of graduate school.

To my fellow lab mates in the Laboratory for Mechanics of Energy Materials and Biological Tissues, whom I worked alongside of for many hours, I would like to thank you for encouraging me to push forward with my research and class work.

I would like to thank the members of my committee, Dr. Kara Peters and Dr. Alexei Saveliev, for providing me their valuable input on my thesis and research project. The classes taught by these professors directly contributed to my academic and professional development through graduate school.

Most of all I would like to thank my advisor, Dr. Hsiao-Ying Shadow Huang for reaching out to me when I was still completing my undergraduate degree and helping me make my decision to come to NCSU; whose continued guidance made this all possible. Thank you for your help in shaping me to be the engineer I am today.

TABLE OF CONTENTS

LIST OF TABLES .... **vii**

LIST OF FIGURES .... **viii**

CHAPTER 1: INTRODUCTION **1**

1.1 Lithium-Oxygen Batteries 1

1.2 The Demand for Batteries 3

1.2.1 Electric Vehicles 5

1.3 Government Funded National Labs and Private Research 7

1.3.1 Argonne National Laboratory 7

1.3.2 NASA Glenn Research Center 8

1.3.3 Yardney Technical Products, Inc 9

1.4 Objectives of the Study 11

CHAPTER 2: LITERATURE REVIEW **13**

2.1 Lithium Oxygen Batteries Attractive Properties 13

2.2 Challenges with Lithium-Oxygen Batteries 14

2.3 Transport Limitations in $Li-O_2$ Batteries 18

2.3.1 Li_2O_2 Distribution in Cathodes 22

2.4 Formation of Discharge Product (ORR) – Li_2O_2 25

2.5 Li_2O_2 Reactivity with Carbon Cathodes 30

2.6 Lithium Dendrite Growth in Lithium Metal Batteries 33

2.6.1 Dendrite Growth in Lithium/Polymer Cells 35

2.6.2 Dendrite Growth in $Li-O_2$ Cells with Ionic Liquid 38

2.7 Dendrite Growth and Battery Capacity Loss 40

2.8 Computational Modeling of Lithium Dendrite Growth 41

2.9 Mitigating Dendrite Growth 44

CHAPTER 3: MODEL DEVELOPMENT **49**

3.1 Fuel-Cell Module Theory 49

3.2 Model Construction and Parameters 51

CHAPTER 4: SIMULATION RESULTS **56**
4.1 Flat Anode vs. Small Dendrite Model 56
4.2 Comparisons of Flat Anode, Small Dendrite, and Long Dendrite Models 62
4.3 Small Dendrite Model vs. Long Dendrite Model 66
4.4 Capacity Loss – Experimental Results vs. Computational Modeling 70
4.5 Cathode Porosity Effect on Discharge Properties 71
4.5.1 Adjusting Cathode Porosity – Flat and Small Dendrite Models 71
4.5.2 Adjusting Cathode Porosity – Dendrite Models 77
4.6 Mass Fraction of O_2 on Discharge Properties 79
4.6.1 Mass Fraction of O_2 Effect on Flat Anode Model 79
4.6.2 Mass Fraction of O_2 Effect on Dendrite Models 82
4.7 Mass Flow Rate of O_2 Effect on Discharge Properties 85
CHAPTER 5: SUMMARY AND CONCLUSIONS **88**
5.1 FUTURE WORK 90
REFERENCES **92**
APPENDIX **97**
Appendix A: ANSYS Project Reports 98
A1: Geometry and Mesh of the Flat Anode Model 98
A2: Fluent Iterations of Flat Anode Model 101
A3: Mesh of the Long Dendrite Anode Model 108
A4: Fluent Iterations of Long Dendrite Anode Model 109
A5: Mesh of the Small Dendrite Anode Model 116
A6: Fluent Iterations of Small Dendrite Anode Model 117
A7: ANSYS Fluent – Fuel Cell Module Setup 123

LIST OF TABLES

Table 1: Physical properties of common Lithium-oxygen and Li-ion battery discharge products (and Li metal) [2] 4
Table 2: Summary of Calculations and Results to Present 12
Table 3: Formula Constants and Parameters of Butler-Volmer Formulas [30].....................50
Table 4: Material Properties of Lithium-Oxygen Battery Reactants 54
Table 5: Default Operating Parameters of Lithium-Oxygen Model 54

LIST OF FIGURES

Chapter 1
Figure 1: Lithium-ion battery vs. Lithium-oxygen battery. (a) Conventional lithium-ion battery (b) Lithium-oxygen battery (c) Schematic of dendrite forming on anode surface and effects on battery cell [3]. 2
Figure 2: Sales of Plug-In electric vehicles. Numbers include both all electric vehicles (EVs) and plug-in hybrid electric vehicles (PHEVs). These numbers do not include non-plug-in hybrid vehicles [5]. 6
Figure 3: The experimental lithium-oxygen battery cell used in the experiments by Reid et al. The battery itself was developed by Yardney Lithium [7] 9
Figure 4: An SEM image of the porous cathode used in the experiments conducted by Yardney Technical Products [8]. 10

Chapter 2
Figure 5: Estimated Gravimetric and Volumetric Energy Densities of Practical $LiCoO_2$ and Lithium-Oxygen Batteries [1] 14
Figure 6: Cyclability of Lithium-Oxygen Cells with Carbonate Electrolytes [2] 16
Figure 7: Oxygen Reduction Reaction Schematic [1] 18
Figure 8: Air-Cathode Capacity Restriction with Carbon Black Cathode Materials. (A) Small discharge rates leasing to Li_2O_2 forming within cathode with poor conduction characteristics leading to poor volume utilizations. (B) Higher discharge rates leading to transport issues and cathode clogging [13]. 19
Figure 9: Different structures of Graphene and Carbon Nanotubes (a) Single wall carbon nanotube (b) multi-walled carbon nanotube (c) Single graphene sheet (d) a crumpled graphene sheet configuration [13]. 21
Figure 10: Li_2O_2 Formation within cathode. From left to right, increase oxygen diffusion rates: (a) D_{O2}=0.5 (b) D_{O2}=1 (c) D_{O2}=3. Increasing diffusion coefficient of O_2 resulted in increased precipitation growth of 1.8 and 3.8 times for cases (b) and (c), respectively [9]. .. 23
Figure 11: (Top) Lithium concentration for cases a, b, and c from Figure 10 (Bottom) Oxygen concentration for cases a, b, and c from Figure 10 [9]. 24
Figure 12: SEM Images of Discharged Toroid-Like Particles [1] 26
Figure 13: (a) Discharge current vs. capacity of lithium-oxygen cell with CNT. Discharged potentiostatically from 2.76 to 2.0 V (b) Discharge current vs. capacity of lithium-oxygen cell with CNT. Discharge galvanostatically from 10 to 1000 mA/g_c (c) Tafel plot of discharge voltage vs. discharge current normalized by active surface area of carbon. [16]... 27

Figure 14: Discharge curve of lithium-oxygen battery. Through discharge, the cell voltage slowly deceases to 2.6 V due to increasing discharge products where voltage dropped off and ORR stops [18]. 29
Figure 15: Li_2O_2 morphology as the lithium-oxygen cell goes through discharge [18]. 30
Figure 16: Morphology of Li_2O_2 and Li_2CO_3 on Carbon Nanotubes [1]. 31
Figure 17: (a) Growth of Li_2CO_3 through cycling (b) Effect of parasitic products on charging voltage [1]. 32
Figure 18: (a) Needle-Like Dendrite Formation (b) Bush-Like Dendrite Formation [12]. ... 33
Figure 19: Dendrite Length in Ionic Liquid as a function of time [22]. 35
Figure 20: High-Current density discharge within lithium/polymer cell [23]. 36
Figure 21: Low current density resulting in the formation of the thin needle-like dendrite [23]. 37
Figure 22: Morphology of Lithium Dendrite Growth at Different Current Densities [22]. .. 39
Figure 23: Lithium metal cell capacity vs. cycle number at different cycling rates [24]. 40
Figure 24: Schematic of System Modeled by Monroe et al. [11]. 42
Figure 25: Dendrite Growth with Uniform and Step-Function Diffusion Coefficients (a) Dendrite Position (b) Lithium-ion Concentration at Dendrite Tip (c) Kinetic Potential at Dendrite Tip [12]. 43
Figure 26: The change in cell capacity as the battery is cycled. Each line represents a different amount of lithium metal used in the initial anode [29]. 45
Figure 27: Images using SEM technique of Li-O_2 anode surface after 10 cycles (a) Li = 0.9 mg (b) Li = 7 mg (c) Li = 14 mg [29]. 46
Figure 28: Lithium Deposition Process through “self-healing process” [21]. 48

Chapter 3

Figure 29: Schematic of PEM Fuel Cell for Fluent Fuel Cell Module [30]. 51
Figure 30: Schematic of x-y plane of lithium-oxygen cell with flat, homogeneous anode surface(not drawn to scale). 52
Figure 31: Schematic of x-y plane of lithium-oxygen cell with small dendrites on lithium metal surface (not drawn to scale). 53
Figure 32: Normalized I-V Curve of Flat and Small Dendrite Models. The Flat model portrays a better performing cell since the discharge voltage does not fall as quickly as the dendrite model when the discharge voltage is lowered to 2.6 V. 57

Chapter 4

Figure 33: Normalized kMol of Li_2O_2 Formation of Flat and Small Dendrite Models. The lower the discharge voltage, the greater the kMol of Li_2O_2 formed. 58

Figure 34: Contour Plots of Flat and Small Dendrite Models at 2.75 V and 2.70 V............ 60
Figure 35: Contour Plots of Flat and Small Dendrite Models at 2.65 V and 2.60 V............ 61
Figure 36: I-V curve of flat, small, and long dendrite models at a cathode porosity of 0.75. As the dendrites grew to represent a cell that had been continuously cycled, the discharge current of the cell greatly decreased. 63
Figure 37: Normalized kMol of Li_2O_2 Formation of Flat, Small, and Long Dendrite Models at cathode porosity of.75. The lower the discharge voltage, the greater the kMol of Li_2O_2 formed. 64
Figure 38: Contour plots of the formation of Li_2O_2 within the cathode of the three different anode models at different discharge voltages. Note the depth of discharge of the flat anode as well as total amount of Li_2O_2 formed is much greater.. 65
Figure 39: I-V Curve of the long dendrite and small dendrite models. A porosity of 0.75 was used for each model. The discharge current was normalized based on the values of the small dendrite model. 66
Figure 40: Amount of discharge product forming in the cathode of the dendrite models. A cathode porosity of 0.75 was used. The formation of Li_2O_2 was normalized based on the values of the small dendrite model. 67
Figure 41: Contour plots of the two dendrite models. A cathode porosity of 0.75 was used. The scaling of the images shows a much higher depth of discharge in comparison to the previous contour plots in Figure 38. The total cathode utilization of the small dendrite model was much greater than the long dendrite model's utilization. 69
Figure 42: I-V Curve of Flat and Small Dendrite Models at Varying Porosities. Varying porosites had little effect on polatization curves of cells... 72
Figure 43: Normalized kMol of Li_2O_2 Formation of Flat and Small Dendrite Models at cathode porosities of 0.25, 0.5, and 0.75. The lower the discharge voltage, the greater the kMol of Li_2O_2 formed... 73
Figure 44: Contour Plots of Flat Model at 2.75 V and 2.70 V 75
Figure 45: Contour Plots of Small Dendrite Model at 2.75 V and 2.70 V 76
Figure 46: I-V Curve of Small Dendrite and Long Dendrite Models at Varying Porosities. Varying porosites had little effect on polatization curves of cells... 77
Figure 47: Normalized kMol of Li_2O_2 Formation of Flat and Small Dendrite Models at cathode porosities of 0.25, 0.5, and 0.75. The lower the discharge voltage, the greater the kMol of Li_2O_2 formed... 78
Figure 48: I-V Curve of Flat Model with Limited Oxygen. Decreasing the amount of oxygen to react in cell decreases the discharge current faster than the cell with more oxygen. 80
Figure 49: Normalized kMol of Li_2O_2 Formation of Flat models with small mas fractions of O_2. The lower the discharge voltage, the greater the kMol of Li_2O_2 formed. 81

Figure 50: Contour Plots of Flat Anode Model at different mass fraction of O_2. Mass fraction of O_2 of 0.75 shown on the left. Mass fraction of O_2 of 1 shown on the right. 82
Figure 51: I-V Curve of dendrite models with a 25% reduction in mass fraction of oxygen available in cathode.. 83
Figure 52: Formation of Li_2O_2 within cathode of cells with a 25% reduction in mass fraction of oxygen available in cathode. 84
Figure 53: I-V Curves of Flat and Dendrite models at increased oxygen mass flow rate through battery cell. The I-V curves of the dendrite models are significantly decreased compared to the values of the flat anode model. 85
Figure 54: The kMol of discharge product within the cathodes of the flat and dendrite models. The amount of Li_2O_2 shown in the cathode structures is decreased even further in the dendrite models compared to the flat anode model when the mass flow rate of oxygen was increased. 86

CHAPTER 1: INTRODUCTION

1.1 Lithium-Oxygen Batteries

Lithium-oxygen batteries, also commonly referred to as lithium-air batteries, have received a great deal of attention over the years due to their high theoretical gravimetric energies and energy densities [1]. These batteries can theoretically supply a car with power and speed characteristics comparable to gasoline. A big reason these lithium-oxygen batteries have such greater theoretical energy densities and gravimetric energies is because they do not require a transport metal (such as Cobalt, Co) to bond to the lithium as it travels between the electrodes of the battery [2]. Without the need of a heavy transport metal, the gravimetric energies of the battery are increased [2].

Lithium-oxygen batteries are composed of three different parts: a pure lithium metal anode, electrolyte, and a cathode. The three components work together to store and release energy through charging and discharging of the battery cell. While the cell discharges, lithium undergoes an oxidation process, releasing electrons through the circuit and moving to the cathode where the lithium bonds with oxygen to form lithium peroxide (Li_2O_2). Through charging, a high voltage is applied to the cell leading to a reduction reaction and the lithium bonding again with the lithium metal anode [2].

A basic schematic of a lithium-oxygen battery can be seen in Figure 1. In this diagram the anode is pure lithium metal and the cathode is usually made up of a carbon nanotube structure. These two electrodes are separated by some type of electrolyte. During discharging of the battery, electrons are released from the lithium into the circuit resulting in positively charged lithium-ions within the battery. The positive lithium-ions then travel through the electrolyte and bond with the negatively charged oxygen to form Li_2O_2 [2]. During charging, a specified voltage and current is applied to the battery to reverse this process. Another unique characteristic of the battery is the theoretical ability of the battery to absorb and release oxygen into the atmosphere as needed, again leading to greater theoretical gravimetric energies since the oxygen does not have to be stored within the battery [2].

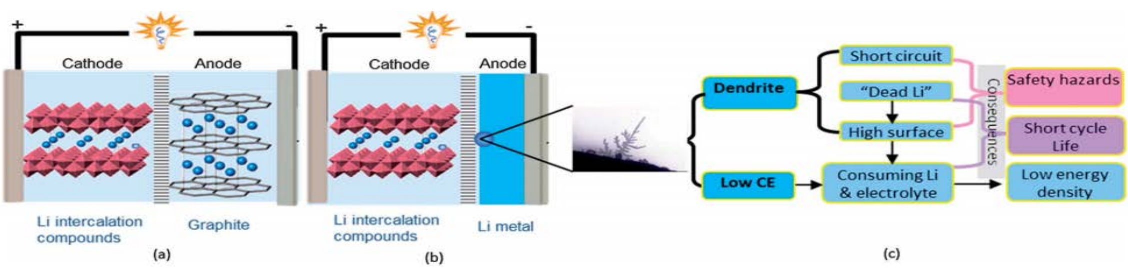

Figure 1: Lithium-ion battery vs. Lithium-oxygen battery. (a) Conventional lithium-ion battery (b) Lithium-oxygen battery (c) Schematic of dendrite forming on anode surface and effects on battery cell [3].

Lithium-oxygen batteries are part of a larger group of batteries known as lithium-metal batteries that are characterized by their pure lithium metal anodes instead of a graphite type anode commonly seen in lithium-ion batteries. Another interesting property of a lithium-oxygen battery is the oxygen permeable layer on the cathode. This layer acts between the outer cathode surface and the atmosphere. The permeable layer is designed to allow oxygen to pass into the battery cell as needed but does not allow other outside containments to enter the cell while also releasing oxygen back into the atmosphere as the cell is recharged and the oxygen is no longer needed [2]. While some lithium-oxygen battery designs do omit the oxygen permeable layer by including a small oxygen storage tank as part of the battery design, these cells have significantly smaller volumetric energies

1.2 The Demand for Batteries

As the global demand for energy increases, the need for suitable energy storage devices continues to grow. Our current energy storage technology of choice is the lithium-ion battery which is commonly found in handheld devices, electric vehicles, and other portable electronics. Since the lithium-ion battery was first introduced in the mid-1970s, it has grown to become an extremely popular commercial technology with specific energies of 0.58 kWh/kg and 2.09 kWh/L for the $LiFePO_4$ discharge product [2]. While one of the main benefits of a lithium-ion battery is the technology's maturity and cyclability, lithium-oxygen batteries present great benefits with their greater theoretical energy. As seen in Table 1 below, the discharge product Li_2O_2 has theoretical specific energies of 3.46 kWh/kg and 7.99 kWh/L [2].

With the greater theoretical energies of lithium-oxygen batteries, there is a great potential for these batteries to be used in many different applications. These applications range from electric vehicle applications to reduce "range-anxiety" to portable electronic energy storage. With the growing interest in renewable energy sources such as solar and wind, lithium-oxygen batteries also pose a benefit for storing the energy generated by the sources to be tapped into again when the sun is not shining or the wind is not blowing.

Table 1: Physical properties of common Lithium-oxygen and Li-ion battery discharge products (and Li metal) [2]

Active material	Specific capacity (mAh/g)	Density (g/cm^3)	Capacity density (mAh/cm^3)	U^θ vs. Li metal (V)	Theoretical specific energy (vs. Li metal) (kWh/kg)	Theoretical energy density (vs. Li metal) (kWh/L)
Li_2O	1794	2.01	3606	2.91	5.22	10.49
Li_2O_2	1168	2.31	2698	2.96	3.46	7.99
$LiOH \cdot H_2O$	639	1.51	965	3.45	2.20	3.33
LiOH	1119	1.46	1634	3.45	3.86	5.60
$LiMO_2$, M = Mn, Ni, Co	275	4.25	1169	3.75	1.03	4.36
$LiFePO_4$	170	3.6	612	3.42	0.58	2.09
Li metal	3861	0.534	2062	0.0		

1.2.1 Electric Vehicles

With the continuous rise in oil prices leading to the rise in the price of gasoline, the demand for electric vehicles has continued to grow since they came back on the market in 2010. Although oil prices have fallen as of late, it is widely believed that the low price of oil is temporary and will eventually rise again, raising the price of gasoline as well.

The idea of electric vehicles is old and has been around as long as cars have been on the road. But while the idea of electric vehicles (EVs) has been around for some time, the battery technology needed for these ideas has not been up to the task until recently. This was seen with the development of the GM EV-1, a battery powered car that was released in 1996 and ran off of lead-acid batteries and had an advertised range of 70-100 miles. The car was a disaster and was scrapped several years later [4]. In 2010, EVs were reintroduced to the market and sales have been growing ever since. Figure 2 below portrays the sales of pure electric vehicles and plug-in electric vehicles (PEVs) each year in the United States [5]. Even in 2014, with gas prices beginning to fall in the United States, the sales of plug-in vehicles grew 23% [5].

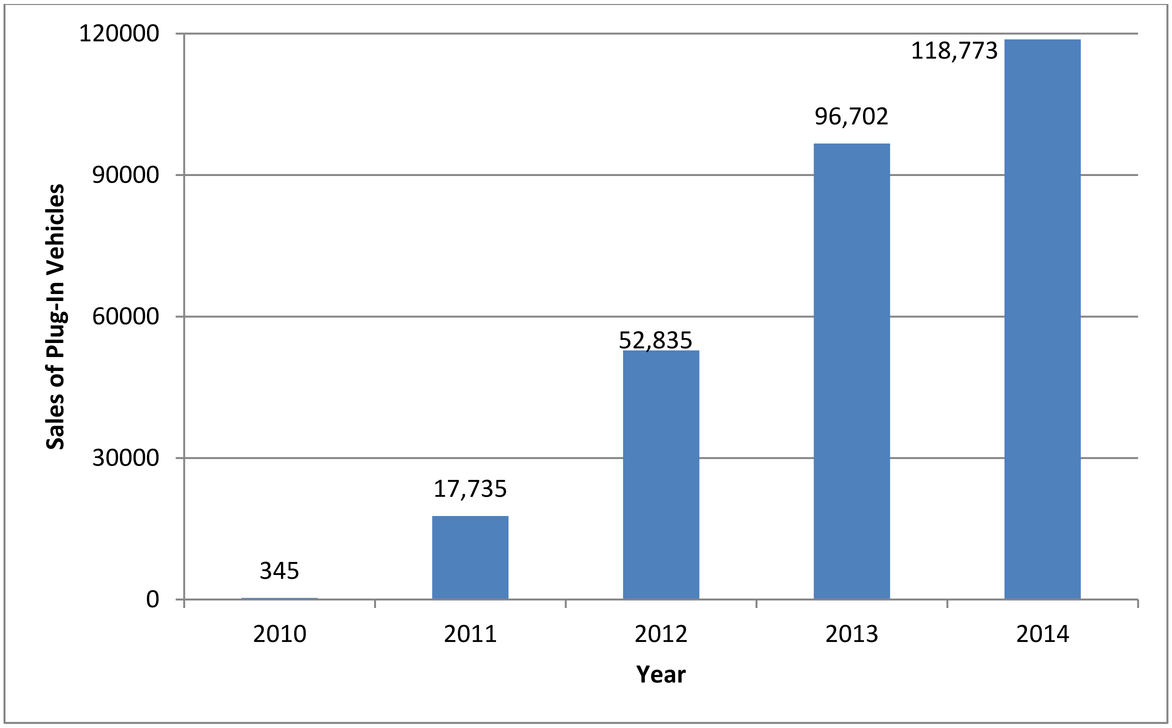

Figure 2: Sales of Plug-In electric vehicles. Numbers include both all electric vehicles (EVs) and plug-in hybrid electric vehicles (PHEVs). These numbers do not include non-plug-in hybrid vehicles [5].

The electric vehicles on the road today use lithium-ion battery technology, utilizing huge battery packs that can often take up most, if not all, of the undercarriage of the vehicle. These batteries at best can deliver a 200 mile range in the Tesla Model-S while other electric vehicles such as the Nissan Leaf, can only go 75-120 miles on a single charge. These relatively short ranges are due to the possible energy densities of the battery packs requiring large and heavy packs installed in these vehicles. With further development of the lithium-oxygen battery, it is theoretically possible to install batteries that can delivery 4-6 times the vehicle range due to the greater specific energies.

1.3 Government Funded National Labs and Private Research

Many nationally recognized labs have been conducting extensive research on lithium-oxygen batteries for years. Some of the more notable research that has been conducted in these labs has been briefly summarized below. A more extensive review of previous lithium-oxygen battery research is presented in Chapter 2.

1.3.1 Argonne National Laboratory

Argonne National Laboratory has been conducting research on lithium-oxygen batteries for several years. A team of engineers and scientists led by Khalil Amine and Michael Thackeray has begun to develop their own lithium-oxygen batteries that will have the capacity to store five to ten times the energy of conventional lithium-ion batteries [6]. The interdisciplinary staff at Argonne National Labs has developed a deep understanding of the challenges of lithium-oxygen batteries and has been using this understanding to develop a safe rechargeable lithium-oxygen battery for the last five years [6]. With their extensive experience researching and developing lithium-ion batteries, the researchers at Argonne National Labs have access to the most advanced research facilities such as their Advanced Photon Source, the Center for Nanoscale Materials, and some of the world's fastest super computers [6].

1.3.2 NASA Glenn Research Center

Groups working at the NASA Glenn Research Center have been developing their own lithium-oxygen battery with a theoretical specific capacity of 11,400 Wh/kg. The batteries under investigation by Reid et al. are being developed for Mobile Oxygen Concentrators, equipment that requires extremely lightweight energy storage [7]. Their group is constructing their own battery cells for experiments with various cathode catalysts and carbon cathode structures to develop a cathode with the optimal active surface area [7]. Other experiments are underway to stabilize the lithium metal surface and prevent dendrite growth on the pure lithium metal anode [7]. One of the experimental cells used in their experiments is shown in Figure 3 below. It is important to note that the work published by Reid et al. is done on primary lithium-oxygen batteries, meaning these experimental cells are not designed to be continuously cycled and are not rechargeable.

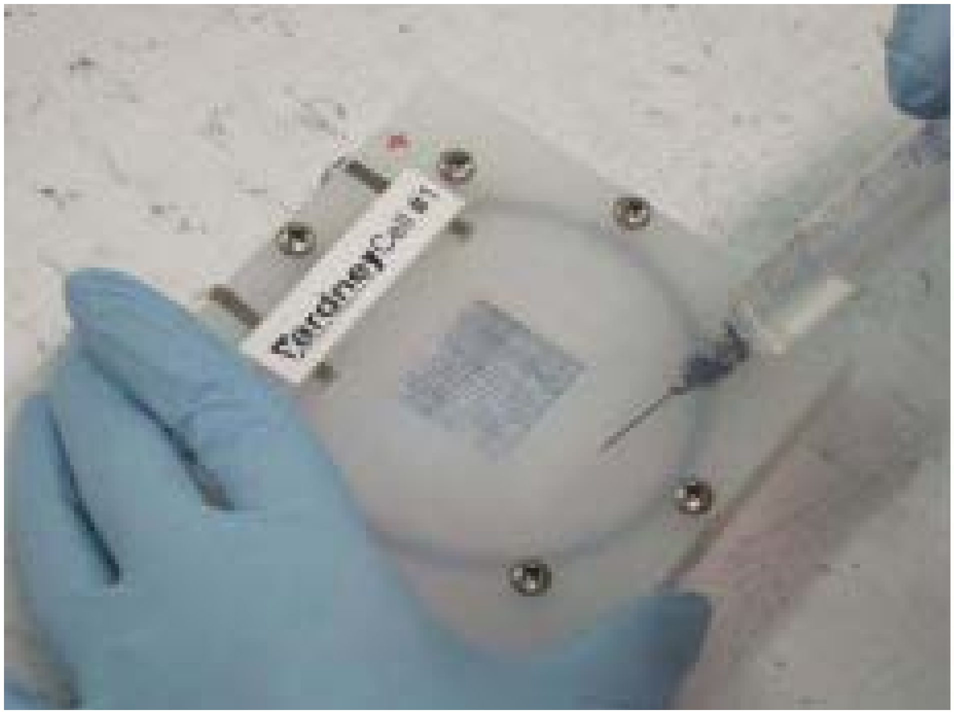

Figure 3: The experimental lithium-oxygen battery cell used in the experiments by Reid et al. The battery itself was developed by Yardney Lithium [7]

1.3.3 Yardney Technical Products, Inc.

Dobley et al. have published work of their own to develop a higher capacity lithium-oxygen battery by incorporating transition metal catalysts with improved cathode structures. While it is widely known that the main limiting factor in lithium-oxygen battery cells is the poor rate of oxygen diffusion within the positive electrode [8]. Recognizing this as the limiting factor of lithium-oxygen batteries, Dobley et al. focused on developing and improving the cathode design and structure [8]. The air cathode used is a layered structure of carbon composite, constructed using carbon, a metal Manganese (Mn) catalyst, and a Teflon and latex binder [8]. Through discharging the lithium-oxygen cells, it was found that increasing the discharge rate of the cell by two times resulted in less than half of the capacity loss of the cell – likely due to poor clogging in their carbon cathode structure [8]. Figure 4 below shows the SEM images of the porous carbon cathode used in their experiments.

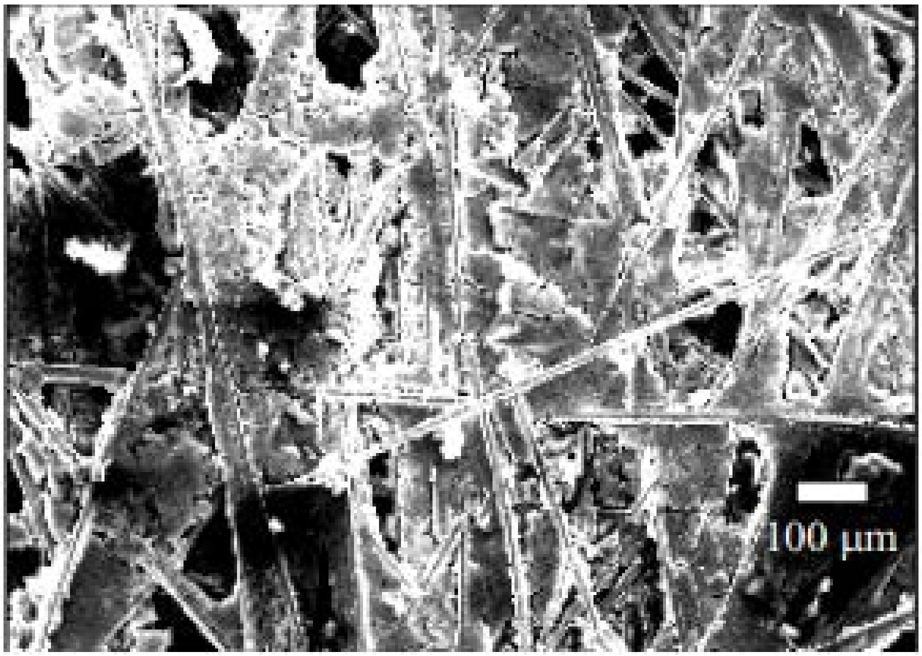

Figure 4: An SEM image of the porous cathode used in the experiments conducted by Yardney Technical Products [8].

The interest in developing future energy storage technologies such as lithium-oxygen and lithium metal batteries is apparent from the extensive research conducted by national and private labs. Despite this continuous work, there is still a great opportunity to contribute to this conversation and help develop the general understanding of these battery cells. The research presented in this study aims to help develop our understanding of anode and cathode designs of the lithium-oxygen battery on the battery performance and will be discussed further.

1.4 Objectives of the Study

Many of the problems with lithium-oxygen batteries can be categorized as issues related to either the lithium-metal anode or the carbon cathode structure. Both electrodes provide their own challenges for developing a commercially viable lithium-oxygen battery. Many studies have been published to better understand the morphology and formation of lithium dendrites on metal anodes and model the growth of dendrites in lithium-oxygen cells using numerical methods. At the same time extensive work has also been done to model the precipitate growth (Li_2O_2) within the cathode numerically and through in-situ techniques [9-12]. Despite these studies, the effects of dendrite growth on the formation of Li_2O_2 within the cathode at discharge have not been studied together to a satisfactory degree. The main objective of the study is to complete our own comprehensive finite elements model of a lithium-oxygen battery that can take into account the structure of the lithium metal anode as well as various design aspects of the carbon cathode to understand how these different behaviors affect the discharge performance of a lithium-oxygen battery. Table 2 below summarizes the calculations that will be carried out on our models.

Table 2: Summary of Calculations and Results to Present

Tabular Summary of Parameters				
Anode Surface Model	**Discharge Voltages**	**Cathode Porosity**	**Mass Fraction of O2**	**Mass Flow Rate of O2**
Flat Model	2.75 V 2.725 V 2.7 V 2.675 V 2.65 V 2.625 V 2.6 V	0.25 0.5 0.75	100% 75%	Default x10
Short Dendrite Model (4 µm)	2.75 V 2.725 V 2.7 V 2.675 V 2.65 V 2.625 V 2.6 V	0.25 0.5 0.75	100% 75%	Default x10
Long Dendrite Model (12.5 µm)	2.75 V 2.725 V 2.7 V 2.675 V 2.65 V 2.625 V 2.6 V	0.25 0.5 0.75	100% 75%	Default x10

CHAPTER 2: LITERATURE REVIEW

2.1 Lithium Oxygen Batteries Attractive Properties

Lithium-oxygen batteries have been receiving a lot of attention in the last few years due to their great theoretical gravimetric energies and energy densities when compared to current lithium-ion batteries. One of the great advantages of lithium-oxygen is that instead of relying on intercalation reactions where the electrode crystal structure is maintained, these technologies use a conversion reaction where the electrode crystal structure is altered [1].

In the lithium-oxygen battery, the oxygen ions within the cathode are reduced by electrons and bond with lithium ions that travel from the anode, without any type of transport metal (such as Co). These products help to form Li_2O_2 as shown in equation 1 below.

$$2Li + O_2 = Li_2O_2 \tag{1}$$

Gravimetric energies of lithium-oxygen are calculated to range between 1800-2800 Wh/kg. The range largely comes from various possible electrode materials in non-carbonate electrolytes. With typical lithium-ion batteries showing gravimetric energies of about 600 Wh/kg, lithium-oxygen batteries may have 3-5 times higher specific energies [1].

Figure 5 displays the advantage of lithium-oxygen batteries over typical lithium-ion batteries but also shows that the calculated volumetric energy densities of the batteries are similar. It should also be noted that Polyplus Inc. believes that a practical lithium-oxygen battery can be constructed with specific energies between 700 and 800 Wh/kg [1].

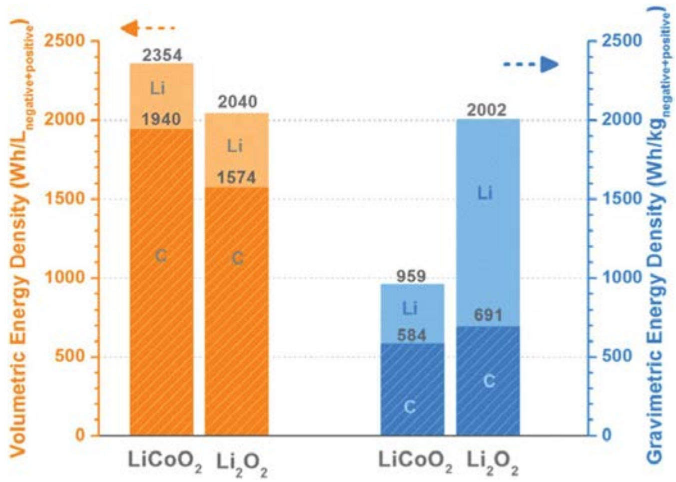

Figure 5: Estimated Gravimetric and Volumetric Energy Densities of Practical $LiCoO_2$ and Lithium-Oxygen Batteries [1]

There are many different issues that must be addressed before cyclable lithium-oxygen batteries can be made commercially available. To address many of these issues such as finding a stable electrolyte and lithium metal electrode, the oxygen reduction and evolution reaction mechanics must be further understood.

2.2 Challenges with Lithium-Oxygen Batteries

Despite some of the major advantages of lithium-oxygen batteries, there are still several major challenges that must be overcome before these batteries will be available for commercial use. These issues range from finding a stable electrolyte, preserving the stability of the lithium metal anode, designing an applicable oxygen permeable membrane, and accommodating volume changes within the cell [2].

One of the main barriers to developing a suitable lithium-oxygen battery is the design of a suitable electrolyte that will promote a cyclable reaction within the cell. Carbonate solvents have proven to be poor candidates for these systems due to the fact that CO_2 becomes a discharge product rather than O_2 as the battery is charged [2]. This leads to Li_2O_2 not being a principal discharge product and therefor limits the cyclability of a cell with carbonate electrolytes. Figure 6 below, taken from Christensen et al., demonstrates the diminishing performance of lithium-oxygen cells with different electrolytes. So far, no publication has been able to cycle a lithium-oxygen cell 100 times with 90% cyclability [2]. Several other electrolytes that have been investigated include ethers and ionic liquids but these still have cyclability issues [2].

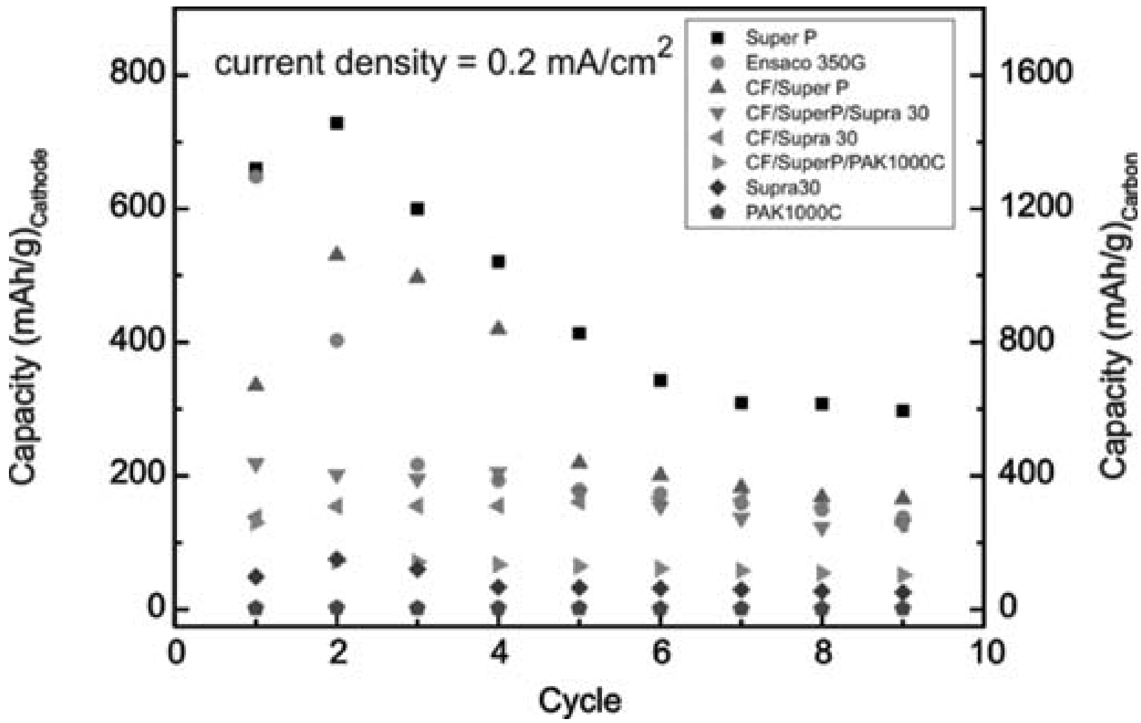

Figure 6: Cyclability of Lithium-Oxygen Cells with Carbonate Electrolytes [2]

Another major issue that must be addressed is the development of an oxygen permeable membrane that would allow oxygen to enter and exit the system as needed. This membrane also must prevent contaminants from entering the cell [2]. Several papers have been published showing promising developments in this field by Zhang et al. and Max Power Inc., where polymer derived membranes are currently being designed [2]. Unfortunately, these membranes have only been demonstrated to work at limited current densities and are still being developed. It is worth noting that on-board storage has been explored (such as utilizing a small tank of oxygen) but it greatly reduces the energy density and specific energy of the cell and would not be ideal [2].

Another roadblock in the development of a commercially available lithium-oxygen battery is a better understanding of the reaction mechanics of the system represented in Figure 7 below; it represents the basic reaction scheme of the oxygen reduction reaction (ORR) that takes place in a nonaqueous electrolyte [1]. The first two branches (r_1 and r_2) represent the ORR reactions of large cations in a nonaqueous media, forming O_2^- as an intermediate species through a one electron transfer before forming YO_2 (where Y represents a large cation). By replacing the large cations with lithium ions (r_3) disproportionation may occur as represented by r_4 in Figure 7. The disproportionation from LiO_2 to Li_2O_2 occurs because of lithium's inability to stabilize O_2^-. The other possible reaction is a second electron transfer to occur as represented by r_5 to still form Li_2O_2. X-ray diffraction results further prove that Li_2O_2 is the main discharge product in nonaqueous media instead of Li_2O and reactions such as r_6 are not observed [1].

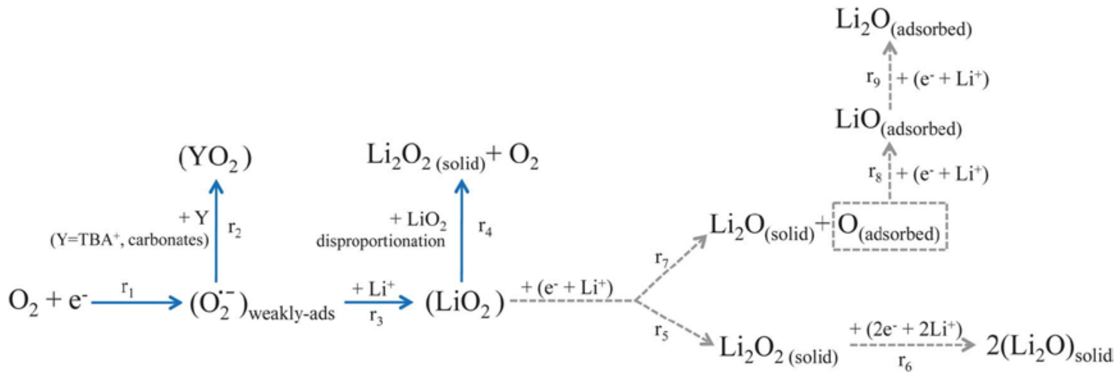

Figure 7: Oxygen Reduction Reaction Schematic [1]

2.3 Transport Limitations in Li-O_2 Batteries

One of the challenges in manufacturing a rechargeable lithium-oxygen battery is due to the inability of typical cathode materials to accommodate large amounts of lithium-peroxide, limiting the overall capacity of the battery. This issue is demonstrated in Figure 8. The cathode material demonstrated in the material is battery grade carbon black. Studies show that upon discharge the internal volume filling is low with most cases suggesting a small ~10-15% internal pore volume being filled [13]. Figure 8a demonstrates the dense low conducting Li_2O_2 films forming at low current rates, leading to low internal volume filling [13]. Figure 8b demonstrates how higher discharge rates can lead to transport issues resulting in a cathode internal volume closure [13].

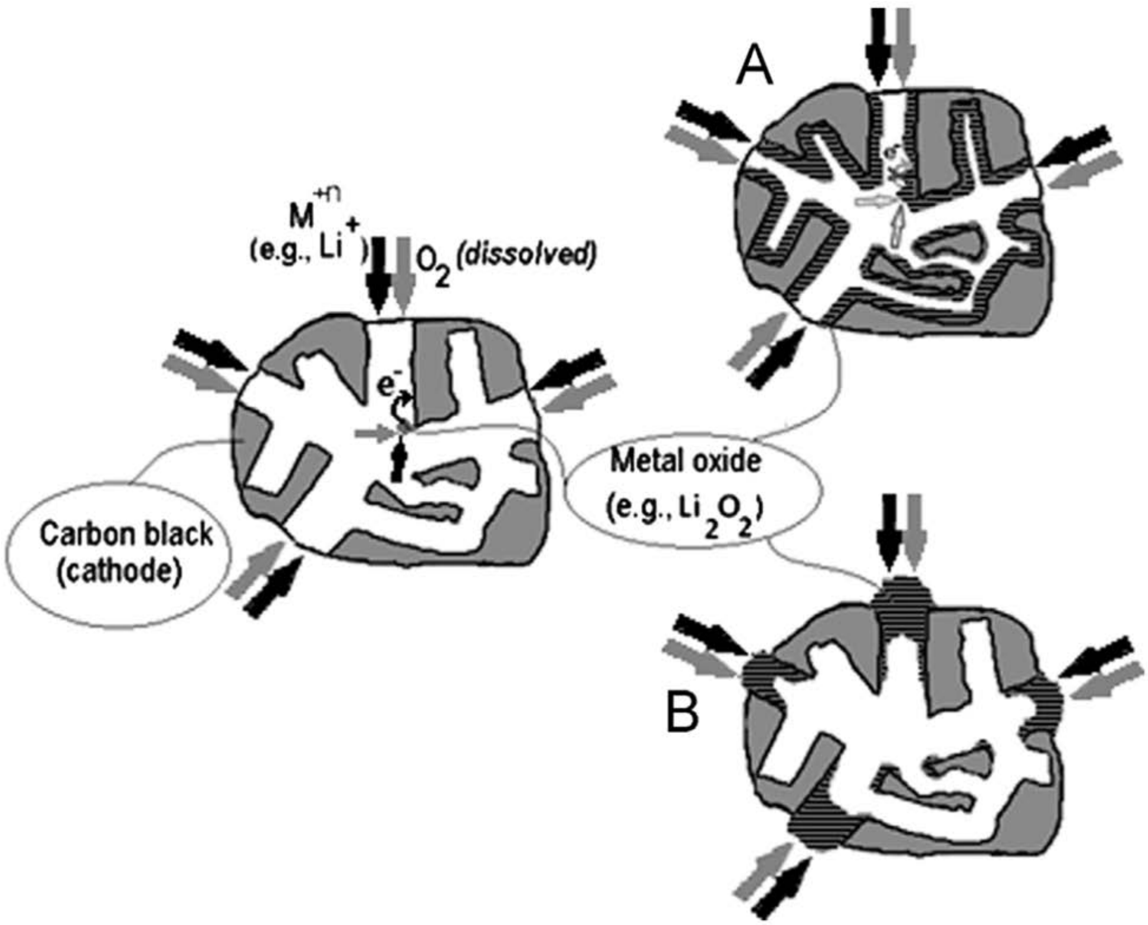

Figure 8: Air-Cathode Capacity Restriction with Carbon Black Cathode Materials. (A) Small discharge rates leasing to Li_2O_2 forming within cathode with poor conduction characteristics leading to poor volume utilizations. (B) Higher discharge rates leading to transport issues and cathode clogging [13].

A cathode's ability to accommodate the lithium peroxide on discharge depends on the cathode pore system structure rather than the internal cathode pore volume [13]. The logic is that the cathode pore size, if too narrow, will be blocked quickly by discharge products, but if it is too large the side surfaces of the pore will be plated with oxides thick enough to stop charge transfer since Li_2O_2 is a known insulator. It is suggested that meso-pore volumes (5-10 nm diameter) may be the most effective cathode system, allowing the formation of the characteristic 5 nm thick layers of oxides on cathode pore surfaces. Pores less than 4 nm were found to lead to pore orifice clogging, meaning the 5-10 nm diameter pore orifices may be optimal for cathode filling [13].

Other studies point to the capacity of lithium-oxygen cells increasing as the pore size of the carbon cathodes grows larger. A linear relationship is reported between the average pore cathode diameter and the capacity of the lithium-oxygen cell with the majority of lithium oxides residing in the larger pores of the cathode [14].

The most extensively studied nanostructures for energy storage capabilities are graphene and carbon nanotube structures with their various structures represented in Figure 9 [13]. Figure 9a represents a single wall carbon nanotube (SWCNT), consisting of a single rolled up graphite sheet. Figure 9b represents a multi-walled carbon nanotube, consisting of numerous SWCNTs fitted one inside another. Figure 9c represents a single graphene sheet (of one atom thickness) and 9d portraying the “crumpled graphene sheet configuration” [13]. The cathode structure and design greatly affect the performance of lithium-oxygen batteries, as both have a direct impact on cell cyclability and capacity.

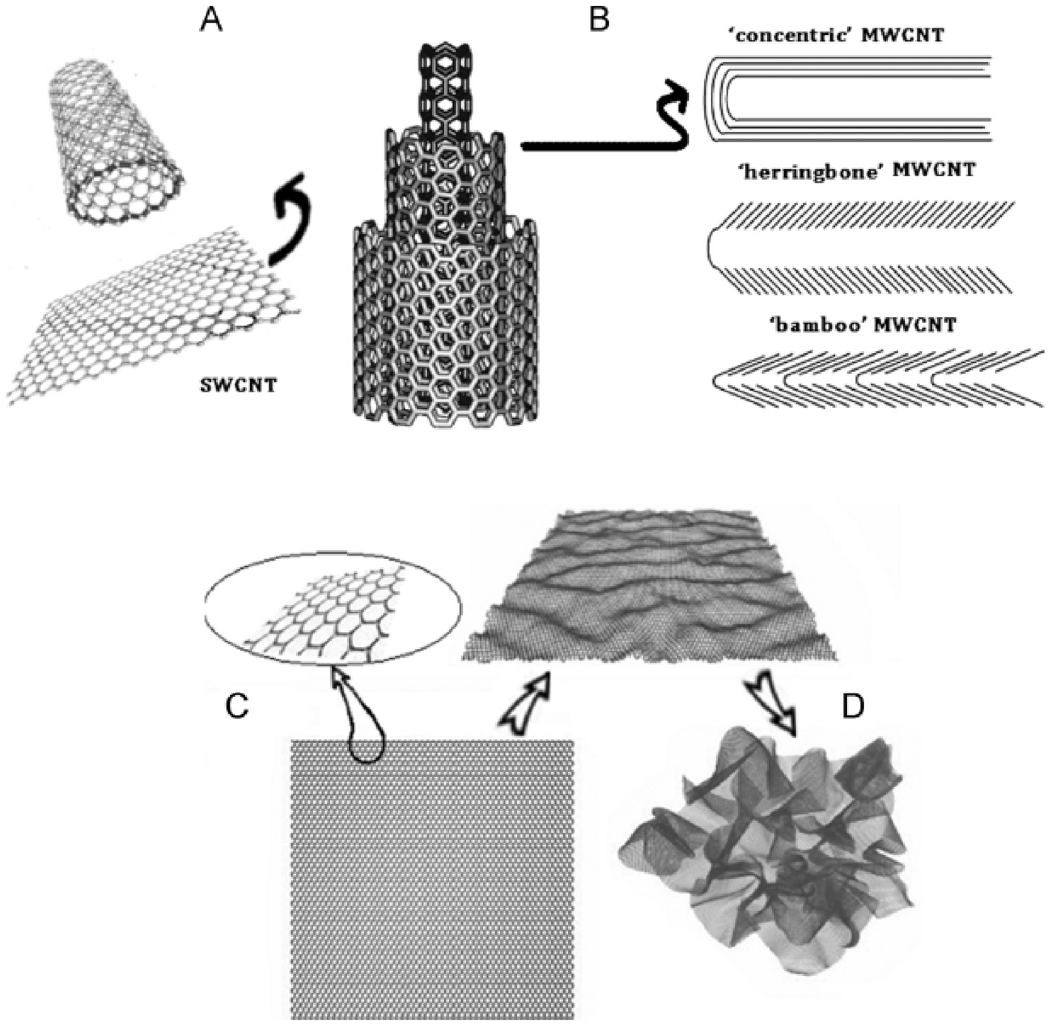

Figure 9: Different structures of Graphene and Carbon Nanotubes (a) Single wall carbon nanotube (b) multi-walled carbon nanotube (c) Single graphene sheet (d) a crumpled graphene sheet configuration [13].

2.3.1 Li_2O_2 Distribution in Cathodes

The distribution of precipitate in the cathode has been studied using high energy x-ray diffraction methods, and they have been carried out to investigate mass-transport limitations during discharging. The work done by Shui et al. cycled a lithium-oxygen battery 11 times, and each time finding similar charging/discharging cycles [10]. It was found that Li_2O_2 is not distributed evenly through the cathode and that the highest concentration of precipitate was found closer to the separator than the oxygen permeable membrane [10]. It makes intuitive sense as the mixing front between lithium and oxygen would occur closer to the separator than the membrane, leading to the highest concentration of Li_2O_2.

Further, the transport limitation of lithium-oxygen batteries further limits the depth of discharge and the capacity and cyclability of the cells [9]. Ryan et al. has investigated the growth of precipitate in the cathode by modeling the reactions of lithium and oxygen within a porous cathode using models developed by Tartakovsky et al [15]. General advection-diffusion-reaction equations are solved to model the movement and reactions of lithium and oxygen within the cathode [9]. The reaction that occurs as the lithium-oxygen battery is discharged is shown below.

From their numerical analysis, it was found that increasing the diffusion coefficient of oxygen does help to move the mixing front deeper into the wetted area of the cathode but does not help to utilize more of the cathode and increase the capacity of the battery [9]. Blockage quickly occurs at the mixing front in the cathode, decreasing the capacity and preventing further formation of lithium peroxide. In the case where a catalyst was utilized, it was found that if the reaction rates deep in the wetting portion of the cathode can be increased in relation to the reaction rates closer to the air side, a larger portion of the cathode can be utilized before pore blockage occurs and the electrochemical reaction stops [9]. The results from Ryan et al. are demonstrated in Figure 10 where the increase in oxygen diffusion rates can be seen to affect the depth of discharge within the cathode as well as the amount of Li_2O_2 formed [9].

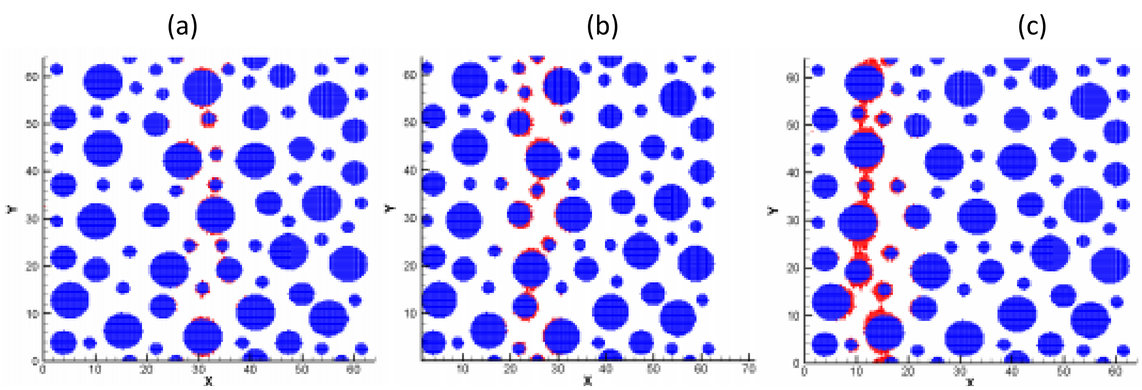

Figure 10: Li_2O_2 Formation within cathode. From left to right, increase oxygen diffusion rates: (a) D_{O2}=0.5 (b) D_{O2}=1 (c) D_{O2}=3. Increasing diffusion coefficient of O_2 resulted in increased precipitation growth of 1.8 and 3.8 times for cases (b) and (c), respectively [9].

Figure 11 demonstrates the concentrations of oxygen and lithium moving through the cathode. It can be seen that the pore blockage caused by the Li_2O_2 formations prevents further mixing of the species.

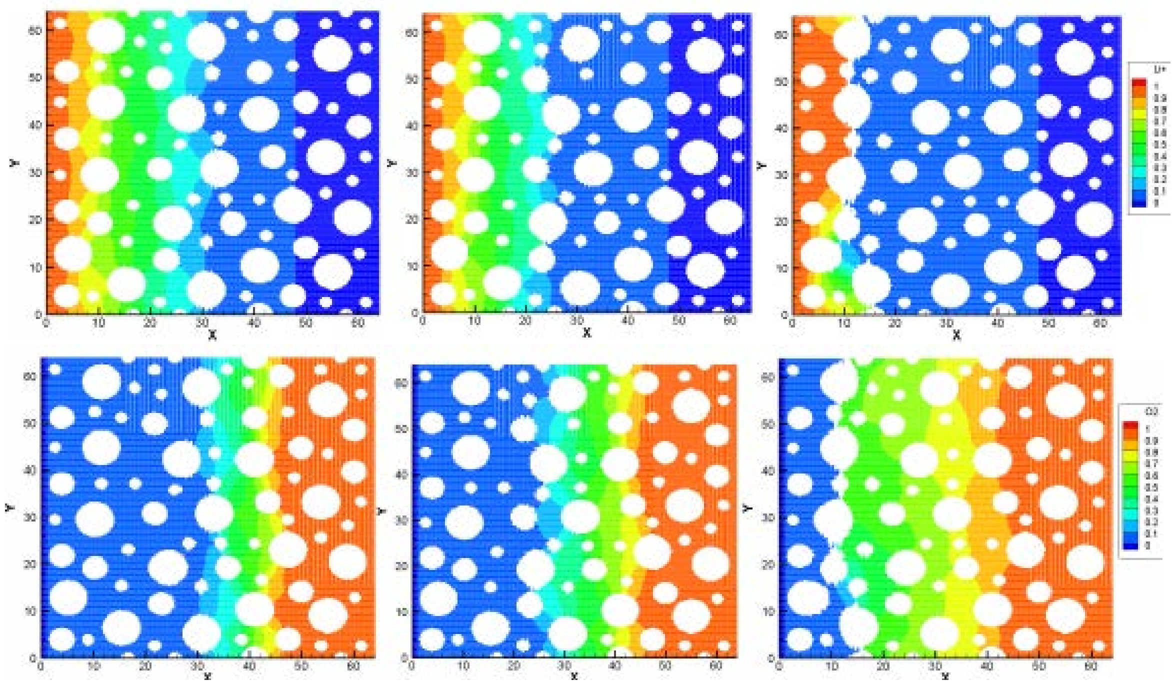

Figure 11: (Top) Lithium concentration for cases a, b, and c from Figure 10 (Bottom) Oxygen concentration for cases a, b, and c from Figure 10 [9].

The results of this analysis contend that a cathode for a lithium-oxygen battery must be developed that can increase the reaction rates as specified above, likely by the use of some catalyst within the cathode [9]. While the paper does not go further into suggesting how to achieve these greater capacities, the results do shed some light on the precipitate growth behaviors in the cathode of lithium-oxygen batteries.

2.4 Formation of Discharge Product (ORR) – Li_2O_2

The morphologies of the Li_2O_2 formed during discharge were found to depend on the applied potential with small particles (10-20 nm) forming at lower discharge potentials and larger disc-like particles (~50 nm thick, 200 nm diameter) forming at higher potentials [16]. These discs are the intermediate to the formation of the toroid-like particles. These findings suggest that larger discharge potentials ($E > 2.7$ V) promote the growth of Li_2O_2 on Li_2O_2 while smaller discharge potentials ($E < 2.7$ V) promote the growth of Li_2O_2 on carbon [16]. The abrupt change between the morphology of Li_2O_2 with respect to different potentials is due to a nucleation barrier of Li_2O_2 on carbon and this nucleation barrier may change with different electrode materials [16].

The formation of thicker discharge products (hundreds of nm instead of several nm) must be achieved in order to reach higher discharge capacities. The formation mechanisms of bulk Li_2O_2 must be better understood and analyzed before higher discharge capacities can be achieved.

It has been reported that discharge in non-carbonate electrolytes forms large Li_2O_2 particles (on the order of one µm) with distinct toroid-like shapes as can be seen in Figure 12 [1]. These toroid shapes appear to be characteristic of Li_2O_2 and not dependent on electrolyte or electrode materials. Toroid-like shapes begin as small particle shapes before evolving into the toroid shapes at higher discharge capacities [1].

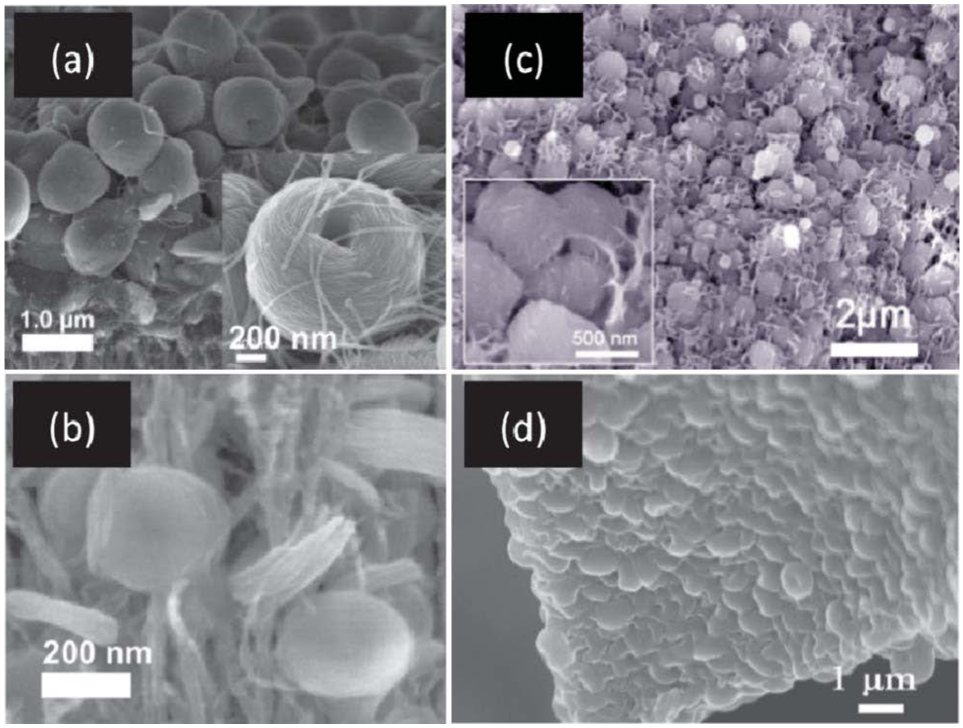

Figure 12: SEM Images of Discharged Toroid-Like Particles [1].

Studies have shown that the Li_2O_2 morphology directly influences the oxygen reduction reactions and the oxygen evolution reactions within lithium-oxygen cells [16]. Figure 13 portrays the discharge potentiostatic (a) and galvanostatic (b) discharge profiles as well as the Tafel plot of discharge voltage versus discharge current (c). A decrease in current can be seen with the potentiostatic discharge plot, especially at lower voltages (less than 2.6 V). This is likely due to electronic limitations that increase as more Li_2O_2 forms and acts as an electronic insulator.

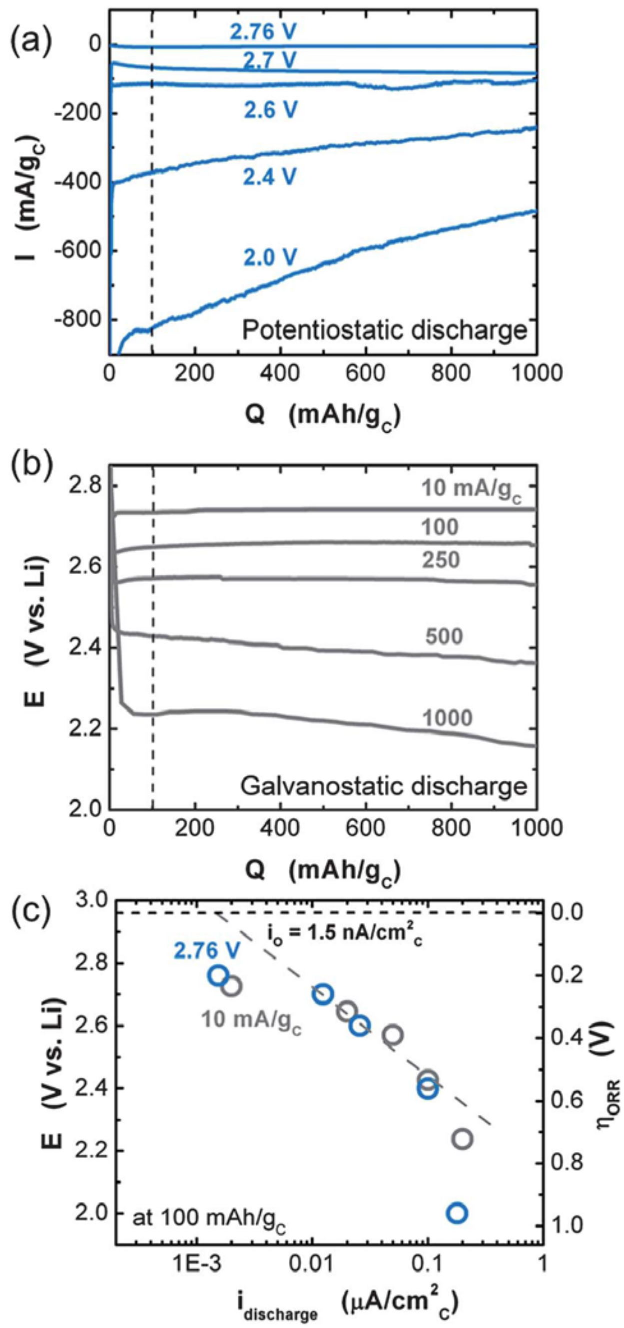

Figure 13: (a) Discharge current vs. capacity of lithium-oxygen cell with CNT. Discharged potentiostatically from 2.76 to 2.0 V (b) Discharge current vs. capacity of lithium-oxygen cell with CNT. Discharge galvanostatically from 10 to 1000 mA/g_c (c) Tafel plot of discharge voltage vs. discharge current normalized by active surface area of carbon. [16].

The galvanostatic discharge plot agrees well with the results seem from the potentiostatic discharge profile at low discharge capacities as can be seen by the linear relationship of the Tafel plot in Figure 13 [16]c. The slope of the Tafel plot in Figure 13c is ~ 290 mV/dec [16]. The “dec” unit is short for “decade” and is referring to the fact that the x-axis of Figure 13c is on a logarithmic scale. At low discharge currents, it can be seen that the discharge voltage and overpotential deviated from a linear relationship and begins to approach ~2.8 V and 0.16 V respectively, or a minimum overpotential. At very high discharge currents, the discharge voltages again deviated from the linear relationship and decreased very quickly, greatly increasing the overpotential [16]. These results are supported by previous studies by Viswanathan et al., however, other reported recent activity but further studies are needed to better understand why these deviations from the linear relationship occur [16, 17].

These findings were confirmed through the work done by Xia et al. where work was done to better control Li_2O_2 properties and morphologies to improve lithium-oxygen cell cyclability [18]. Their experimental cell would discharge to a voltage of 2.6 V before the buildup for discharge products which caused the voltage to drop off and cease discharge as seen in Figure 14. It was found that at low discharge current, Li_2O_2 deposits were found on carbons surfaces resembling small disc-like particle before more Li_2O_2 nucleated on disc-like particles led to an increase in disc size and crystalline Li_2O_2 shells [18].

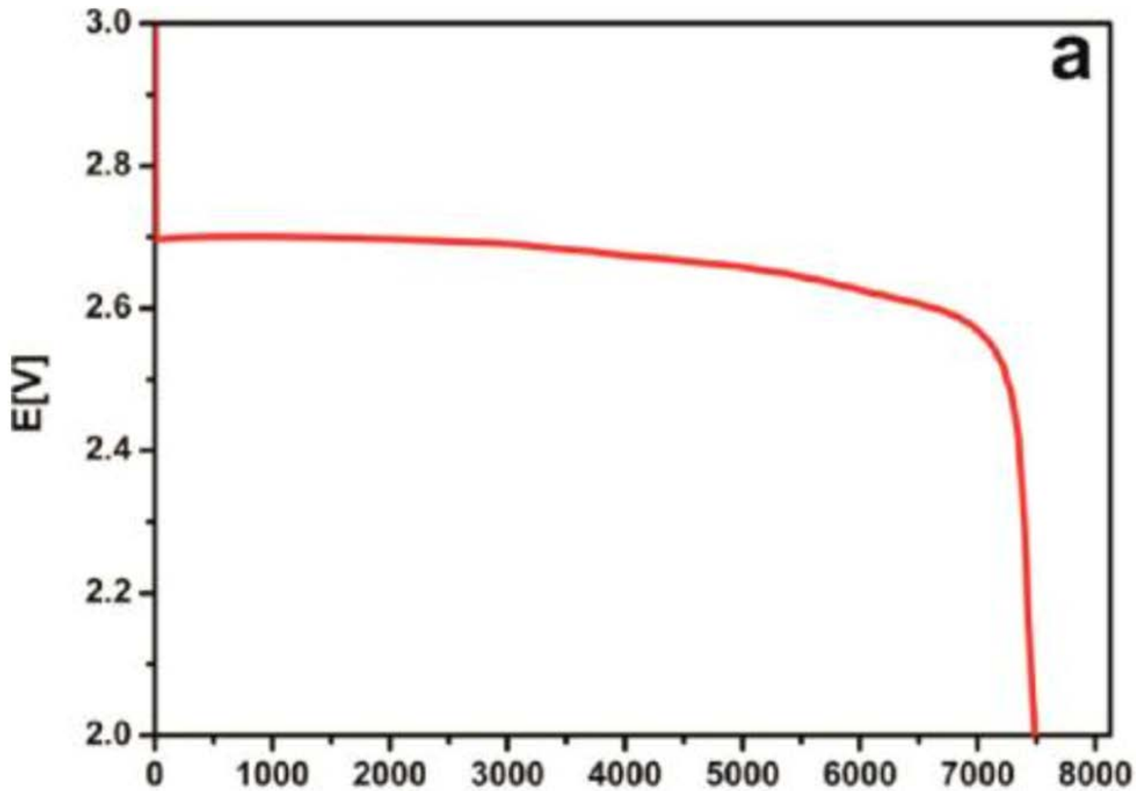

Figure 14: Discharge curve of lithium-oxygen battery. Through discharge, the cell voltage slowly deceases to 2.6 V due to increasing discharge products where voltage dropped off and ORR stops [18].

As the experimental cell continued to discharge, a defective super-oxide phase was found to form on the rims of the disc-like particles, forming a toroid shape that is highly chemically reactive and degrades the cell [18]. These reactions can be seen in Figure 15.

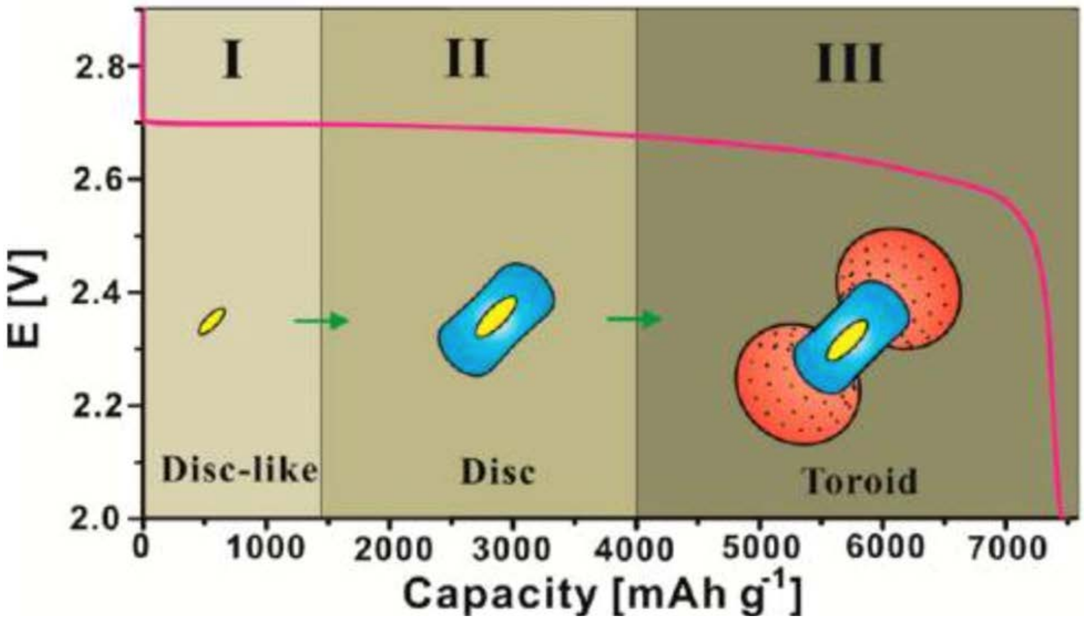

Figure 15: Li_2O_2 morphology as the lithium-oxygen cell goes through discharge [18].

2.5 Li_2O_2 Reactivity with Carbon Cathodes

Another issue resulting from the reduction reactions is the Li_2O_2 reacting with carbon (from ether-based electrolytes) to form Li_2CO_3. Products such as Li_2CO_3 have been seen to form on carbon nanotubes and can represent an irreversible reaction and should be prevented as seen in Figure 16 below [1]. Recent experiments utilizing XANES have shown Li_2CO_3 present at lower loadings (~1000mAh/g) but have not been observed at higher capacities (2000 and 4700 mAh/g). Gallant et al. proposes the apparent absence of Li_2CO_3 at higher capacities is due to the large Li_2O_2 particles covering up the Li_2CO_3 as seen in Figure 14 [1]. McCloskey et al. supports this statement using a differential electrochemical mass spectroscopy study in which CO_2 (with ^{13}C from the electrode surface) was detected with a small Li_2O_2 thickness [19]. Further, Thotiyl et al. reports that the formation of Li_2CO_3 is largely related to electrolyte decomposition (instead of cathode decomposition) on discharge [20] . This was found experimentally when it was discovered that the parasitic products contained ^{12}C (from the electrolyte) instead of ^{13}C (from the electrode) upon discharge. However when the battery was charged, the presence of ^{12}C or ^{13}C in the parasitic products depended on the charge potential [1, 16]. These findings again highlight the importance of developing a noncarbonated electrolyte so these parasitic products can be mitigated.

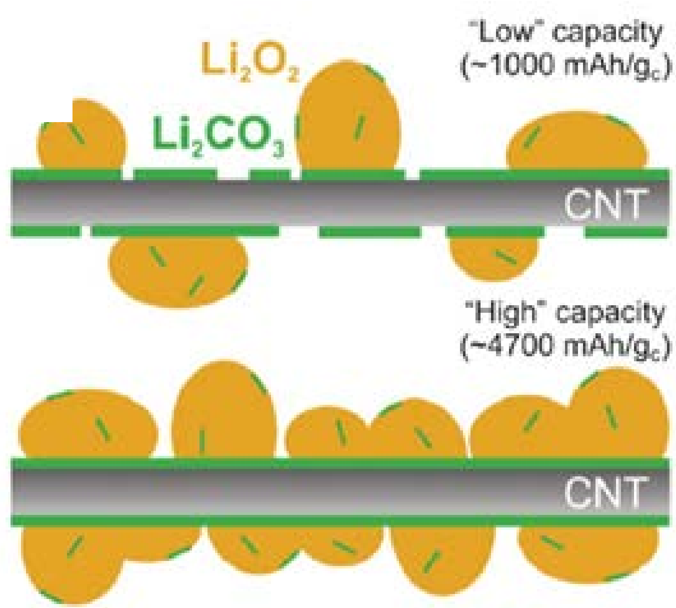

Figure 16: Morphology of Li_2O_2 and Li_2CO_3 on Carbon Nanotubes [1].

Figure 17 below portrays the effect that parasitic products such as Li_2CO_3 can have on the discharge profiles of a lithium-oxygen battery. Figure 17a shows the formation and growth of parasitic products upon cycling while Figure 17b shows the increase in charging voltage required through cycling. It can be seen that at higher cycles, the charging voltage required increases as the parasitic products (Li_2CO_3) continue to grow.

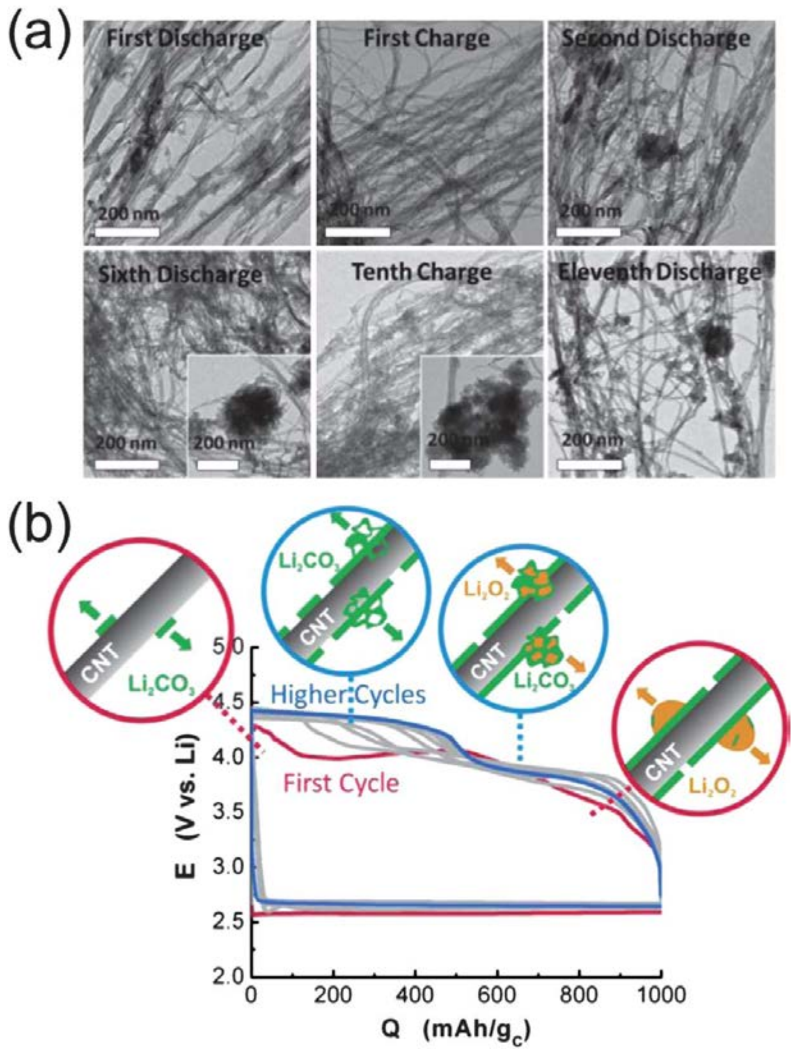

Figure 17: (a) Growth of Li_2CO_3 through cycling (b) Effect of parasitic products on charging voltage [1].

2.6 Lithium Dendrite Growth in Lithium Metal Batteries

Another problem in the development of lithium-oxygen batteries is the growth of dendrites (tree-like structures) on the lithium metal anode of the battery. The growth of dendrites on pure lithium metal has been a known issue for several decades and has been a subject of study for over 40 years [21]. These dendrites can lead to low columbic efficiency of the battery and eventually catastrophic failure of the system due to shorts. These dendrites form through the cycling of the battery and are observed not just in lithium-oxygen batteries, but in all battery systems with a pure lithium metal anode. Figure 18 below shows an image of dendrites forming within a lithium-oxygen cell, with Figure 18a portraying a needle-like dendrite and Figure 18b portraying the bush-like dendrite formation, two different dendrite formations that form at low and high current densities, respectively [12].

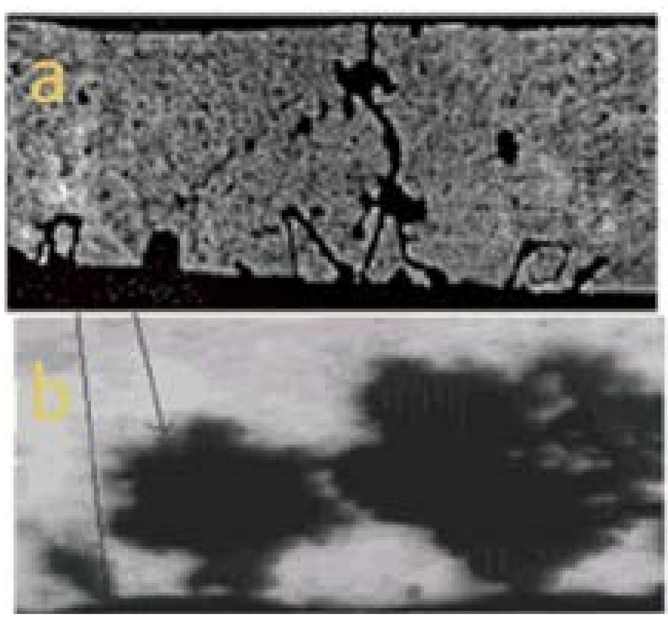

Figure 18: (a) Needle-Like Dendrite Formation (b) Bush-Like Dendrite Formation [12].

These dendrites can lead to changes in local transport properties, increased in joule heating in the anode, and eventual breakage of the dendrites (and shorts in the system) [21]. These events are unacceptable and a suitable solution must be found to mitigate these structures from forming before a safe and cyclable lithium-oxygen battery is developed.

The length of the dendrite arms as a function of time are measured and are demonstrated in Figure 19 below where it can be seen that the dendrite growth is proportional to the square root of time. Figure 19 demonstrates the initial dendrite growth is slow while the dendrite growth begins to increase once it exceeds a specific certain length. This is due to the slow growth rate of the smaller whisker-like dendrite growing initially that then are followed by the growth of longer spiny deposits [22].

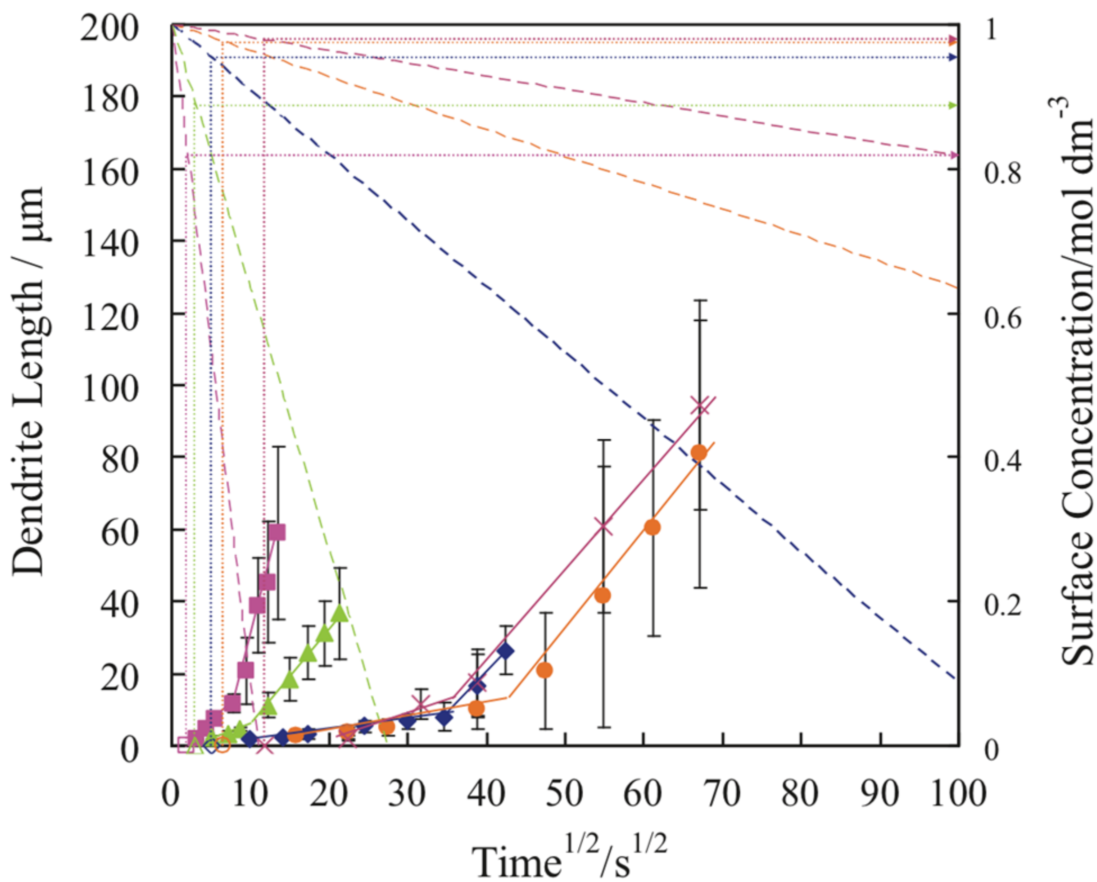

Figure 19: Dendrite Length in Ionic Liquid as a function of time [22].

2.6.1 Dendrite Growth in Lithium/Polymer Cells

Dendrites are known to grow in all battery systems with a pure lithium metal electrode. All lithium-oxygen batteries utilize this metal anode and thus dendrite growth is something that must be dealt with in every type of lithium-oxygen cell. One common type of lithium-oxygen battery cell that was introduced in the 90s is the lithium/polymer cell [23]. This type of battery cell is known for its solid state, adhesiveness, and elastomer-like properties of the electrolyte [23]. It is known that a solid state electrolyte can help mitigate dendrite growth through the application of some pressure on the anode surface and thus pose an interesting investigation.

Brissot et al. published in-situ work, experimenting with their own lithium/polymer cells under galvanostatic conditions. It was found that the lithium dendrites grow and had different structures based on the discharge current density of the battery cell. In the high-current density, the dendrites take on the previously discussed “bush” like morphology as seen in Figure 20. It was also observed that these dendrite structures were not able to grow past a certain length of the electrode surface [23].

Figure 20: High-Current density discharge within lithium/polymer cell [23].

When the cell was discharged at a low-current density, the thin needle-like dendrite was formed as seen in Figure 21. Unlike the bush like dendrites previously discussed, the needle-like dendrites do not have a limit to how long they can grow and pose a safety hazard with the potential to short out the battery cell.

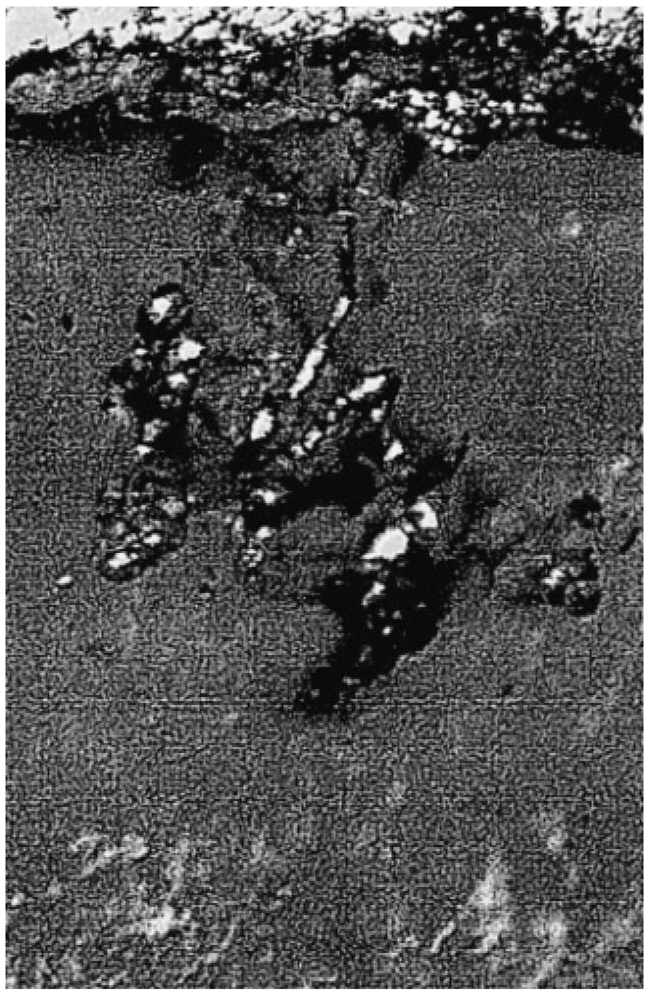

Figure 21: Low current density resulting in the formation of the thin needle-like dendrite [23].

While it is not yet fully understood how the current density affects the formation of dendrite on the anode surface through cycling, it is thought that various inhomogeneity's that already exist in the anode surface can lead to the formations of these structures [23].

2.6.2 Dendrite Growth in Li-O_2 Cells with Ionic Liquid

The potential use of lithium metal as the anode of lithium-ion batteries in order to increase the energy density of the batteries has been investigated for decades. One of issues with battery cells with pure lithium metal anodes is dendrite growth that inhibits electrochemical reversibility as well causing short-circuit issues. The use of ionic liquids as the electrolyte has also been explored for use in both lithium-ion and lithium-oxygen batteries.

The effects of both the ionic mass transfer rate and the electrodeposited surface morphology and how these characteristics affect lithium deposition onto metal was investigated by Nishida et al. 5mm square Ni sheets were used as the working electrode while the "counter" electrode was made of Li metal foils of 200 μm thickness [22]. The lithium dendrite growth was observed using a digital optical microscope and the current densities imposed on the experimental cells ranged from 0.1 to 5.0 mA/cm^2. The results from the study can be seen in Figure 18.

Figure 22 demonstrates the dendrite growth observed based on different current densities. It can clearly be seen that the movement of the dendrites is dependent on the applied current densities with the smaller current densities (<0.5 mA/cm^2) forming long needle-like dendrites [22]. The larger current densities shift the formation of lithium dendrites from needle-like structures to a seaweed-like form. These dendrites do not form right away as these cases present smooth surfaces up to about 300 mC/cm^2. Also worth noting from Figure 22 are the needle-like dendrites appear to form at lower capacities as the discharge current of the battery cell is decreased.

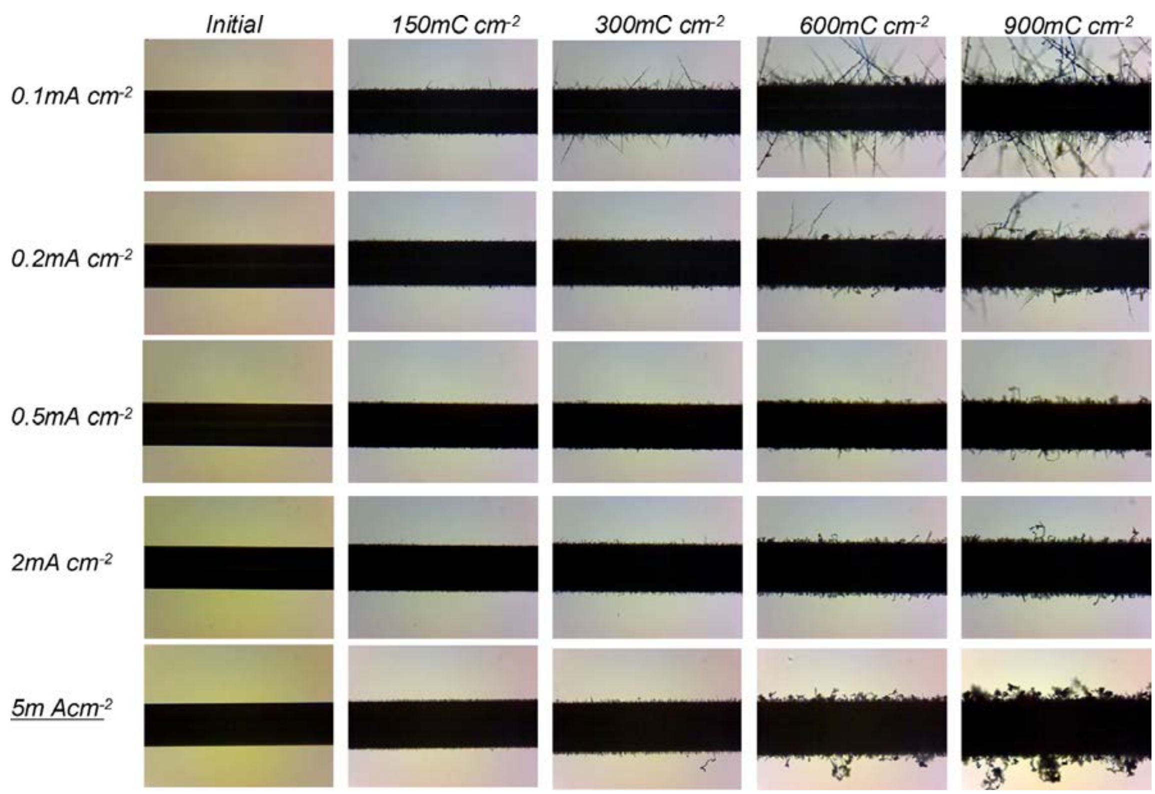

Figure 22: Morphology of Lithium Dendrite Growth at Different Current Densities [22].

2.7 Dendrite Growth and Battery Capacity Loss

The work published by Orsini et al studied the lithium dendrite growth within lithium metal battery cells and the associated capacity loss as the cells were cycled [24]. It is well documented that lithium dendrites grow as the lithium-oxygen batteries are continuously cycled. From the work published by Orsini, the experimental lithium cells experienced a 90% capacity loss as the cells were cycled as few as 25 times [24]. Figure 23 below demonstrates the decrease in capacity of their lithium metal cells as they were continuously cycled, with y-axis representing the normalized cell capacity. The smaller the discharge current density of the cell the smaller the capacity loss [24].

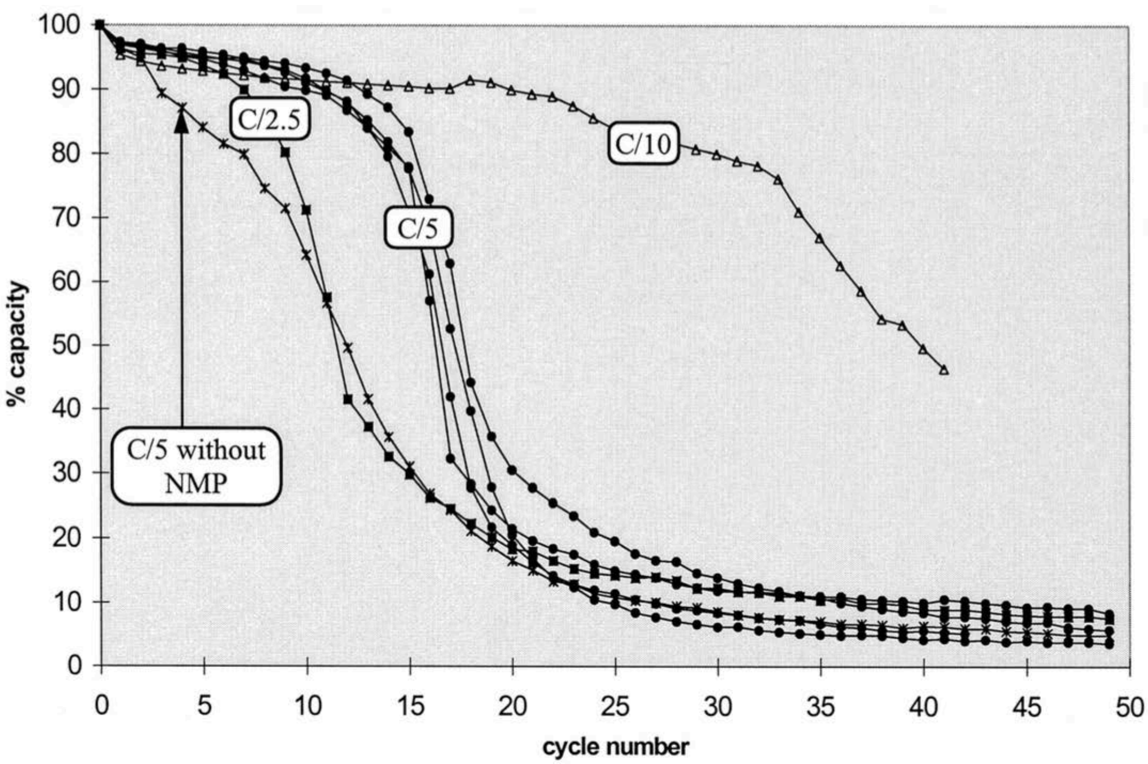

Figure 23: Lithium metal cell capacity vs. cycle number at different cycling rates [24].

The study on lithium metal batteries revealed that the higher discharge current densities of the battery led to larger dendrite formations and deposits [24]. The formation of the mossy, or bush-like, dendrites was shown to be the cause of the rapid deterioration of the lithium-electrolyte interface and led to the rapid decrease in battery cell capacity [24].

2.8 Computational Modeling of Lithium Dendrite Growth

Many papers have been published relating to the modeling of dendrite growth in lithium metal batteries. Monroe et al. published a paper in 2003 that provides a summary relating to dendrite growth in lithium metal systems. They compiled the most relevant research in this field and developed their own comprehensive numerical dendrite growth model. A large part of the model developed by Monroe et al. was based off of modeling work done by Barton and Bockris. Their group developed a dendrite model that made several critical assumptions such as neglecting mechanical and inertial forces, incorporating surface forces to resist infinite dendrite thinning, spherical diffusion dominates linear diffusion, and mass transfer and surface forces dominate kinetics of dendrite growth [11].

Monroe et al. took the assumptions and theories developed by Barton and Bockris, and other groups such as Diggle et al. and Chazalviel et al., in order to produce their own model [25-27]. Based off of the schematic in Figure 24 below, the concentration profile and mass transfer profiles were derived [11].

Through non-dimensionalizing the formulas for the transient diffusion equations for the salt concentration and the boundary conditions of their system, the current density applied at dendrite tips, and dendrite tip velocity were calculated [11].

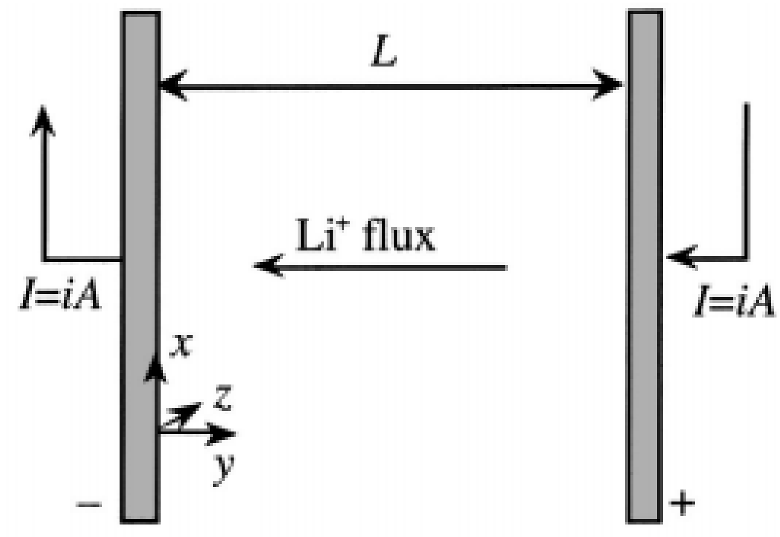

Figure 24: Schematic of System Modeled by Monroe et al. [11].

It is interesting to note that while the methods developed by Monroe et al. are able to model simple dendrite growth within lithium metal systems; several major assumptions had to be made in order to simplify the system. Of the many assumptions made, one was that the diffusion coefficient of lithium was constant throughout the entire system [11]. As explained in the more recent work completed by Tan et al., it can be shown that the diffusion coefficient of the lithium within the system may not be uniform in all cases [12].

When applying modeling to the dendrite growth in lithium-oxygen battery systems, Tan et al. found that a uniform diffusion coefficient was actually able to model the growth of needle-like dendrites well but failed to model the growth of bush-like dendrite growth accurately [12]. The group did find that when the diffusion coefficient was changed to represent a step function, the dendrite growth rates were greater and could represent the growth of bush-like dendrites much better, although this actual comparison was not made [12]. This can be seen in Figure 25 where the lithium concentration as well as the cell potential increases much more rapidly with a step-function diffusion coefficient, leading to much greater dendrite velocities [12].

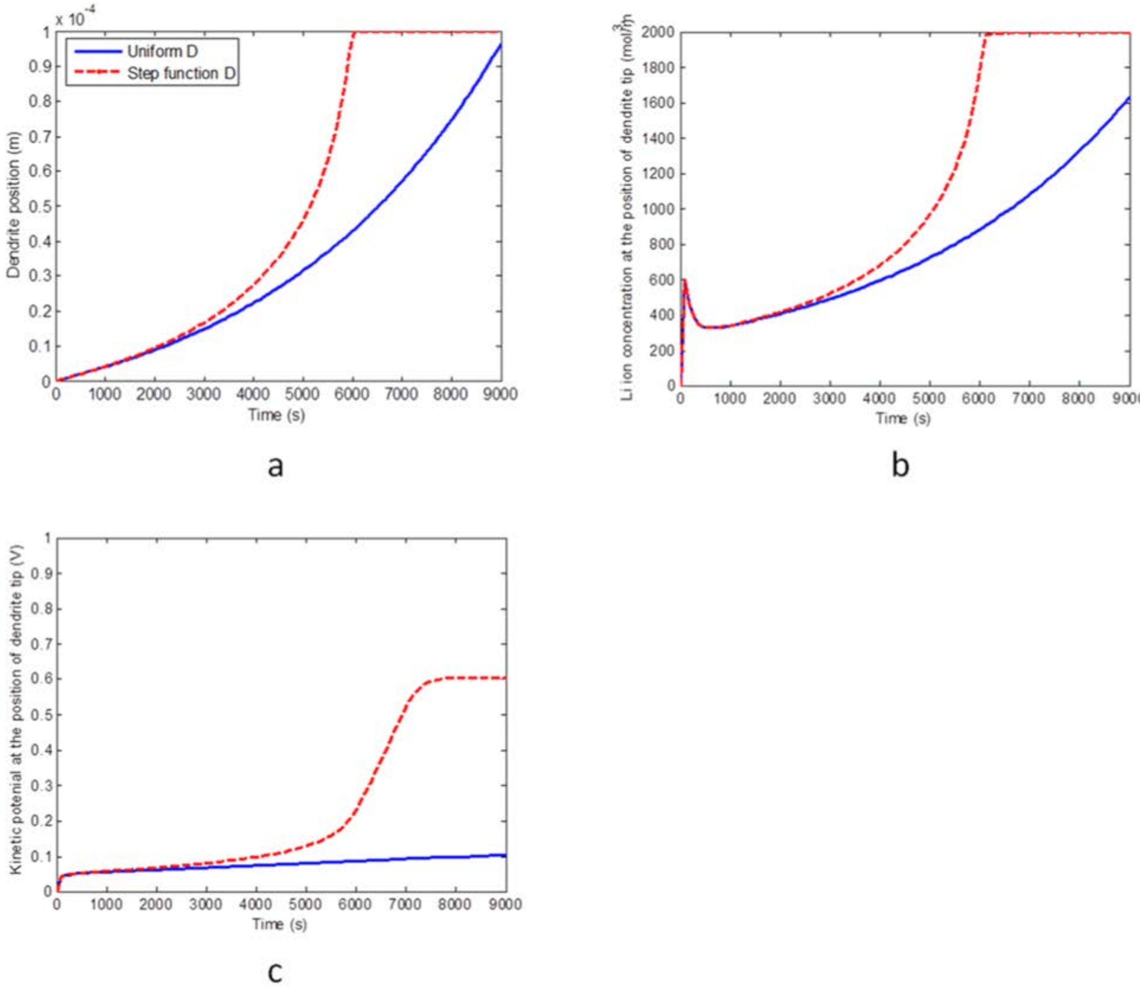

Figure 25: Dendrite Growth with Uniform and Step-Function Diffusion Coefficients (a) Dendrite Position (b) Lithium-ion Concentration at Dendrite Tip (c) Kinetic Potential at Dendrite Tip [12].

Various mathematical models have been developed that do not require some of the assumptions taken by Monroe et al. One of such was developed by Akolkar, using similar boundary conditions and taking into account a concentration dependent diffusion coefficient, developed a lithium-ion transport model and electrochemical reaction model to consider the activation, concentration, and surface curvature overpotentials of the dendrites [28]. Akolkar found that if the concentration of lithium near the dendrite surface is known, then the tip current density can be calculated as a function of the dendrite tip radius [28]. It leads to a much more simple formula to calculate the dendrite tip current density than previously developed.

2.9 Mitigating Dendrite Growth

Other areas that have been explored to mitigate dendrite growth in lithium metal batteries include utilizing the changing battery cell volume through cycling. Jang et al. experiments with different amounts of lithium metal to observe the effects on both the cell capacity and dendrite growth through cycling [29]. With cells ranging from 0.9 mg to 14 mg of lithium metal, it was found that a cell with 0.9 mg of lithium could utilize almost all of the metal anode during discharge before cycling back and depositing on the remaining lithium metal through charging [29]. Each cell was shown to decrease in capacity as the cells were cycled and the smaller the volume of lithium that was available, the smaller the total capacity of the cell [29]. These results can be seen in Figure 26.

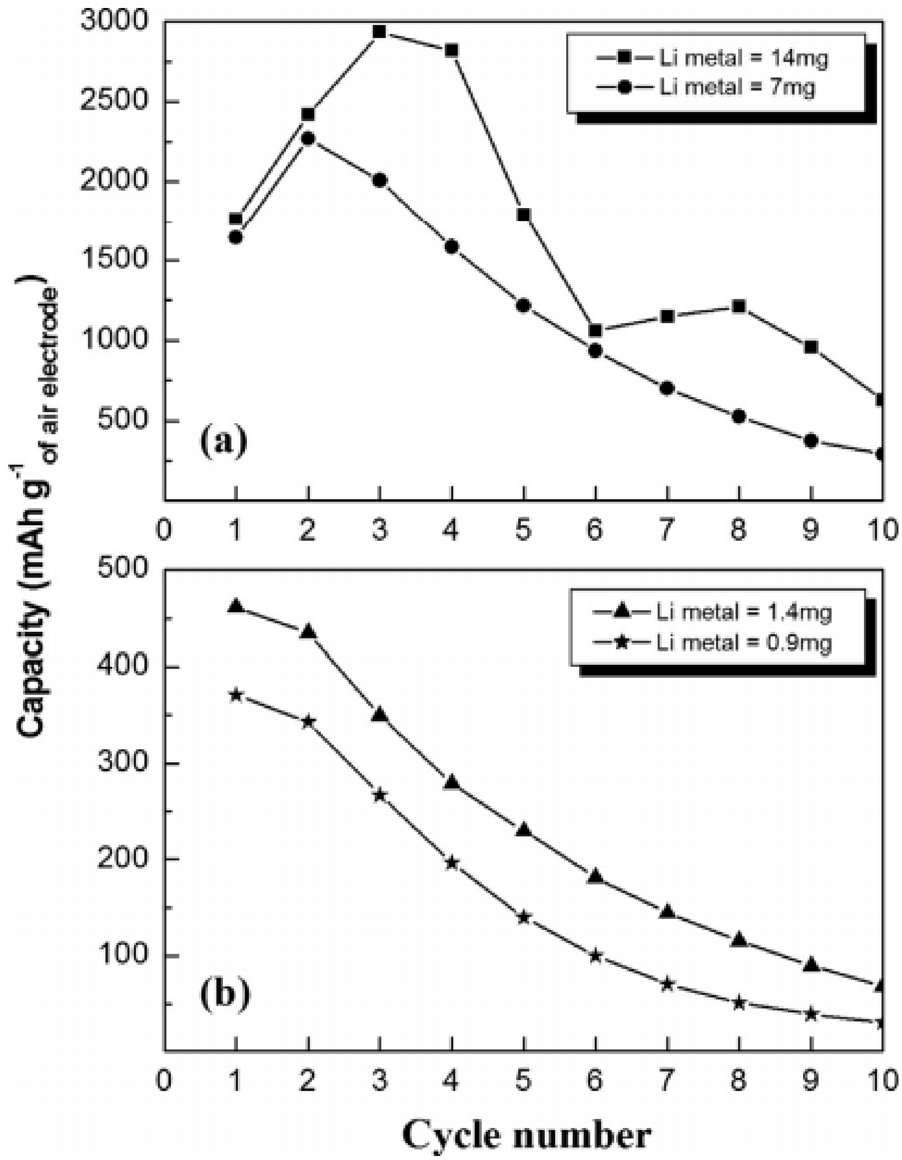

Figure 26: The change in cell capacity as the battery is cycled. Each line represents a different amount of lithium metal used in the initial anode [29].

Although it may be counterintuitive, as the amount of lithium in the anode was increased the anode became more porous and experienced more dendrite growth through cycling when compared to the cells with less lithium [29]. It can be seen in Figure 27 where the anode surfaces of three different anodes are shown. Figure 27c shows a more porous and rough anode surface after cycling due to the greater amounts of lithium used in the anode.

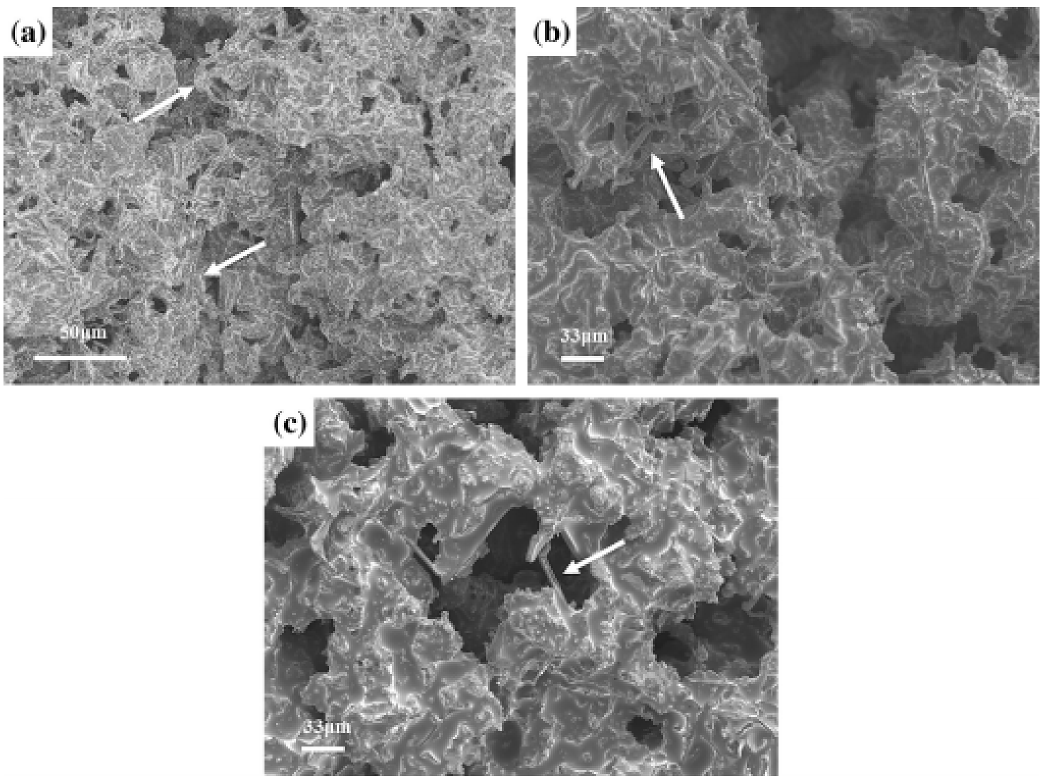

Figure 27: Images using SEM technique of Li-O_2 anode surface after 10 cycles (a) Li = 0.9 mg (b) Li = 7 mg (c) Li = 14 mg [29].

Figure 28 portrays a step-by-step process of the “self-healing” shield developed through experiment. In the first diagram (Figure 28a), both lithium and the cation additive begin to deposit onto the surface of lithium metal through charging. It is important to note that charging voltage in this case must be slightly lower than the lithium reduction potential but higher than the cation reduction potential. Figure 28b shows the beginning of the formation of a protuberant tip of lithium on the lithium metal, which as stated previously, will continue to grow due to the higher electric field of the protrusion.

As the lithium-protrusion (dendrite) continues to grow, the cation additives will begin to “accumulate around the tip to form an electrostatic shield” due to their smaller reduction potential (Figure 28c and 28d). Because of their positive charge, this electrostatic shield from the cations will drive the lithium ions to deposit in the surrounding regions of the lithium metal (Figure 28e) until a smooth surface is once again formed on the lithium metal (Figure 28f).

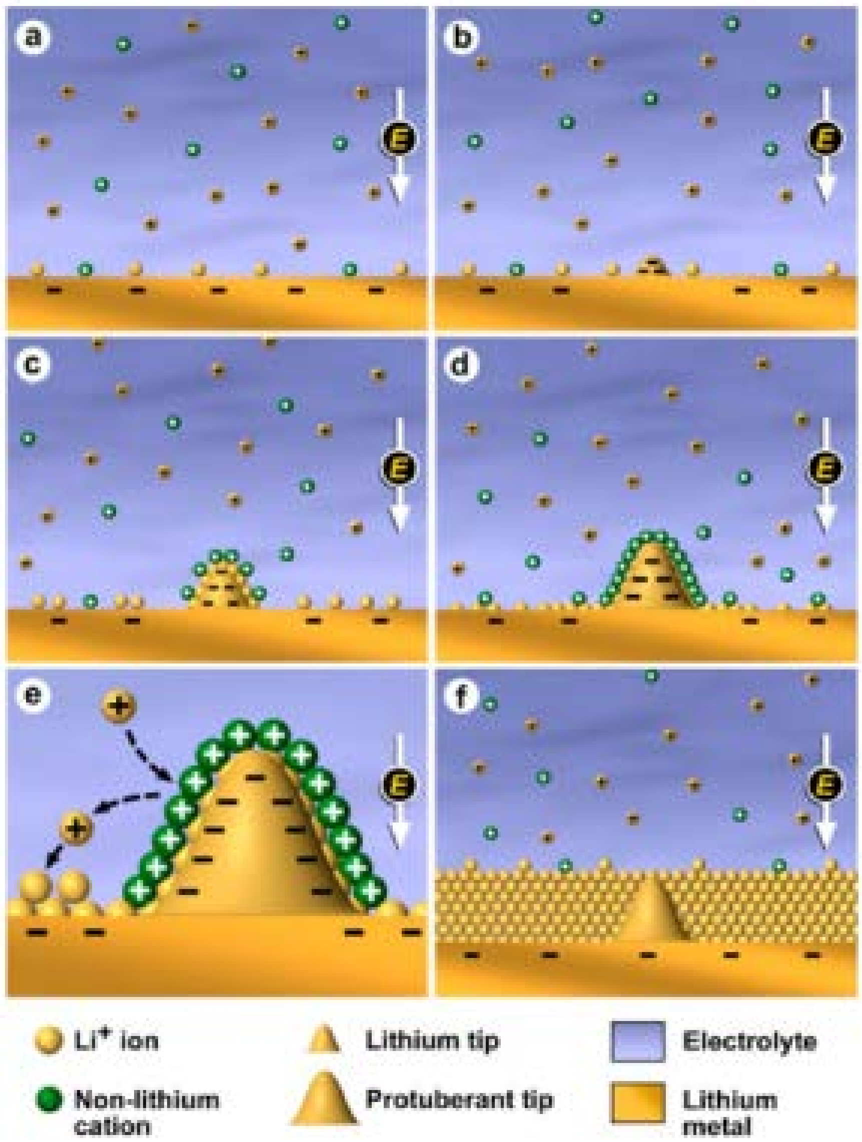

Figure 28: Lithium Deposition Process through “self-healing process” [21].

CHAPTER 3: MODEL DEVELOPMENT

We are hopeful that a better understanding of the operating mechanisms of the lithium-oxygen cell can be obtained by studying the effects of the anode and cathode together through a finite element model. The goal is to construct three different models within ANSYS Fluent with different anode surface structures – one smooth/homogeneous and two differing anode surface structures reflecting lithium dendrite growth.

3.1 Fuel-Cell Module Theory

The Fuel-Cell Module will be used within ANSYS Fluent due to the ability to model chemical reactions that can be modified to reflect the well-known reactions of a lithium-oxygen cell shown below in equation 2.

$$O_2 + 2e^- + 2Li^+ \longleftrightarrow Li_2O_2 \tag{2}$$

The Fluent Fuel-Cell module solves two potential equations shown in equations 3 and 4 as the driving force for the reactions lies in the cell overpotential. Equation 3 represents the potential equation for the electron transport through the anode while equation 4 solves for the protonic transport of species transport [30].

$$\nabla * (\sigma_{sol} \nabla \phi_{sol}) + R_{sol} = 0 \tag{3}$$

$$\nabla * (\sigma_{mem} \nabla \phi_{mem}) + R_{mem} = 0 \tag{4}$$

Further, the volumetric transfer current (R) are computed through the Butler-Volmer and Tafel equations shown in equations 5 and 6 [30]. Table 3 below demonstrates the constants and parameters taken from the ANSYS manual [30].

$$\mathrm{R}_{an} = \zeta_{an} j_{an}^{ref} * \left(\frac{[\mathrm{A}]}{[\mathrm{A}_{ref}]}\right)^{\gamma_{an}} * \left(e^{\frac{\alpha_{an} \mathrm{F} \eta_{an}}{\mathrm{RT}}} - e^{\frac{\alpha_{cat} \mathrm{F} \eta_{an}}{\mathrm{RT}}}\right) \tag{5}$$

$$\mathrm{R}_{cat} = \zeta_{cat} j_{cat}^{ref} * \left(\frac{[\mathrm{C}]}{[\mathrm{C}_{ref}]}\right)^{\gamma_{an}} * \left(e^{\frac{\alpha_{cat} \mathrm{F} \eta_{cat}}{\mathrm{RT}}} - e^{\frac{\alpha_{cat} \mathrm{F} \eta_{an}}{\mathrm{RT}}}\right) \tag{6}$$

Table 3: Formula Constants and Parameters of Butler-Volmer Formulas [30]

j	reference exchange current density per active surface area (A/m^2)
ζ	specific active surface area (1/m)
[],[]ref	local species concentration, reference value (kmol/m^3)
γ	concentration dependence
α	transfer coefficient (dimensionless)
F	Faraday Constant

Constructing a finite element model of the lithium-oxygen cell gives the benefit of adjusting parameters such as electrode porosity, oxygen diffusivity, and mass flow rates through potentiostatic or galvanostatic discharge. Examining these cell and experimental characteristics with the different anode surface structures gives us the ability to make observations that may be difficult to conduct through pure experimental work.

Below in Figure 29 is the schematic of the PEMFC fuel cell used in the fuel cell module. Using this schematic, the lithium-oxygen battery models were constructed.

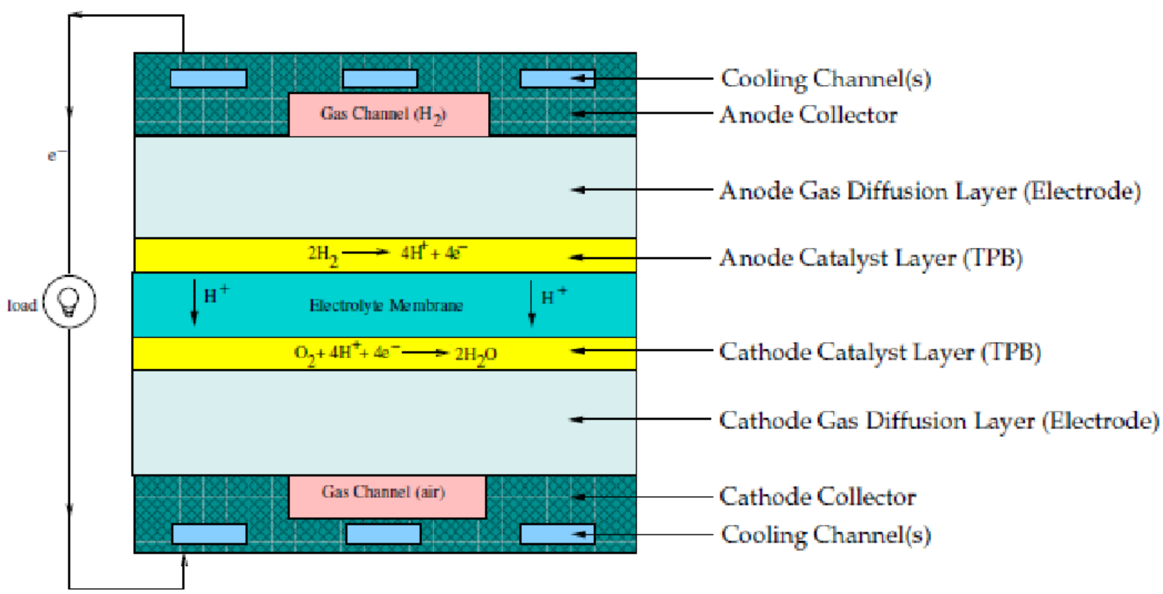

Figure 29: Schematic of PEM Fuel Cell for Fluent Fuel Cell Module [30].

3.2 Model Construction and Parameters

In order to customize the fuel cell module within Fluent to model the reaction of a lithium oxygen battery, we will input the different properties of lithium, lithium peroxide, and oxygen in exchange for the properties of H_2O and hydrogen. A cell will then be drawn with the same dimensions seen in the literature previously discussed with different models to reflect different anode surfaces [31, 32]. Our goal is to observe how the effects of different anode surfaces (and other cell properties) affect the discharge capacity, voltage, species concentration, and other characteristics to get a better understanding of how the entire cell operates. The current dimensions of the model can be seen in Figure 30 and 31 below.

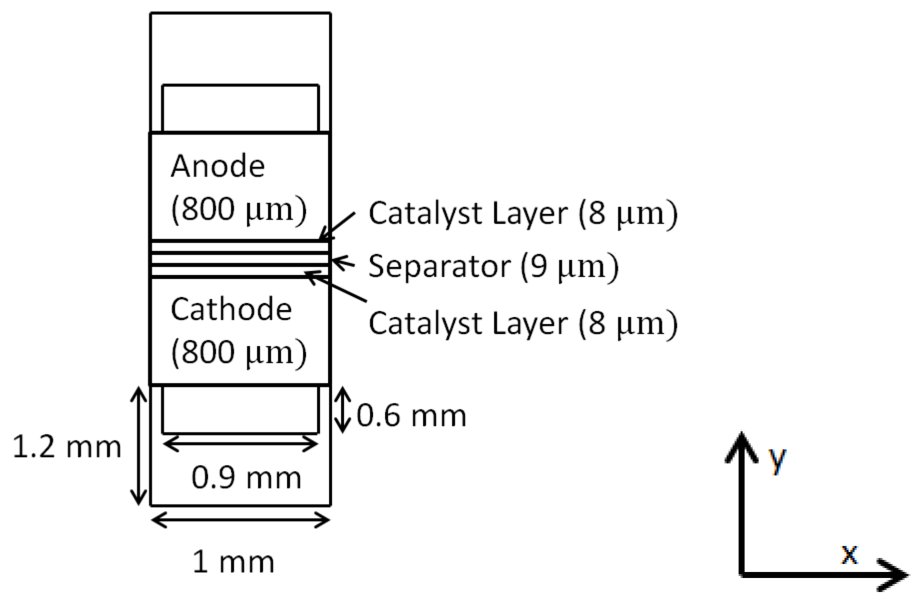

Figure 30: Schematic of x-y plane of lithium-oxygen cell with flat, homogeneous anode surface(not drawn to scale).

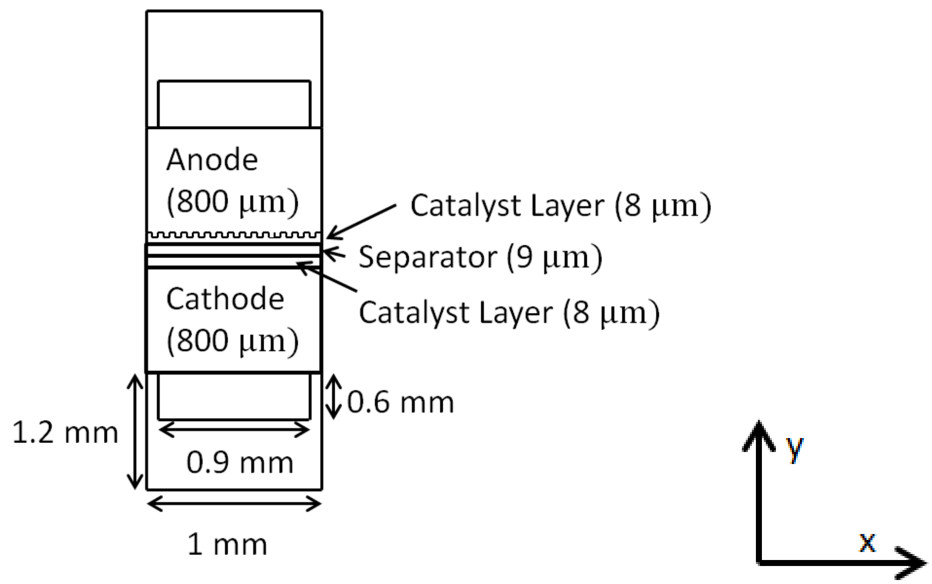

Figure 31: Schematic of x-y plane of lithium-oxygen cell with small dendrites on lithium metal surface (not drawn to scale).

One of the apparent differences between our lithium-oxygen cell models and the PEMFC fuel cell model is the considerably wider gas channels of our models. These are adjusted to span nearly the entire length of the electrodes to ensure an even distribution of lithium and oxygen in the x-direction of the electrodes.

Table 4 below represents the properties of lithium, oxygen, and lithium peroxide used in the model. It is important to note that the molecular weight of lithium in Table 4 is the actual molecular weight of 6.94 kg/kmol. Our model uses a molecular weight of 13.88 kg/kmol to represent Li_2 rather than a single Li. With the 13.88 kg/kmol we can use an accurate molecular weight for Li_2O_2.

Table 4: Material Properties of Lithium-Oxygen Battery Reactants

Property	Units	Lithium	Oxygen	Lithium Peroxide
Thermal Conductivity [32, 33]	W/m*K	85	0.0246	14.5
Viscosity	kg/m*s	8.41E-06	1.92E-05	1.34E-05
Molecular Weight [32]	kg/kmol	6.94	31.9988	45.88
Electrical Conductivity [32, 34]	1/ohm*m	1.1E+7	1.00E-16	5E-18

Table 5 below portrays the operating parameters of the lithium-oxygen battery models. Many of these values were taken from the values given by Li et al. to ensure realistic battery behaviors [32].

Table 5: Default Operating Parameters of Lithium-Oxygen Model

Parameter	Value	Units
Anode Ref. Current Density	3.11	A/m^2
Cathode Ref. Current Density	3.11	A/m^2
Diffusivity of Li	8E-11	m^2/s
Diffusivity of O_2	1E-09	m^2/s
Diffusivity of Li_2O_2	0.00001	m^2/s
Open Circuit Voltage	2.8	V

It is important to note that the diffusivity values of the different species were adjusted so the computational model could better converge. The values portrayed in Table 5 are actual values taken from Li [32]. The diffusivities in the model are larger but the differences in diffusivities remain the same in magnitude. The diffusivity of species used in the model is as follows: O_2: $1e^{-2}$, Li: $8e^{-4}$, Li_2O_2: $1e^{-6}$ m^2/s. The difference in magnitudes comes from the values of Li et al [32].

Several cell parameters were adjusted and the discharge properties compared. The current vs. voltage curves (*i.e.*, I-V curves) of the various cells as well as contour plots of the Li_2O_2 precipitate concentrations within the cathode were all compared. The operating parameters adjusted were listed previously in Table 2.

Potentiostatic calculations are carried out, where the discharge voltage is set for each separate calculation and the discharge current, contour plots for Li_2O_2 formation, and kMol of Li_2O_2 precipitate formation are recorded before another calculation at a different discharge voltage is carried out. With the open circuit voltage of the cell being 2.8 V, the cell was discharged from 2.75 V and decreased until cellular failure, typically around 2.6 V [18].

CHAPTER 4: SIMULATION RESULTS

With the model setup within Fluent, calculations were carried out to better understand the discharge behaviors of lithium-oxygen batteries. Several sections below discuss the observed parameters and their resulting calculations. The contour plots shown below demonstrate the varying distributions of lithium peroxide (Li_2O_2) within the cathode after discharge of the cell.

4.1 Flat Anode vs. Small Dendrite Model

The first set of calculations compared the flat anode model with the model with 4 µm long dendrites. Both models were discharged with a cathode porosity of 0.75, which is suggested from the literature [32]. As expected, the dendrite-free model performed better than the dendrite model when comparing the I-V curves, the amount of discharge product within the cathode, and when comparing a 2D contour plot of Li_2O_2 formation. The decrease in performance is due to the dendrites on the anode surface. In a true experimental setup, these dendrites increase in size as the cell is continuously cycled and the performance of the cell declines, suggesting the dendrite formations negatively affect the performance of the cell.

The plot in Figure 32 below represents the I-V curves of two different lithium-oxygen battery cells. The flat anode model, represented with the red squares, portrays a better performing cell as the discharge current does not drop as quickly as the dendrite model when the discharge voltage is lowered from 2.75 V to 2.6 V.

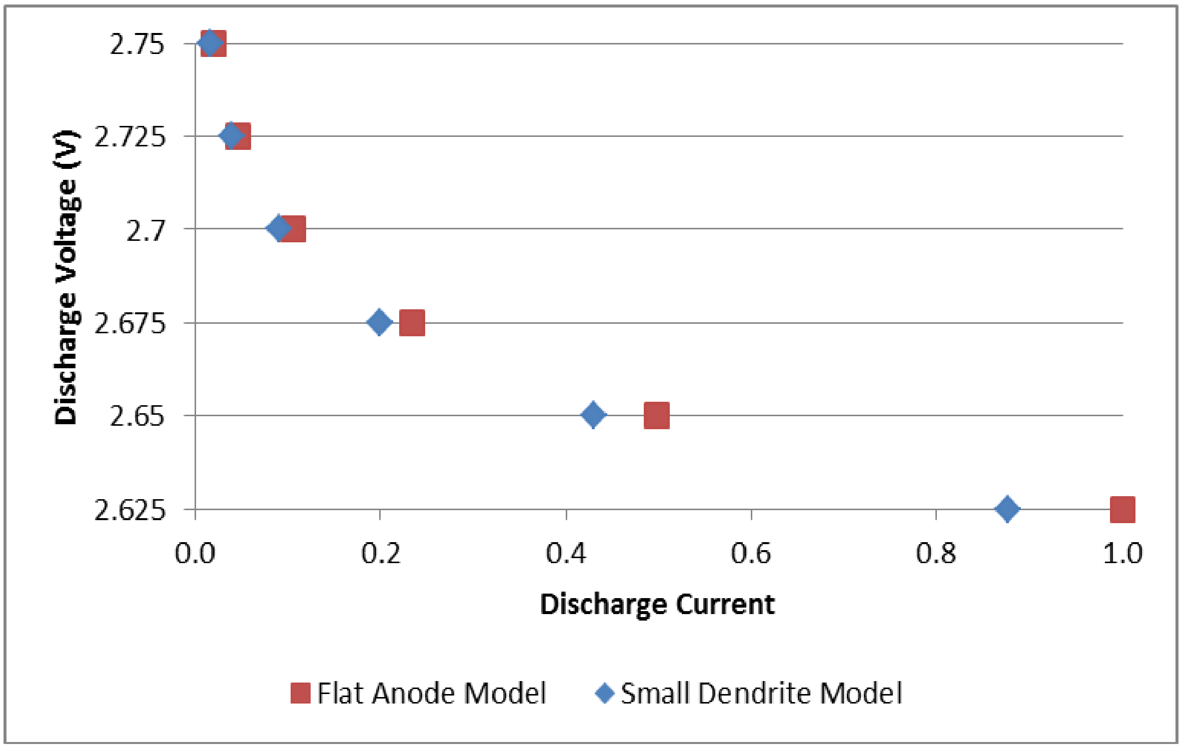

Figure 32: Normalized I-V Curve of Flat and Small Dendrite Models. The Flat model portrays a better performing cell since the discharge voltage does not fall as quickly as the dendrite model when the discharge voltage is lowered to 2.6 V.

The plot below in Figure 33 represents the normalized amount of Li_2O_2 formation within the cathode of the cell as the discharge voltage is decreased. The plot shows that as both cells are discharged and the cell voltage decreases, the amount of discharge product increases. It is again apparent that the flat anode model displays a better performing cell with a higher capacity (where the amount of discharge product formed is assumed to be analogous to cell capacity). At the conclusion of discharge, the flat anode model demonstrated nearly four times the amount of Li_2O_2 formation within the cathode as the small dendrite model.

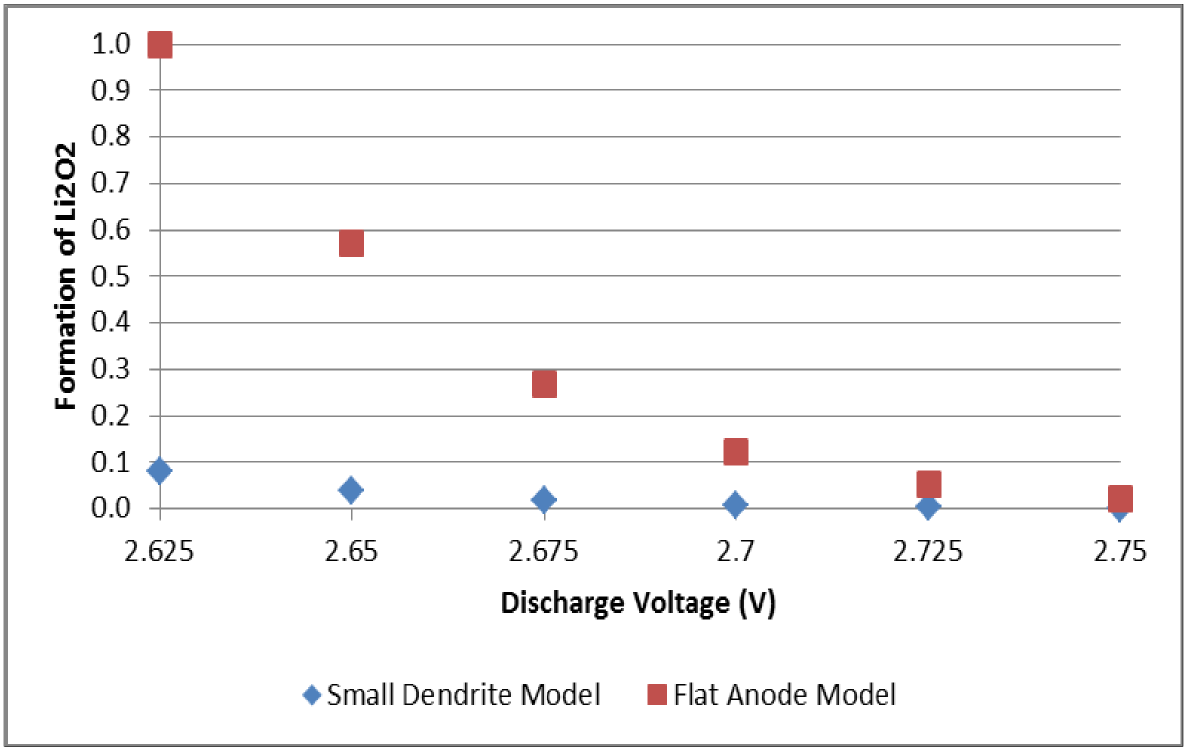

Figure 33: Normalized kMol of Li_2O_2 Formation of Flat and Small Dendrite Models. The lower the discharge voltage, the greater the kMol of Li_2O_2 formed.

The contour plots shown below show the distribution of Li_2O_2 wthin the cathode of the lithium-oxygen cell. Each plot shows the highest concentraiton of lithium peroxide forming close to the separator [10]. From the plots in Figure 34 and Figure 35 below, it is apparent that the Li_2O_2 formation utilizes more of the cathode with the flat model when compared to the dendrite model. The contour plots support the observations made from Figure 33 as the flat anode model utilizes a larger portion of the cathode and therefor demonstrates a higher capacity and larger amount of Li_2O_2 formation. Figure 34 demonstrates the contour plots at discharge voltages of 2.75 V and 2.70 V. Figure 35 shows the contour plots at discharge voltages of 2.65 V and 2.60 V.

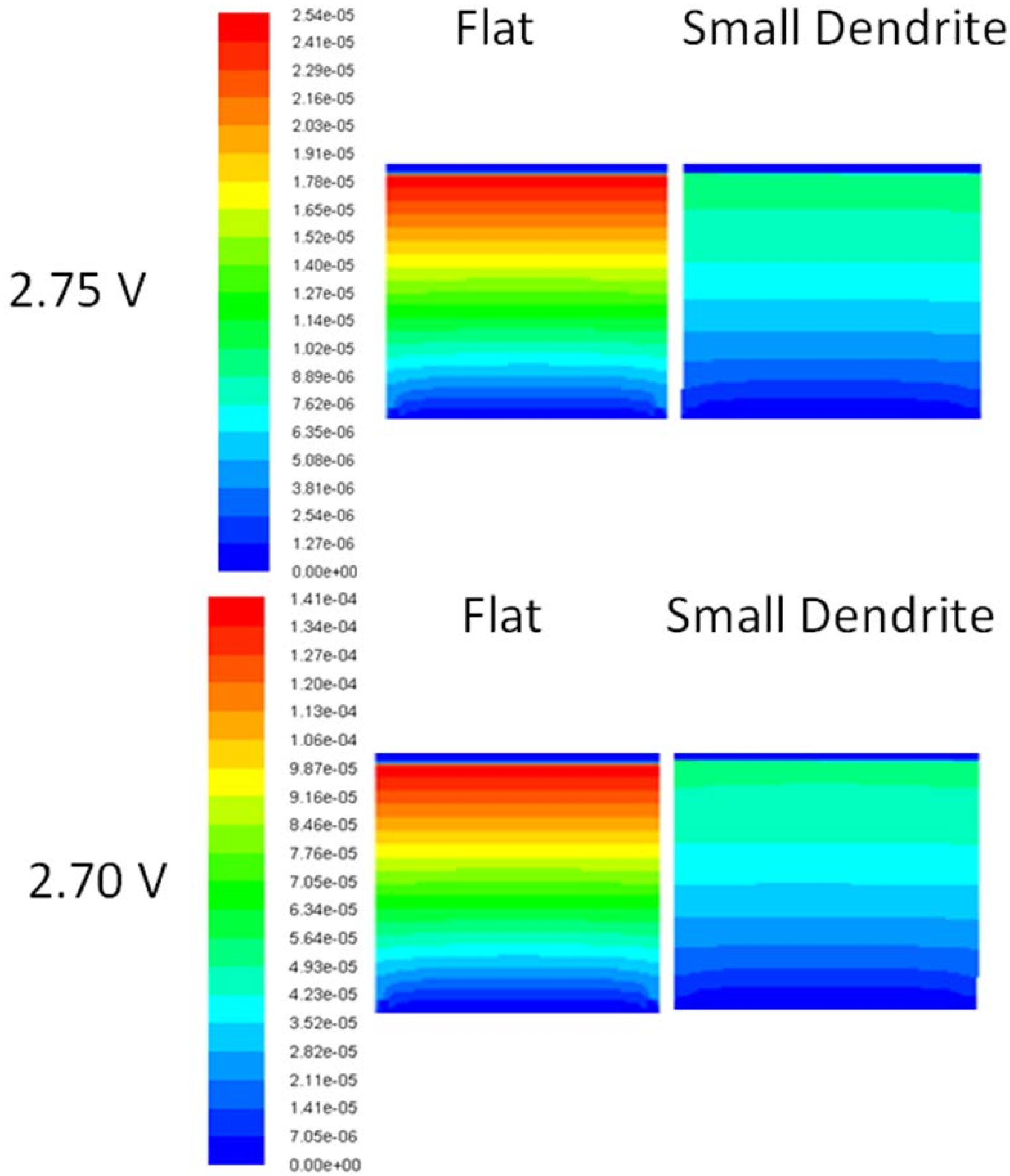

Figure 34: Contour Plots of Flat and Small Dendrite Models at 2.75 V and 2.70 V

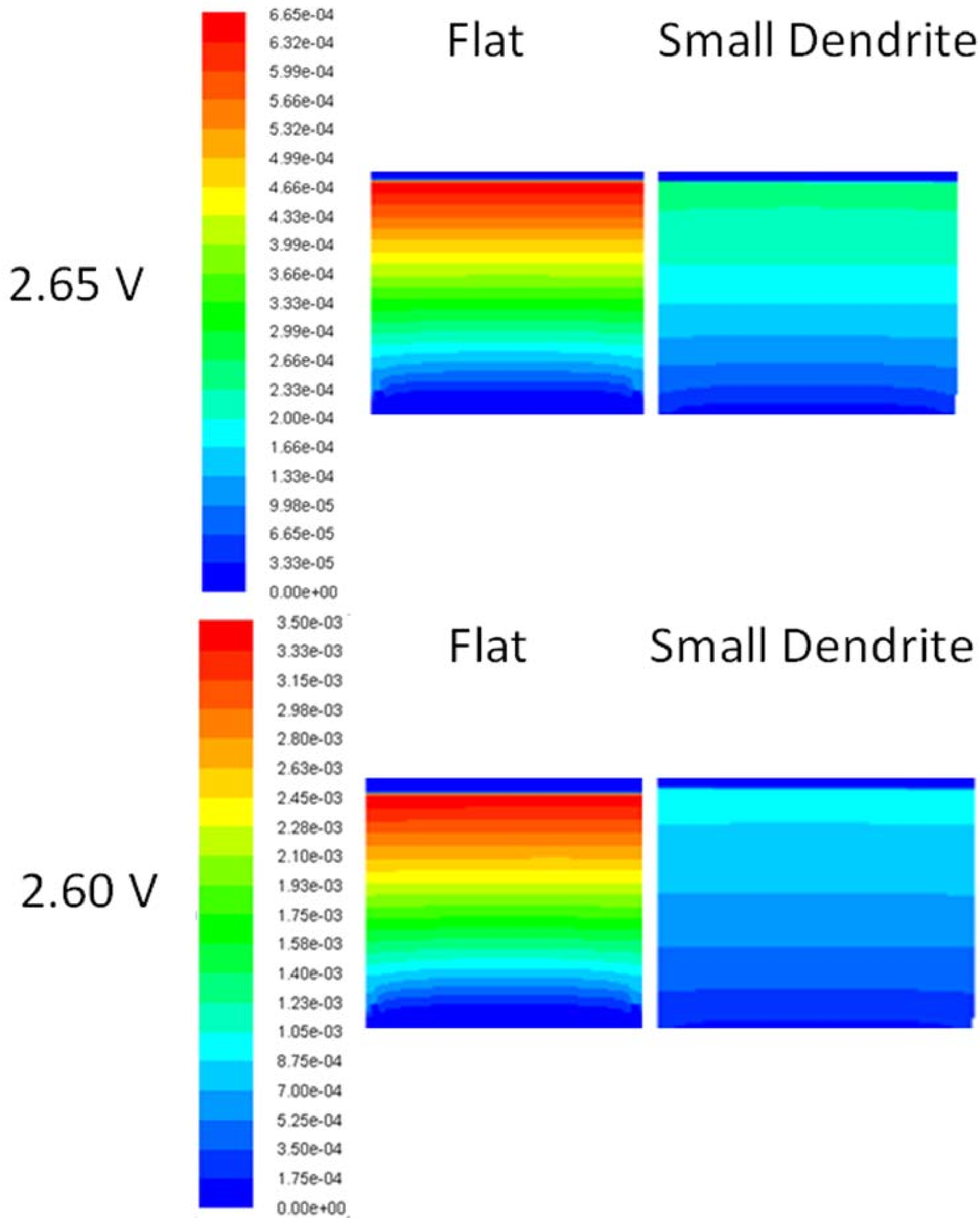

Figure 35: Contour Plots of Flat and Small Dendrite Models at 2.65 V and 2.60 V

4.2 Comparisons of Flat Anode, Small Dendrite, and Long Dendrite Models

It is easy to see in the previous section that the lithium-oxygen cell with a perfectly homogeneous anode surface performs much better than the cell that has theroetically been cycled enough times to begin lithium dendrite growth. The next comparison takes the results of the previous section and compared them to the third model that was constructed, the long dendrite model. The long dendrite model (12.5 μm) resembles a battery cell that has been cycled enough times to grow dendrite structures that pertrude halfway through the separator of the anode and cathode structures.

Through running our models it is easy to see that the long dendrite model's trends fall in line with the decrease in performance compared to both the small densrite model and the flat anode surface model. This can be seen in Figure 36 below where the polarization curve of the three models are compared. As the discharge voltage was decreased, the long dendrite model experienced nearly a 40% decrease in discharge current when compared to the flat anode model.

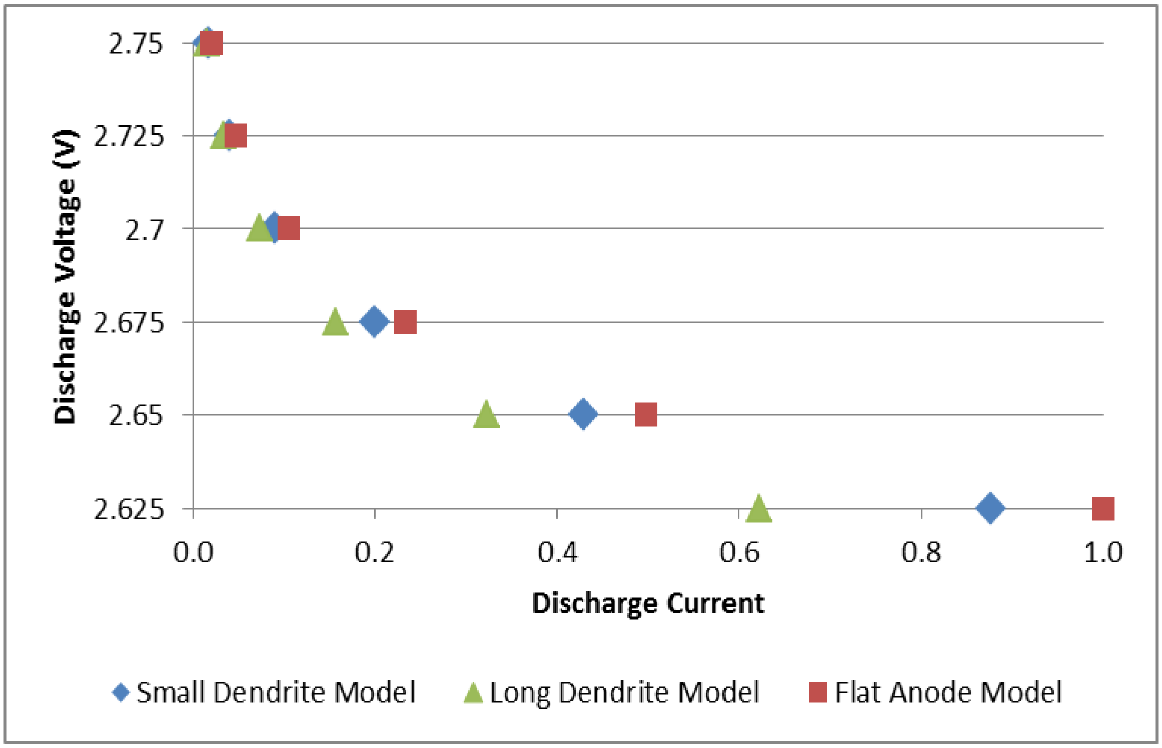

Figure 36: I-V curve of flat, small, and long dendrite models at a cathode porosity of 0.75. As the dendrites grew to represent a cell that had been continuously cycled, the discharge current of the cell greatly decreased.

A comparison was made of the different amounts of Li_2O_2 forming within the cathode of the three different models as well. Similar to the previous study, the amount of Li_2O_2 formation of the long dendrite model greatly dropped off when compared to the flat anode model. From the appearance of Figure 37, the amount of Li_2O_2 of the long dendrite model appears slightly smaller than the small dendrite model. Due to the scale and normalization based on the flat anode model, the two dendrite models are compared closely in the following section.

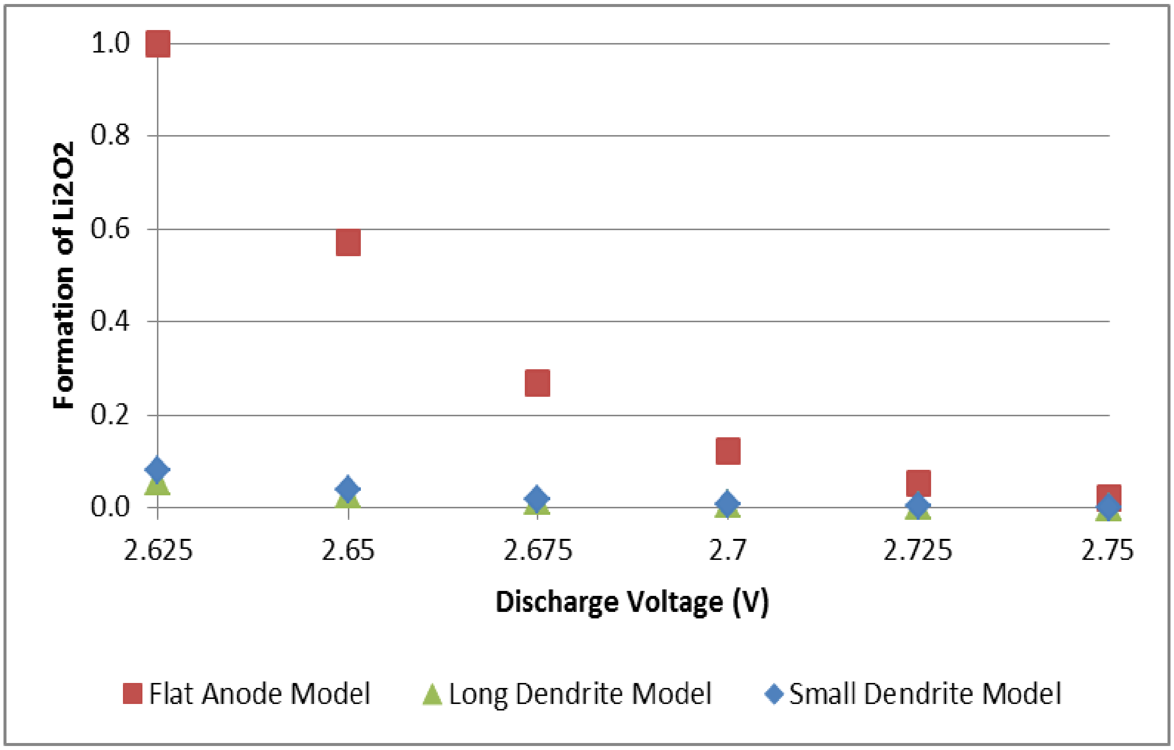

Figure 37: Normalized kMol of Li_2O_2 Formation of Flat, Small, and Long Dendrite Models at cathode porosity of.75. The lower the discharge voltage, the greater the kMol of Li_2O_2 formed.

Figure 38 below demonstrates the amount of discharge product further with the comparison of Li_2O_2 formation within the cathode of the three different models as the cells are discharged. A porosity of 0.75 was used for each model. It is clear to see that when compared to the flat anode model, the battery cells that have theoretically been cycled enough for dendrites to grow on the anode portray a significant decrease in discharge product within the cathode. It is also easy to see that the amount of Li_2O_2 formed within the cathode of the dendrite models are closer in magnitude than the dendrite models compared to the flat anode model.

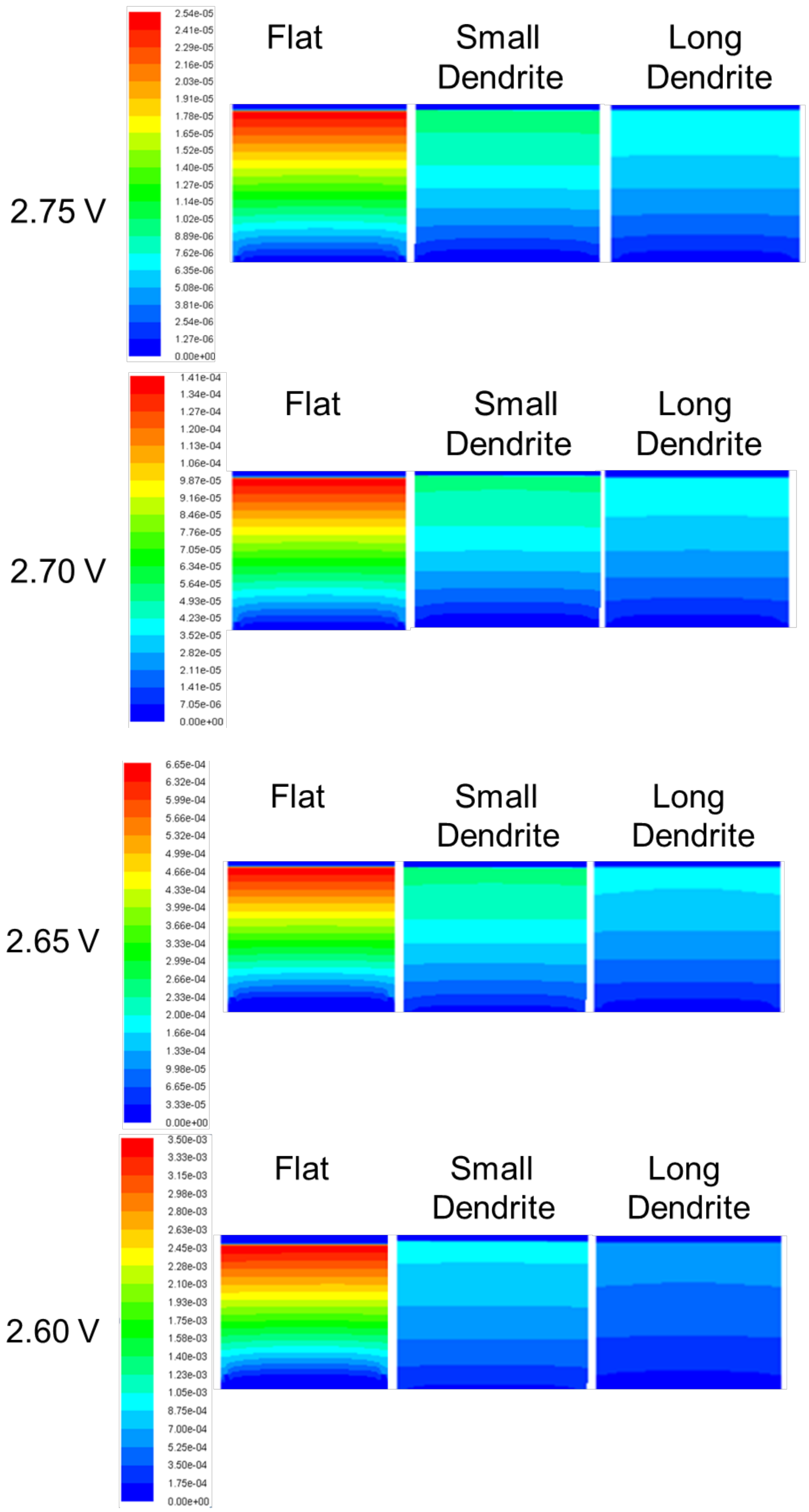

Figure 38: Contour plots of the formation of Li_2O_2 within the cathode of the three different anode models at different discharge voltages. Note the depth of discharge of the flat anode as well as total amount of Li_2O_2 formed is much greater.

4.3 Small Dendrite Model vs. Long Dendrite Model

Form the results of the previous section it is obvious to see that as the dendrites grow on the anode surface of the lithium-oxygen cell, the performance of the battery decreases. The difference in performance is further examined in this section. Figure 39 below portrays the polarization curve of the two dendrite models. It can be seen that the discharge current of the long dendrite model is over 30% lower than the discharge current of the small dendrite model (i.e., 4 μm). Using discharge current values that are normalized based off of the small dendrite model, it is obvious to see the performance drop significantly as the cell is cycled and the lithium dendrite grow.

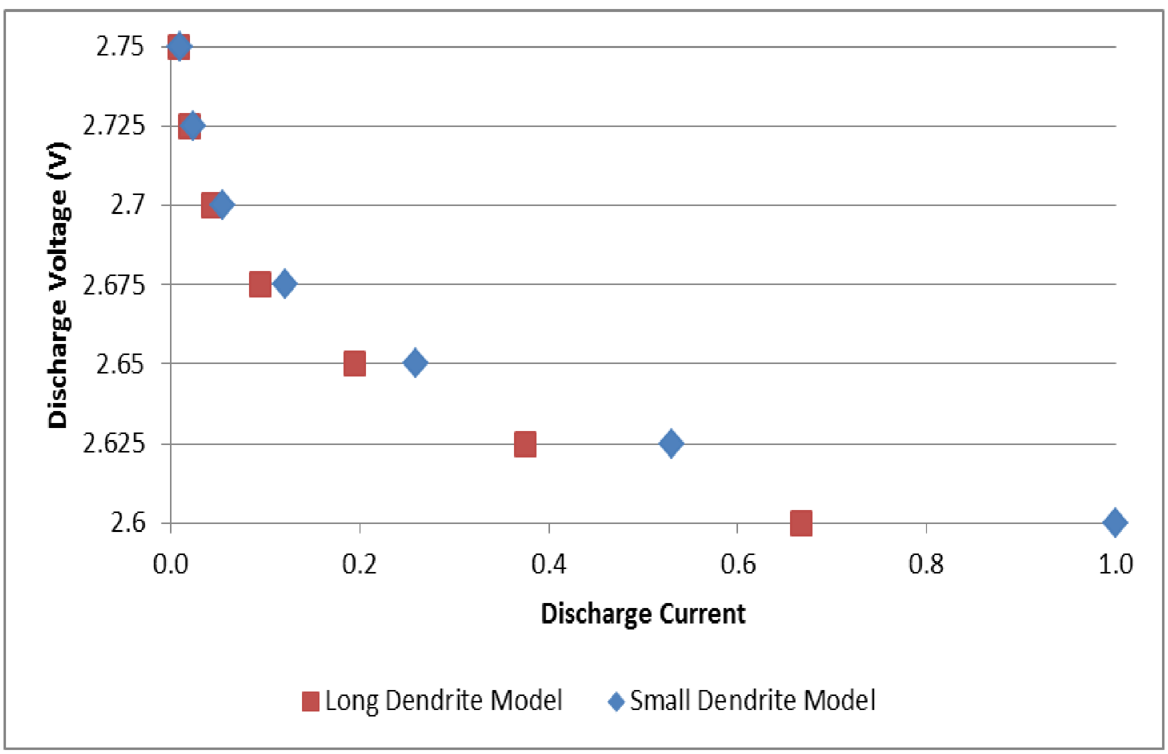

Figure 39: I-V Curve of the long dendrite and small dendrite models. A porosity of 0.75 was used for each model. The discharge current was normalized based on the values of the small dendrite model.

Figure 40 portrays the amount of discharge product forming in the cathode of the dendrite models. As discussed in the previous section, the amount of discharge product decreases as the dendrites grow longer but it is easier to see in this plot that the amount of Li_2O_2 formed within the cathode decreases significantly. The long dendrite model shows a decrease of 35% in discharge product, suggesting a significant drop in cell capacity.

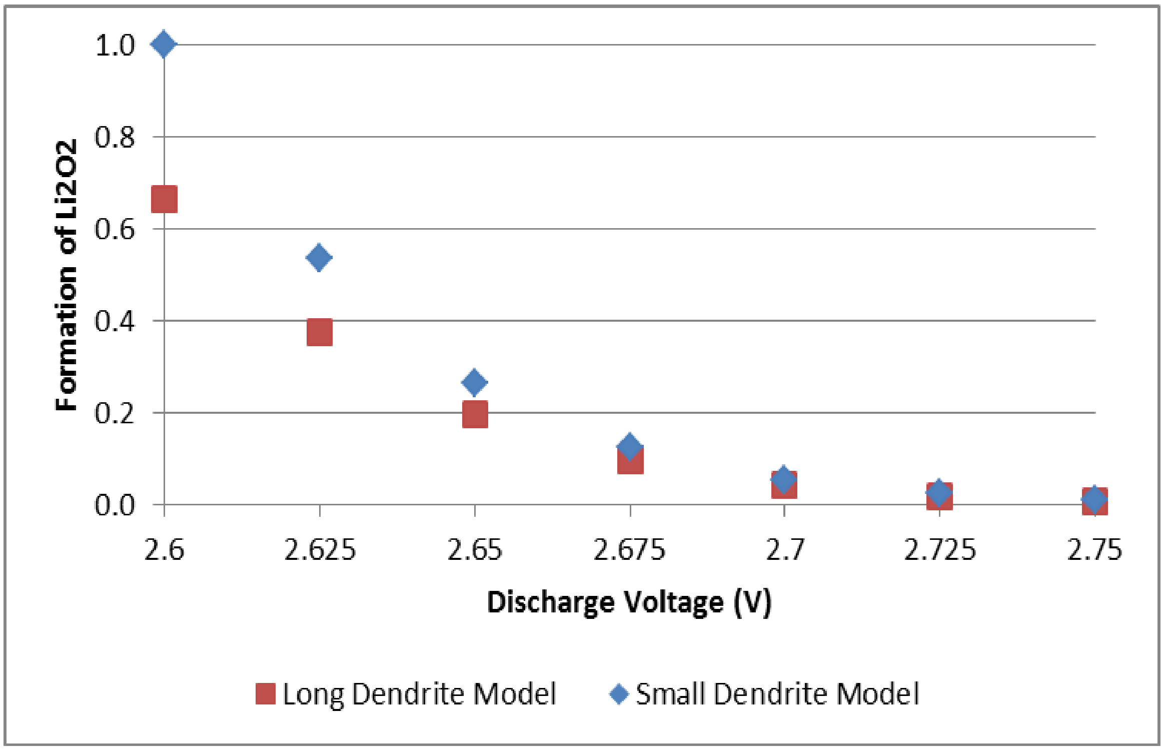

Figure 40: Amount of discharge product forming in the cathode of the dendrite models. A cathode porosity of 0.75 was used. The formation of Li_2O_2 was normalized based on the values of the small dendrite model.

Figure 41 portrays the contour plots of the formation of Li_2O_2 of the dendrite models. Since the scales of the plots are adjusted in Figure 41, it is easier to tell the difference between the models as the discharge voltage is decreased from 2.75 V to 2.60 V. From these plots, the depth of discharge can be seen to decrease as well as the total amount of Li_2O_2 formed within the cathode decreasing. Similar to the discussion in the previous section, the closer to perfect homogeneity the anode surface is, the better performing the cell and more Li_2O_2 with a higher capacity.

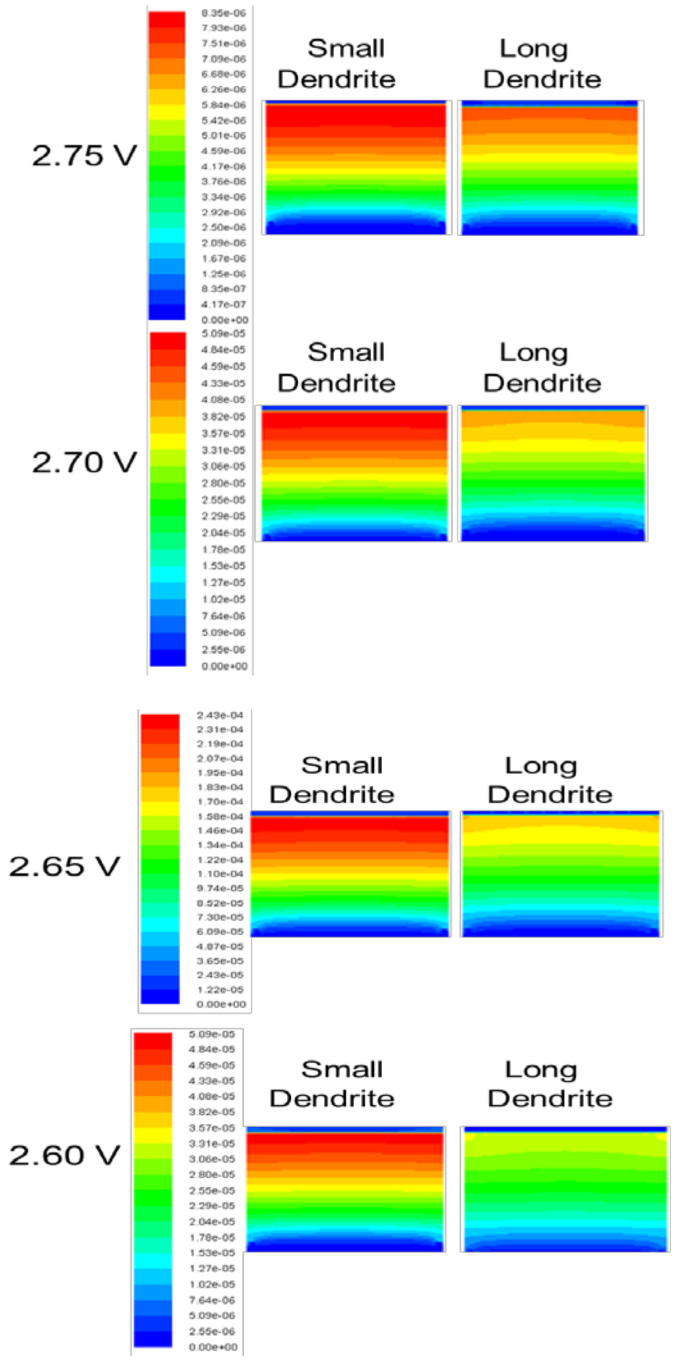

Figure 41: Contour plots of the two dendrite models. A cathode porosity of 0.75 was used. The scaling of the images shows a much higher depth of discharge in comparison to the previous contour plots in Figure 38. The total cathode utilization of the small dendrite model was much greater than the long dendrite model's utilization.

4.4 Capacity Loss – Experimental Results vs. Computational Modeling

The theoretical capacity of the lithium-oxygen models and the associated loss of capacity with dendrite growth can be compared to the experimental work published by Orsini et al. As discussed previously in the literature review, Orsini found that as their lithium metal cells continuously cycled, dendrite growth occurred on the surface of their metal anodes [24]. As their cells were continuously cycled, the bush-like dendrites grew and the capacity of their cells greatly decreased. The decrease in capacity was amplified as the discharge current density increased [24]. As previously shown in Figure 23, the capacity of the lithium metal cells (C/2.5 and C/5 cells) decreased by 80-90%% when cycled only 25 times. The decrease in cell capacity started to flatten out after the initial steep decrease in cell capacity [24].

The results generated from our computational models presented in section 4.2 have a similar quantitatively decrease in the capacity as reported experimentally from Orsini et al [24]. Our flat anode model represents a fresh lithium-oxygen cell that has yet to be cycled with 100% capacity. Our first dendrite model with dendrites that have grown to a length of 4 μm, found that the total amount of Li_2O_2 formed within the cathode had decreased by about 90%. Next, our cell with dendrite structures with a length of 12.5 μm showed a decrease of about 30% in Li_2O_2 formation from the small dendrite model and 93% compare to the fresh anode model.

Our computational results fall in line with the decrease in capacity presented by Orsini et al. where the onset of dendrite growth sparks a large decrease in cell capacity and the continuous cycling of the cells results in a more gradual decrease in capacity. Finally, the dendrite structures in our models represent the bush-like dendrites that are commonly seen in cells with a greater discharge current density, where these effects are again amplified.

4.5 Cathode Porosity Effect on Discharge Properties

One of the common design parameters when assembling a lithium-oxygen battery cell is in the porosity of the carbon cathode. This section closely examines the effects of varying cathode porosities on the discharge characteristics of our computational cells.

4.5.1 Adjusting Cathode Porosity – Flat and Small Dendrite Models

The porosities of the cathode were adjusted to investigate the effects of decreasing electrode porosity on the discharge characterisitcs of the lithium-oxygen cell. As discussed by Tran et al., the porosity of the cathode can greatly affect the performance of the cell [9, 14]. Porosites of 0.75, 0.5, and 0.25 were investigated for the flat and small dendrite models, and the I-V curves, concentration of Li_2O_2 formation, and contour plots were generated as discussed below.

The polarization curve (*i.e.*, I-V curves) below demonstrates similar phenomonon that the flat anode models portray a better performing cell than the small dendrite models. It is interesting to point out that the I-V curves of the models at different porosities are the same. In both cases, all of the calculations for the flat and small dendrite models reveal the same I-V plots at different cathode porosities. It could be due to the fact that the porosity of the cathode has little to no effect on the discharge current of the cells. Figure 42 below demonstrates the I-V curve at different porosities. Our results are different from what Ryan et al. [9] have found, however, it could due to that they only conduct either a cathode model or an anode model (e.g., a half-cell model), without a complete battery cells which include all consituent of a lithium-oxygen battery as shown in the current study.

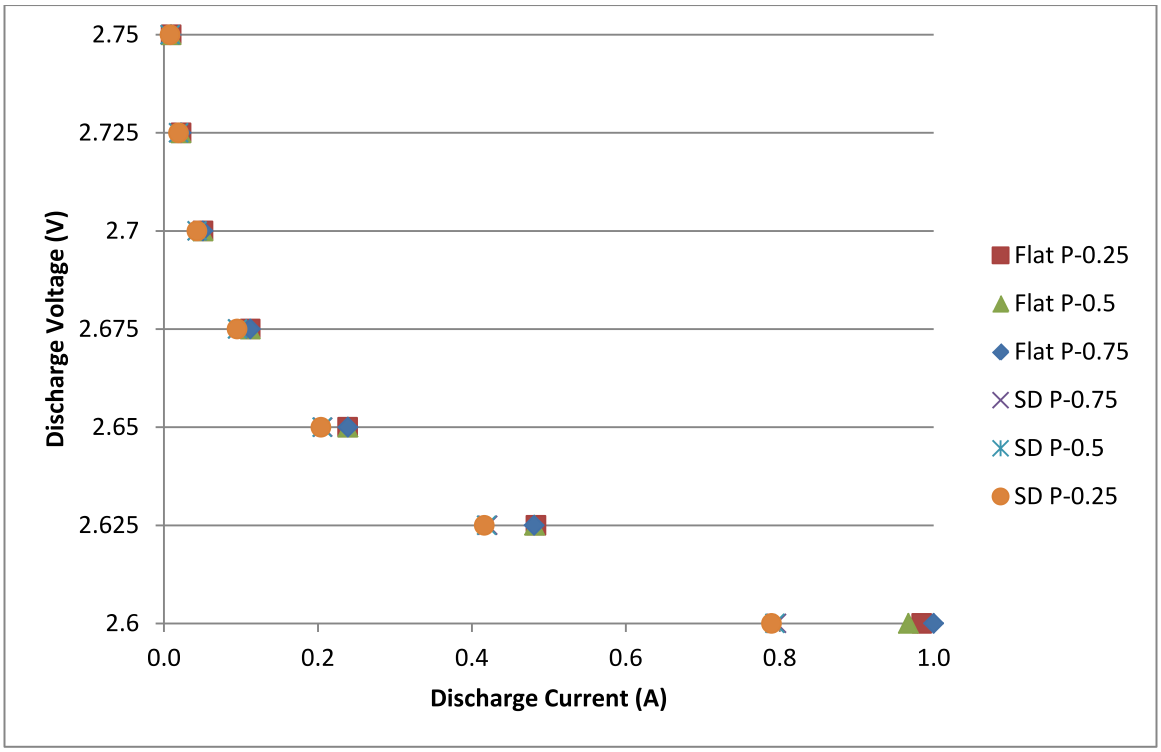

Figure 42: I-V Curve of Flat and Small Dendrite Models at Varying Porosities. Varying porosites had little effect on polatization curves of cells.

The plot portraying the amount of discharge product as the discharge voltage drops is shown in Figure 43. It is interesting to observe that as the porosity of the cathode is decreased, the amount of Li_2O_2 forming within the cathode increases by a proportional amount. That is, as the porosity of the cathode decreases from 0.75 to 0.5 (by 33.3%) the amount of Li_2O_2 formed also decreases by 33.3%. It is suggested that when the porosity of the cathode decreases, the surface area for lithium and oxygen to react decreases, resulting in a reduction of Li_2O_2 formed within the cathode.

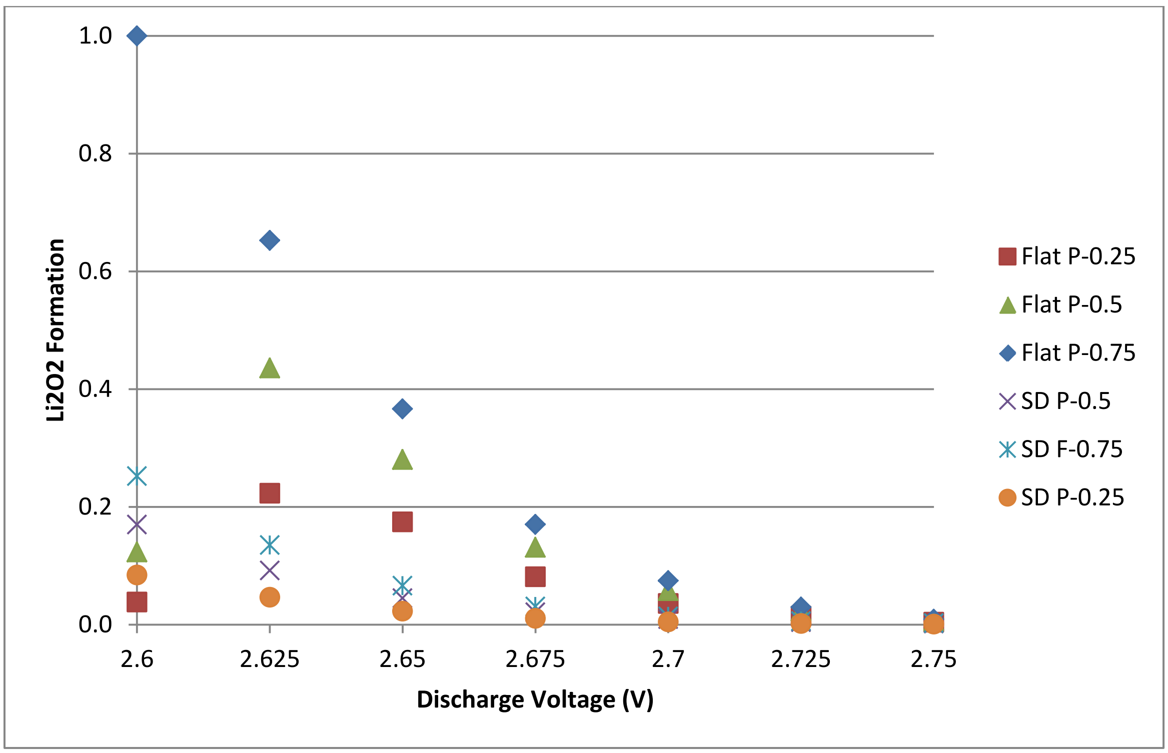

Figure 43: Normalized kMol of Li_2O_2 Formation of Flat and Small Dendrite Models at cathode porosities of 0.25, 0.5, and 0.75. The lower the discharge voltage, the greater the kMol of Li_2O_2 formed.

Figure 44 displays the Li_2O_2 contour plots of flat anode model discharged at three different porosities. While it is apparent that the smaller the porosity the greater the depth of discharge of the Li_2O_2 within the cathode, it is important to remember that the greater porosities reveal a greater amount of discharge product within the entire cathode. It is likely due to the higher porosities revealing a higher amount of Li_2O_2 along the entire z-axis of the cell (out of plane direction). The Li_2O_2 contour plots were observed at a depth of 11 mm in the z-direction of the cell. The two different discharge voltages of 2.75 V and 2.70 are shown for comparison.

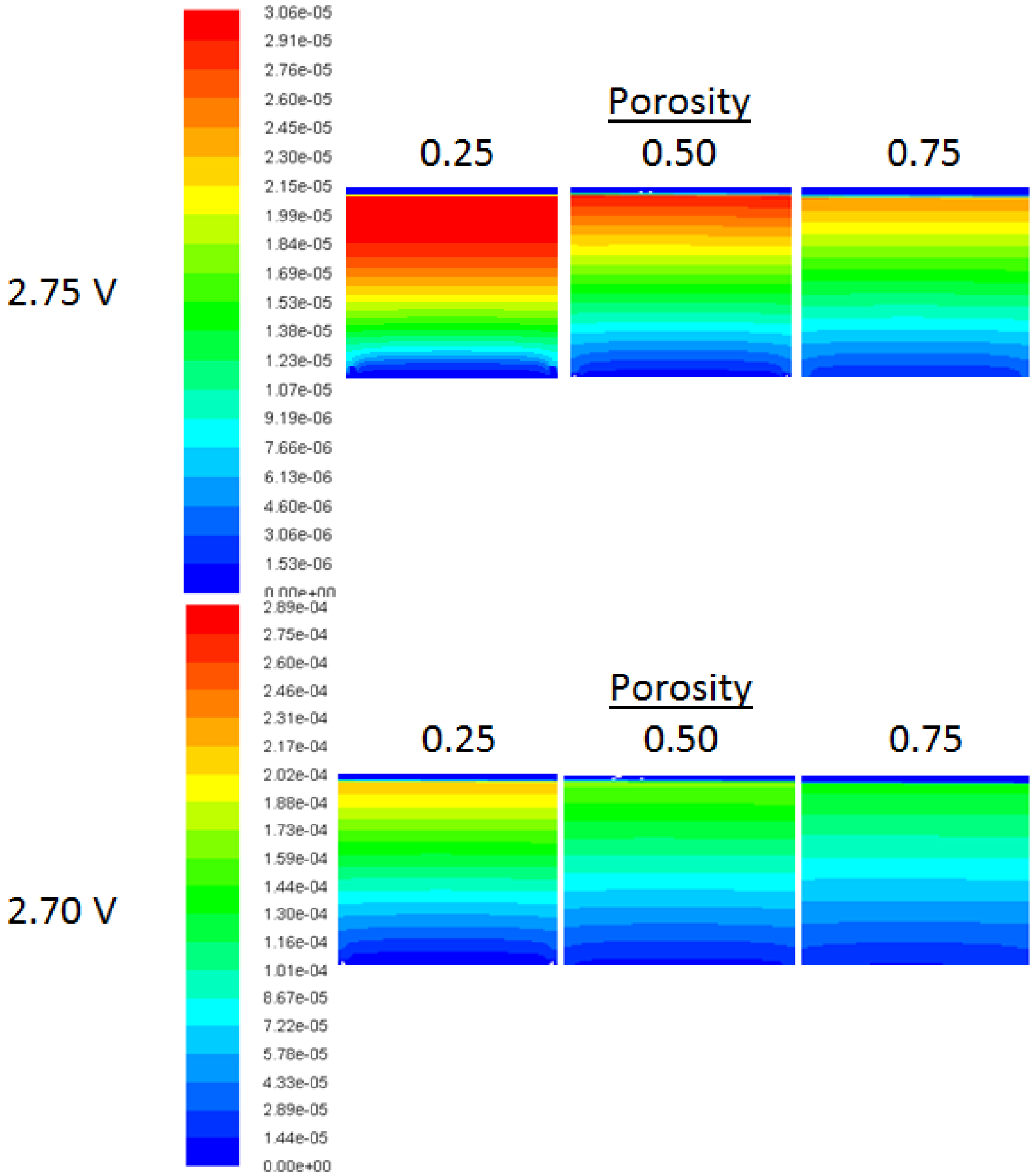

Figure 44: Contour Plots of Flat Model at 2.75 V and 2.70 V

Figure 45 below demonstrates similar results for the small dendrite models. Similar to the flat anode model, this small dendrite model exemplifies a greater depth of discharge at the smaller discharge voltage. The Li_2O_2 contour plots were observed at a depth of 11 mm in the z-direction of the cell. The two different discharge voltages of 2.70 V and 2.60 are shown for comparison.

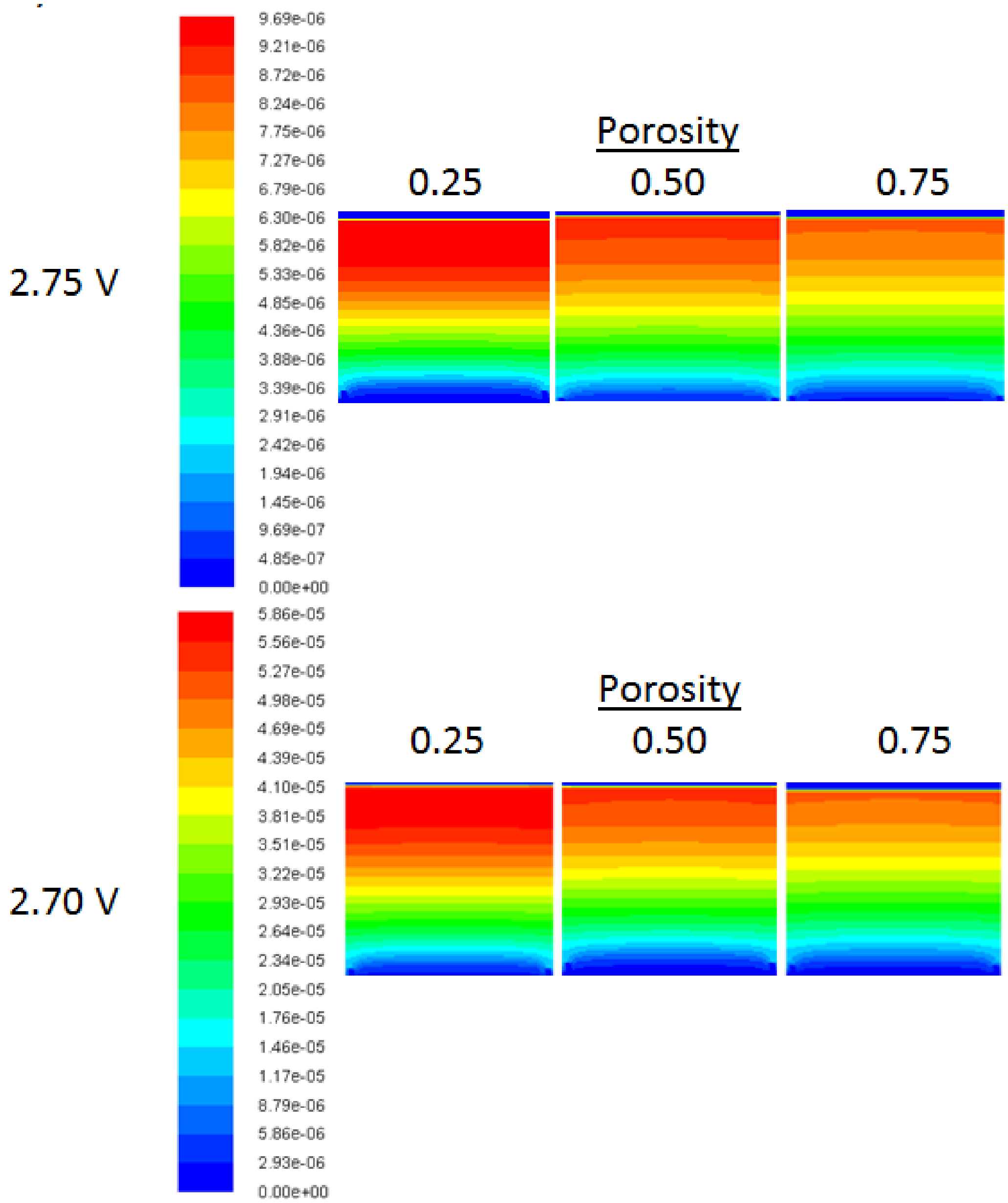

Figure 45: Contour Plots of Small Dendrite Model at 2.75 V and 2.70 V

4.5.2 Adjusting Cathode Porosity – Dendrite Models

The effects of the varying porosities of the dendrite models are compared. Figure 46 below is the polarization curves of the short and long dendrite models discharged at porosities ranging from 0.25 to 0.75. Similar to the previously discussed results, the porosities of the cathode structures were found to have little effect on the polarization curves of the cells but the differences due to dendrite growth can be seen.

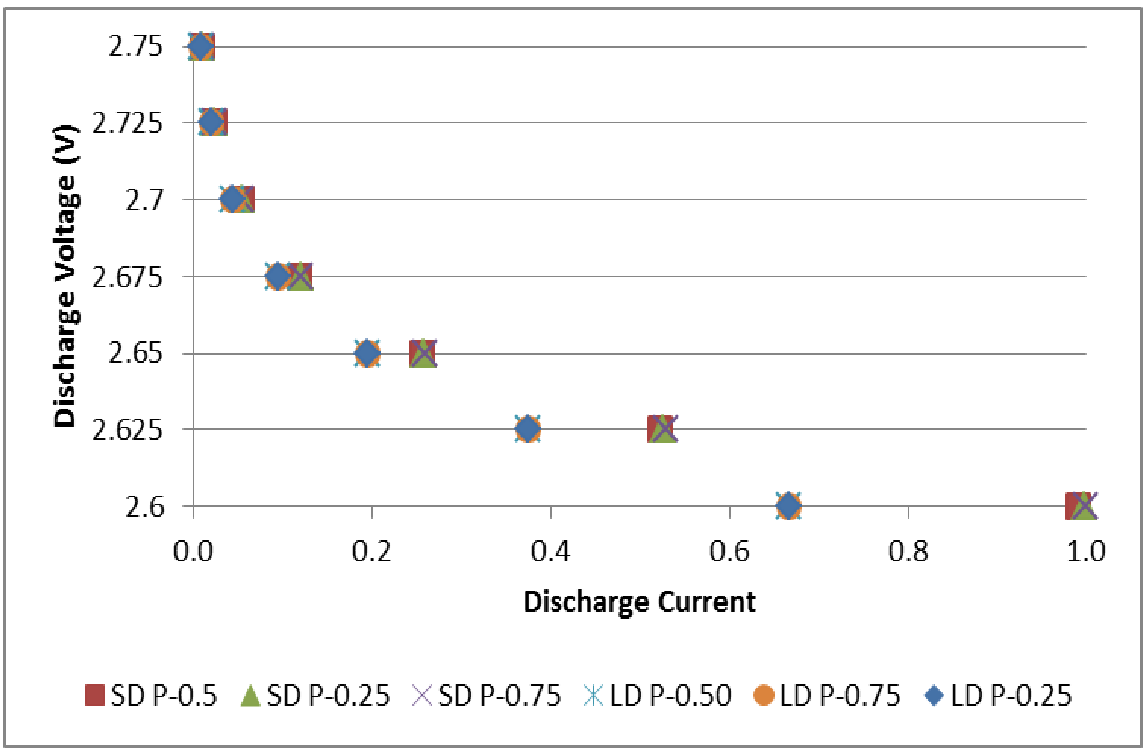

Figure 46: I-V Curve of Small Dendrite and Long Dendrite Models at Varying Porosities. Varying porosites had little effect on polatization curves of cells.

Figure 47 below demonstrates the differences in normalized kMol of Li_2O_2 formed within the cathode structures of the varying porosity models. The porosities of the cathode structures can be seen to significantly decrease the total amount of Li_2O_2 formed and hence lead to a lower capacity cell. One interesting observation is the amount of discharge product formed with the long-dendrite model at a high porosity (0.75) shows the same amount of discharge product as the short dendrite model at a smaller porosity of 0.50.

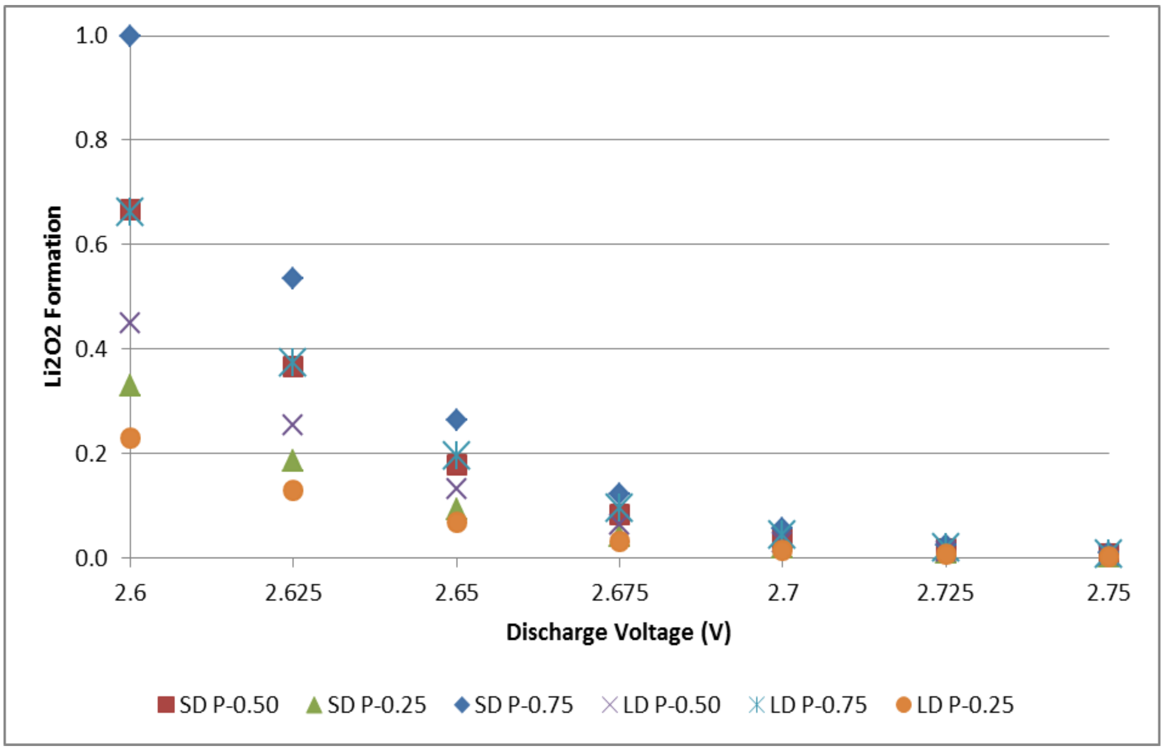

Figure 47: Normalized kMol of Li_2O_2 Formation of Flat and Small Dendrite Models at cathode porosities of 0.25, 0.5, and 0.75. The lower the discharge voltage, the greater the kMol of Li_2O_2 formed.

From the results found in section 4.5.1 and 4.5.2, it can be seen that the change in cathode porosity of our lithium-oxygen cells has a positive, linear relationship with the amount of Li_2O_2 forming within the cathode. These results fall in line with the literature previously discussed by Tran et al. stating that the majority of Li_2O_2 resides in the larger pores of the cathode [14].

4.6 Mass Fraction of O_2 on Discharge Properties

The effects of mass fraction of O_2 available in the cell were explored. Section 4.6.1 examines the effects of the change in mass fraction of O_2 on the polarization and discharge product formation while section 4.6.2 compares the results of the flat anode model to the two dendrite models.

4.6.1 Mass Fraction of O_2 Effect on Flat Anode Model

The mass fraction of O_2 moving through the cathode was adjusted from 100% O_2 in the previously discussed calculations to 75% O_2 to investigate the effects of limited oxygen available for reaction on the cell performance. From Figure 48 below, we can see that as we reduce the amount of oxygen within the cell the I-V curves exhibits different characteristics. The cell with limited oxygen shows a curve where the discharge current of the cell is dropping more quickly as the discharge voltage of the cell is decreased from 2.75 to 2.65 V. It is important to note that these calculations were carried out on the flat anode models.

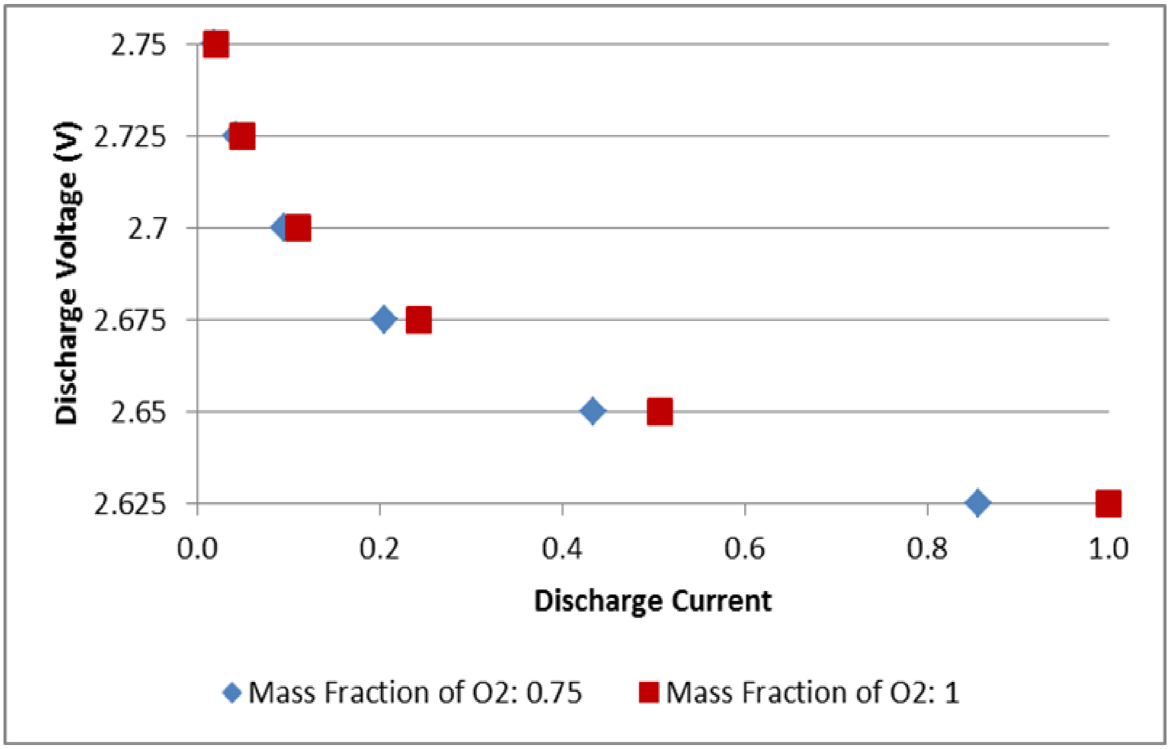

Figure 48: I-V Curve of Flat Model with Limited Oxygen. Decreasing the amount of oxygen to react in cell decreases the discharge current faster than the cell with more oxygen.

Figure 49 demonstrates the amount of Li_2O_2 formed within the cathode of the cells with different mass fractions of O_2 available for reaction. It is apparent that as the amount of oxygen is reduced, the amount of discharge product (*i.e.*, Li_2O_2) that forms is more limited as well. It ultimately effects the discharge capacity of the cell and should be avoided when possible.

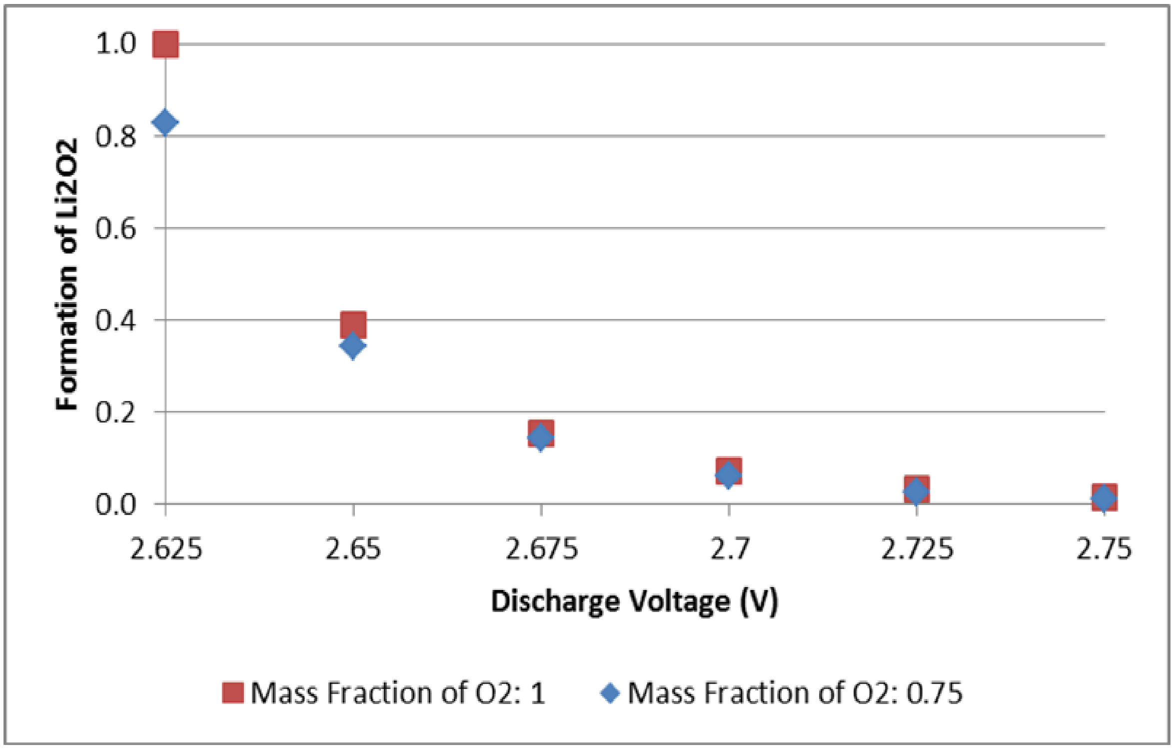

Figure 49: Normalized kMol of Li_2O_2 Formation of Flat models with small mas fractions of O_2. The lower the discharge voltage, the greater the kMol of Li_2O_2 formed.

The contour plots in Figure 50 compare the concentration of discharge product within the cell. The models with a higher amount of O_2 show a much higher Li_2O_2 concentration close to the separator barrier with a slightly better depth of discharge compared to the oxygen restricted model. This could be due to the pore clogging effect disrupting the formation of additional Li_2O_2 and preventing the already limited oxygen from reacting with the lithium.

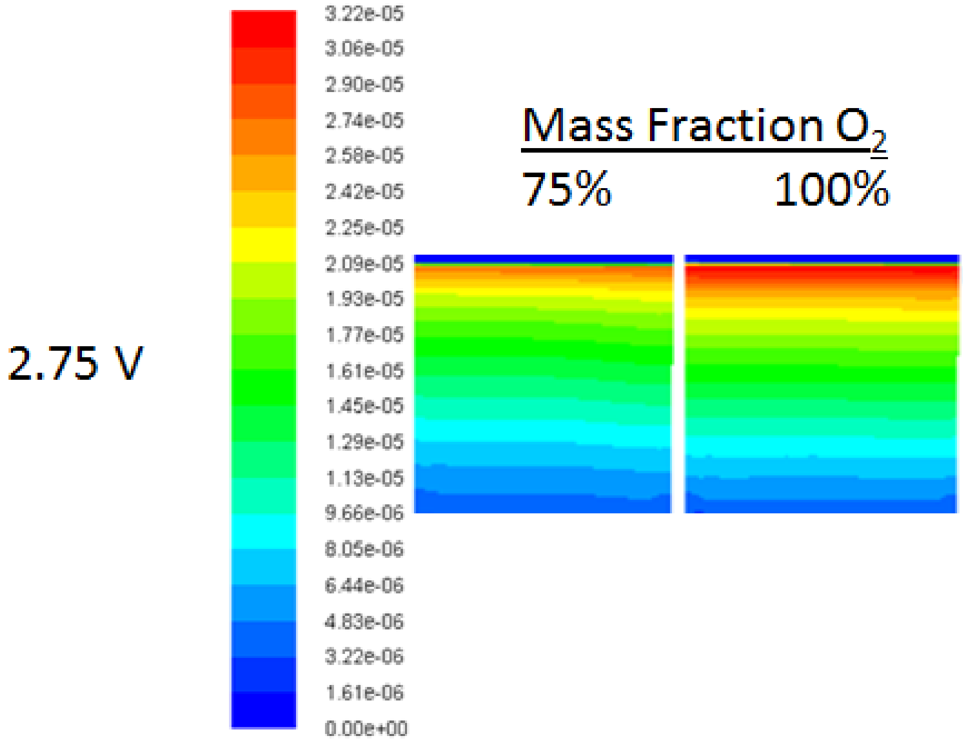

Figure 50: Contour Plots of Flat Anode Model at different mass fraction of O_2. Mass fraction of O_2 of 0.75 shown on the left. Mass fraction of O_2 of 1 shown on the right.

4.6.2 Mass Fraction of O_2 Effect on Dendrite Models

Simulations were conducted for the dendrite models to examine the effects of reducing the mass fraction of oxygen available in the cathode for the small and long dendrite models. From the results presented in the figures below, it can be seen that while both models suffer a decrease in performance from the lack of oxygen available, the difference in magnitude of both the polarization curves and amounts of kMol formed within the cathode remain the same. Figure 51 below shows the I-V curves of the long and small dendrite models with a 25% reduction in oxygen mass fraction.

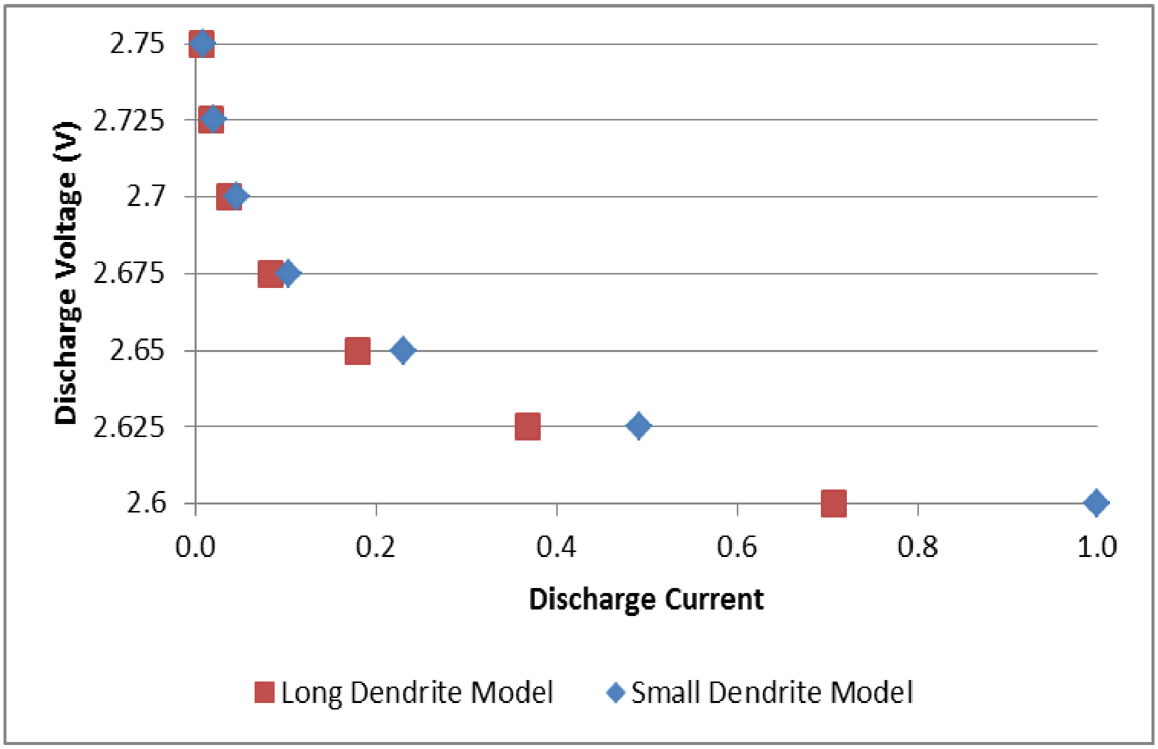

Figure 51: I-V Curve of dendrite models with a 25% reduction in mass fraction of oxygen available in cathode.

Figure 52 below displays the amounts of discharge product forming within the cathodes of the small and long dendrite models as the mass fraction of oxygen is reduced. It can be seen that the difference in magnitude of discharge product forming within the cathode is the same between the two models as shown in Figure 40, despite both models experiencing a decrease in battery cell performance.

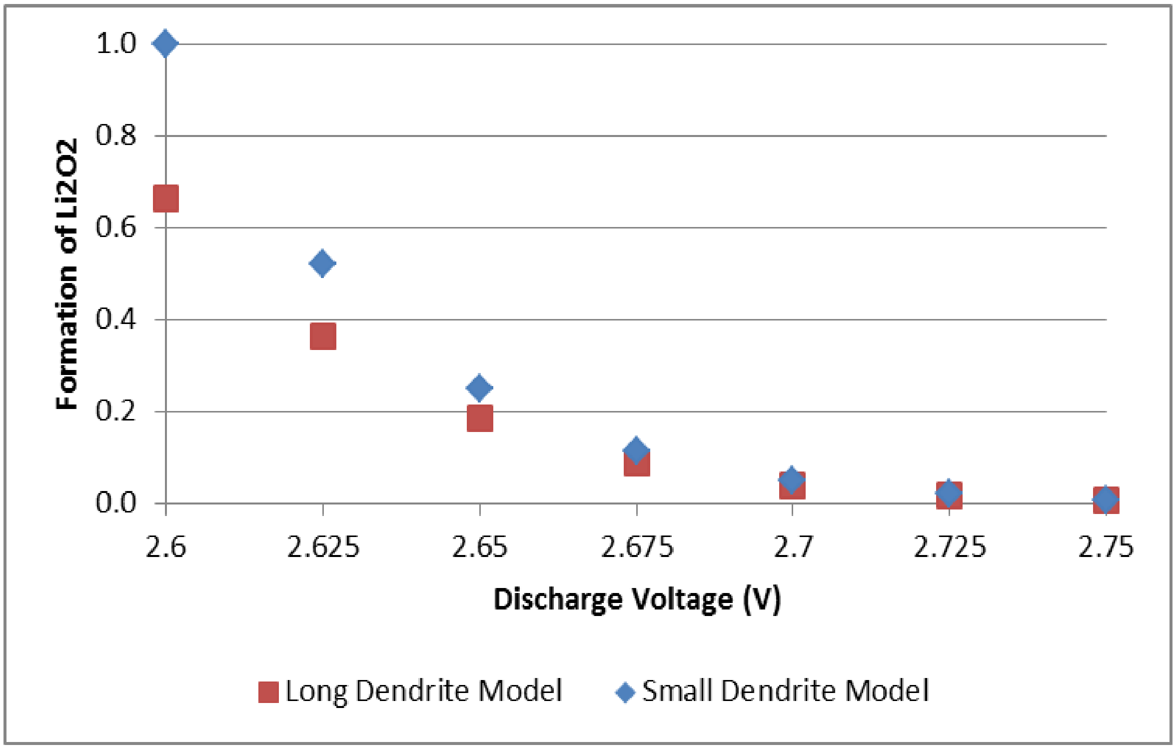

Figure 52: Formation of Li_2O_2 within cathode of cells with a 25% reduction in mass fraction of oxygen available in cathode.

Despite the data in Figures 51 and 52, the results of decreasing the mass fraction of O_2 in the battery cell cathode decreased the performance of both of the cells. It is interesting to note that when the small dendrite model and the flat anode models are compared, the differences in kMol formed within the cathode change, with the small dendrite model showing a 50% decrease in Li_2O_2 compared to previous models with a greater mass fraction of oxygen. This seems to point to the dendrite growth being the major factor leading to the decrease in battery cell performance.

4.7 Mass Flow Rate of O_2 Effect on Discharge Properties

The mass flow rate of oxygen moving through the lithium-oxygen cell was also adjusted to understand the effects on the battery cell. By increasing the mass flow rate of oxygen moving through the gas channels on the cathode side by one magnitude we could observe the effects on the discharge parameters of the cells. Figure 53 below portrays the I-V curves of the models as they were discharged with the increased mass flow rates of oxygen. The increase in mass flow rate further decreased the performance of the dendrite models compared to the flat anode model.

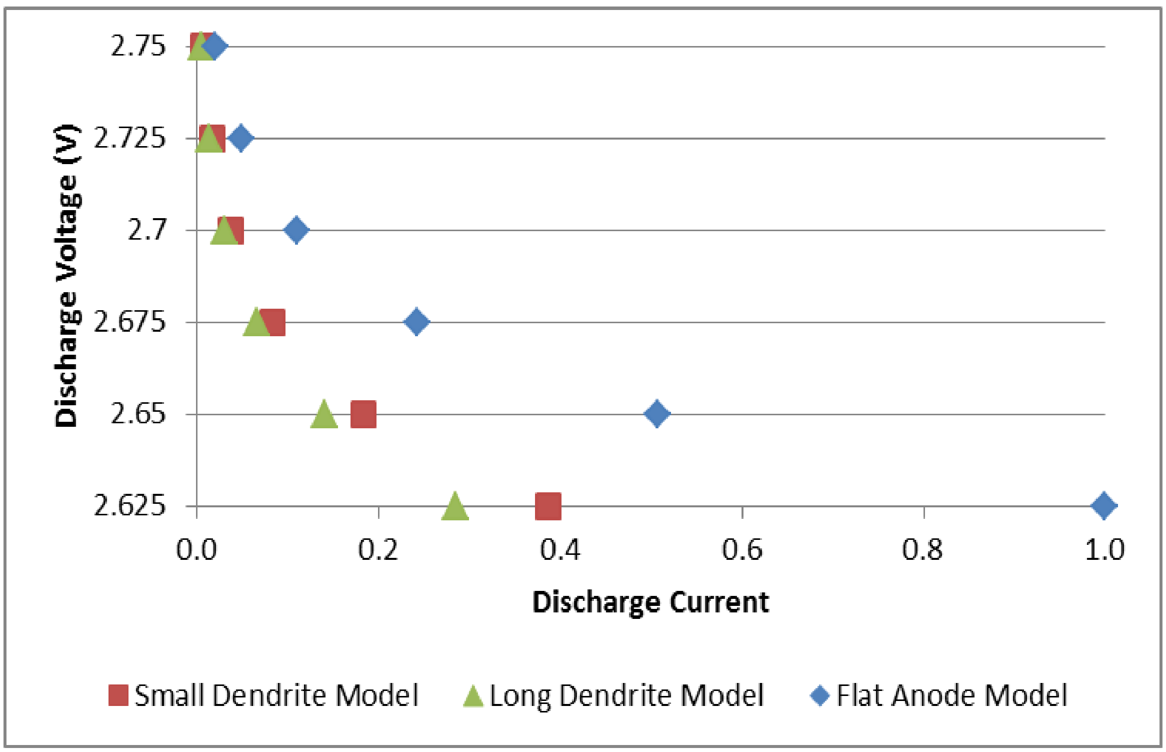

Figure 53: I-V Curves of Flat and Dendrite models at increased oxygen mass flow rate through battery cell. The I-V curves of the dendrite models are significantly decreased compared to the values of the flat anode model.

Figure 54 below portrays the formation of Li_2O_2 within the cathodes of the models. The increase in oxygen again significantly decreases the performance of the dendrite models, decreasing the amount of discharge product much further than the 90% reduction seen in previous sections of this paper.

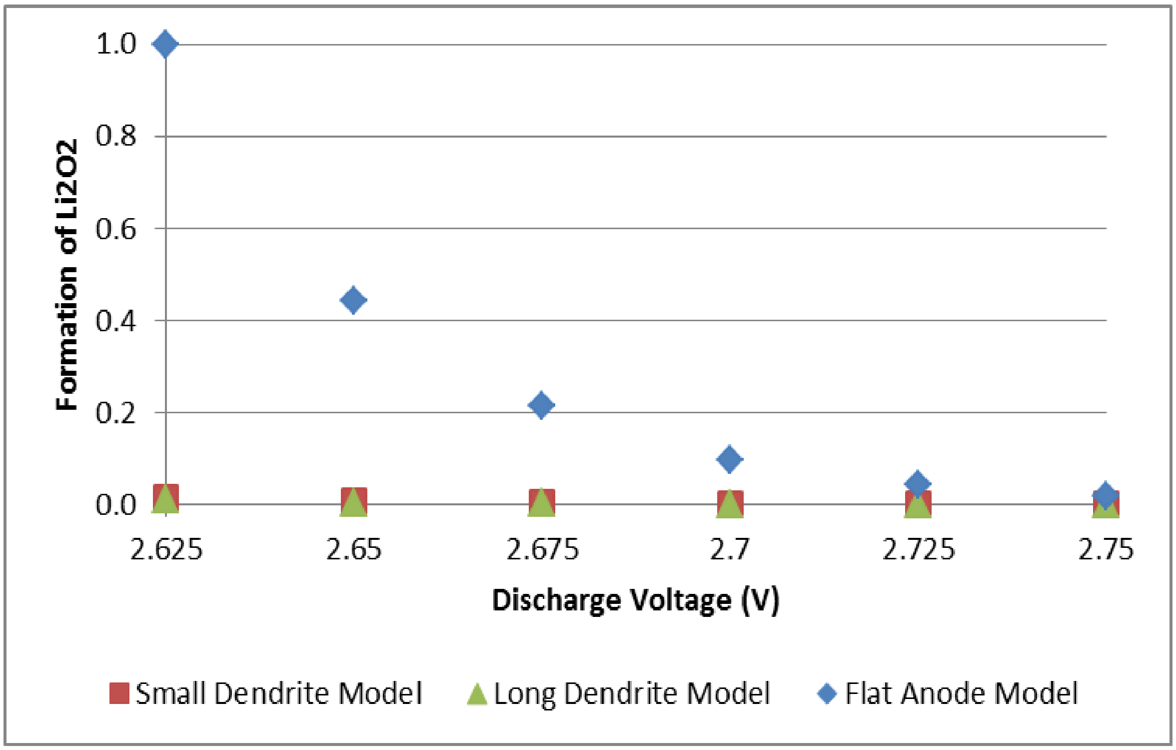

Figure 54: The kMol of discharge product within the cathodes of the flat and dendrite models. The amount of Li_2O_2 shown in the cathode structures is decreased even further in the dendrite models compared to the flat anode model when the mass flow rate of oxygen was increased.

The results shown in Figure 53 and 54 were surprising and went against the intuition that an increase in the mass flow rate of oxygen in the battery cell would increase the performance of the cells. From the results generated, it is clear to see that the increase in O_2 mass flow rate significantly decreased the performance of the cells. This could largely be due to the way the fuel cell module is set-up within Fluent where the oxygen and lithium flowing through the gas channels flow in the z-direction compared to the y-direction in a typical lithium-oxygen battery model. The increase in oxygen mass flow rate could have been too high and forced the oxygen through the gas channels too quickly to react with the lithium to form lithium peroxide, thus decreasing the battery cell performance.

CHAPTER 5: SUMMARY AND CONCLUSIONS

A finite element model of a lithium-oxygen battery was assembled within ANSYS using the CFD Fluent software and the Fuel-Cell Module add-on. Our model was constructed to compare how differing discharge parameters and anode surface homogeneities would affect the discharge characteristics of a lithium-oxygen cell. We found that as the discharge voltage of the cell decreases the kMol of Li_2O_2 formed within the cathode increases greatly as shown in the figures in Chapter 4. It was also noted that an increase in porosity of the cathode resulted in a proportional increase in lithium-peroxide formation. The changes in the cathode porosity had little to no effect on the discharge current of the cell like it does on the amount of lithium peroxide formed.

When comparing a flat anode model to a model with small 4 μm dendrite structures forming on the anode surface, we found that the performance of the cell began to decline. The discharge current of the models with dendrite structures dropped faster than the discharge current of the models with a flat anode surface. The amount of discharge product formed in the cathode was also less, leading to a cell with a smaller capacity. These results were further exemplified when the cathode porosities of the small dendrite models were modified. Like the flat anode model, as the porosities of the cathode was decreased from 0.75 down to 0.25, the amount of Li_2O_2 forming within the cathode reduces considerably. It is interesting to note that the model with the flat anode model at the lowest porosity (0.25) still portrayed a greater amount of Li_2O_2 than the small dendrite model with the greatest porosity

(0.75). Results in this study show how detrimental the formation of dendrite structures can be on the performance of a lithium-oxygen battery.

Further, oxygen limitations were investigated to understand the effects on discharge behaviors. It was found that by decreasing the mass fraction of oxygen available to react with lithium by as much as 25% resulted in the discharge current dropping quickly and a decrease in the amount of Li_2O_2 formed within the cathode, suggesting that the decrease in reactants (O_2) in the electrochemical reaction (Li_2O_2) would clearly negatively affect the performance of the lithium-oxygen cell.

Similar results were seen when the long dendrite model, with dendrites as long as 12.5 µm, was discharged and compared with the flat anode model and small dendrite model. As intuition would suggest, the long dendrite model did not perform well compared to the other two models when examining the formation of Li_2O_2 and I-V curves of the theoretical battery cells.

When comparing all three models and their changes in porosity and oxygen restriction, it can be concluded that although the changes in porosity and oxygen decrease the performance of the lithium-oxygen cells, the dendrites led to the greatest decrease in performance of the battery when examining the capacity of the cell. These results suggest that further work and research must be done to mitigate lithium dendrite growth in lithium-oxygen batteries to generate a commercially available battery cell.

Our results were compared to experimental data that examined the decrease in lithium metal cells as the cells were continuously cycled. The published work found that at high discharge current, bush-like dendrites similar to our computational models, grew large and quickly decreased the capacity of the battery cells [24]. With as few as 25 cycles, a 90% decrease in capacity was found with a slow drop off in capacity after the initial drop. This falls in line with our results with the ~90% decrease in capacity of the small dendrite model and subsequent small decrease in capacity of the long dendrite model.

In this study we constructed three computational lithium-oxygen battery cells and compared their performances under different discharge parameters. Using our models we developed a better understanding of the parameters that have the greatest effect on lithium-oxygen battery performance. Using what the models presented in this study and if we can further mitigate lithium dendrite growth in lithium-oxygen battery cells we may be a couple steps closer to developing a commercially viable lithium-oxygen battery.

5.1 Future Work

Although we have generated results that can help develop our understanding of lithium-oxygen batteries and the effects of varying electrode designs, there is still more we can do to further develop the model and our understanding of Li-O_2 cells.

One change that could be made moving forward would be the modeling method of our dendrite structures. We completed a 3D model by drawing out the cross-sectional shape of the lithium-oxygen battery and extruding the part. This led to what looked like dendrite structures in the 2D x-y plane that were extruded down the entire length of the battery.

However, our model is simplified as the dendrites would be in a random formation across the entire length of the anode surface in a real battery cell. We could improve our model by randomizing the formation of these dendrites and modeling their structures as a more realistic dendrite structure. It is important to point out that this was not carried out yet due to the intense computing power that would be required to run the calculations on such a complex model.

Another possible way to improve the model in the future would be to incorporate the reaction rates of lithium and oxygen and enable this property to be adjusted. Some of the studies published by Ryan et al. focused on adjusting the reaction rates of species to observe the effect on the buildup of Li_2O_2 [9]. The diffusivity of oxygen was also adjusted based on the depth of discharge of the reactions. With similar parameters and functions being incorporated into our model we can compare with the results from the other studies (porosity change, O_2 mass fraction, diffusivity, etc.) then we could draw further conclusions from our own model than previous studies could.

While there are several possible options for future work with this project, the models developed in the current study have shown to be powerful in that the entire lithium-oxygen battery is observed and understood. With the aid of this finite-element model, we have developed a program that can be used to help design real experimental lithium-oxygen batteries and test different electrode designs before real-life construction and testing.

REFERENCES

[1] Lu, Y., Gallant, B., Kwabi, D., 2013, "Lithium–oxygen Batteries: Bridging Mechanistic Understanding and Battery Performance," Energy and Environmental Science, (6) pp. 750-768.

[2] Christensen, J., Albertus, P., Sanchez-Carrera, R., 2012, "A Critical Review of Li/Air Batteries," Journal of the Electrochemical Society, 159(2) pp. R1-R30.

[3] Xu, W., Wang, J., Ding, F., 2014, "Lithium Metal Anodes for Rechargeable Batteries," Energy and Environmental Science, 7pp. 513.

[4] Kim, S., 2014, "Before Tesla's $5B Gigafactory, there was GM's EV1," ABC News, Business.

[5] EDTA, December, 2014, "Electric Drive Sales Dashboard," Electric Drive Transportation Association, January, 2015(1/25/2015) pp. 4.

[6] Khalil, A., 2009, "Argonne to Develop Lithium-Air Battery," .

[7] Reid, C., Dobley, A., and Seymour, F., 2014, "Lithium-Air Cell Development," AIAA Propulsion and Energy Forum, pp. 1.

[8] Dobley, A., DiCarlo, J., and Abraham, K., 2014, "Non-Aqueous Lithium-Air Batteries with an Advanced Cathode Structure: Final Report for NASA SBIR Contract," Yardney Technical Products, Inc. / Lithium, Inc., .

[9] Ryan, E. M., Ferris, K. F., Tartakovsky, A. M., 2013, "Computaitonal Modeling of Transport Limitations in Li-Air Batteries," Journal of the Electrochemical Society, 45(29) pp. 124-136.

[10] Shui, J., Okasinski, J., Chen, C., 2014, "In Operando Spatiotemporal Study of Li2O2 Grain Growth and its Distribution Inside Operating Li-O2 Batteries," CHEMSUSCHEM, 7(2) pp. 543.

[11] Monroe, C., and Newman, J., 2003, "Dendrite Growth in Lithium/Polymer Systems," Journal of the Electrochemical Society, 150(10) pp. A1377-A1384.

[12] Tan, J., and Ryan, E. M., 2013, "Numerical Modelin of Dendrite Growth in a Lithium Air Battery System," Journal of the Electrochemical Society, 53(20) pp. 35-43.

[13] Kraytsberg, A., and Ein-Eli, Y., 2013, "The Impact of Nano-Scaled Materials on Advanced Metal-Air Battery Systems," Nano Energy, 2pp. 468-480.

[14] Tran, C., Yang, X., and Qu, D., 2010, "Investigation of the Gas-Diffusion-Electrode used as Lithium/Air Cathode in Non-Aqueous Electrolyte and the Importance of Carbon Material Porosity," Journal of Power Sources, 195pp. 2057.

[15] Tartakovsky, A. M., Redden, G., Lichtner, P., 2008, "Mixing-Induced Precipitation: Experimental Study and Multiscale Numerical Analysis," Water Resources Research, 44(6) pp. W06S04.

[16] Gallant, B., Kwabi, D., Mitchell, R., 2013, "Influence of Li_2O_2 Morphology on Oxygen Reduction and Evolution Kinetics in Li–O_2 Batteries," Energy and Environmental Science, (6) pp. 2518-2528.

[17] Viswanathan, V., Norskov, J., Speidel, A., 2013, "Li-O_2 Kinetic Overpotentials: Tafel Plots from Experimental and First-Principles Theory," The Journal of Physical Chemistry Letters, 4(4) pp. 556-560.

[18] Xia, C., Waletzko, M., Chen, L., 2014, "Evolution of Li_2O_2 Growth and its Effect on Kinetics of Li-O_2 Batteries," Applied Materials and Interfaces, 6(15) pp. 12083.

[19] McCloskey, C., Speidel, A., Scheffler, R., 2012, "Twin Problems of Interfacial Carbonate Formation in Nonaqueous Li–O_2Batteries," The Journal of Physical Chemistry Letters, 3(8) pp. 997-1001.

[20] Thotiyl, M., Freunberger, S., Peng, Z., 2012, "The Carbon Electrode in Nonaqueous Li-O_2 Cells." Journal of the American Chemical Society, 135pp. 494-500.

[21] Ding, F., Xu, W., Graff, G., 2013, "Dendrite-Free Lithium Deposition Via. Self-Healing Electrostatic Shield Mechanism," Journal of the American Chemical Society, 135(11) pp. 4450-4456.

[22] Nishida, T., Nishikawa, K., Rosso, M., 2013, "Optical Observation of Li Dendrite Growth in Ionic Liquid," Electrochimica Acta, (100) pp. 333-341.

[23] Brissot, C., Rosso, M., Chazalviel, J., 1999, "Dendrite Growth Mechanismsin Lithium/Polymer Cells," Journal of Power Sources, 81(82) pp. 925-929.

[24] Orsini, F., Pasquier, A., Beaudoin, B., 1998, "In Situ Scanning Electron Microscopy (SEM) Observation of Interfaces within Plastic Lithium Batteries," Journal of Power Sources, 76pp. 19.

[25] Chazalviel, J., 1990, "Electrochemical Aspects of the Generation of Ramified Metallic Electrodeposits," Physical Review A, 42pp. 7355-7367.

[26] Diggle, J., Despic, A., and Bockris, J., 1969, "The Mechanism of the Dendritic Electrocrystallization of Zinc," Journal of the Electrochemical Society, 116pp. 1503-1514.

[27] Barton, J., and Bockris, J., 1962, "The Electrolytic Growth of Dendrites from Ionic Solutions," Proceedings of the Royal Society of London. Series A, 268pp. 485.

[28] Akolkar, R., 2013, "Mathematical Model of the Dendritic Growth during Lithium Electrodeposition," Journal of Power Sources, 232pp. 23-28.

[29] Jang, I., Hidaka, Y., and Ishihara, T., 2013, "Li Metal Utilization in Lithium Air Rechareable Batteries," Journal of Power Sources, 244pp. 606.

[30] ANSYS, 2011, "ANSYS FLUENT Fuel Cell Modules Manual," pp. 4.

[31] Read, J., 2002, "Characterization of the Lithium/Oxygen Organic Electrolyte Battery," Journal of the Electrochemical Society, 149(9) pp. A1190.

[32] Li, X., and Faghri, A., 2012, "Optimization of the Cathode Structure of Lithium-Air Batteries Based on a Two-Dimensional, Transient, Non-Isothermal Model," Journal of the Electrochemical Society, 159(10) pp. A1747.

[33] ElementData, M., "Technical Data for Lithium," 2013pp. 1.

[34] Radin, M., and Siegel, D., 2013, "Charge Transport in Lithium Peroxide: Relevance for Rechargeable Metal-Air Batteries," Energy and Environmental Science, 6pp. 2370-2379.

APPENDIX

Appendix A: ANSYS Project Reports

A1: Geometry and Mesh of the Flat Anode Model

Below are the images of the geometry and mesh of the flat anode model.

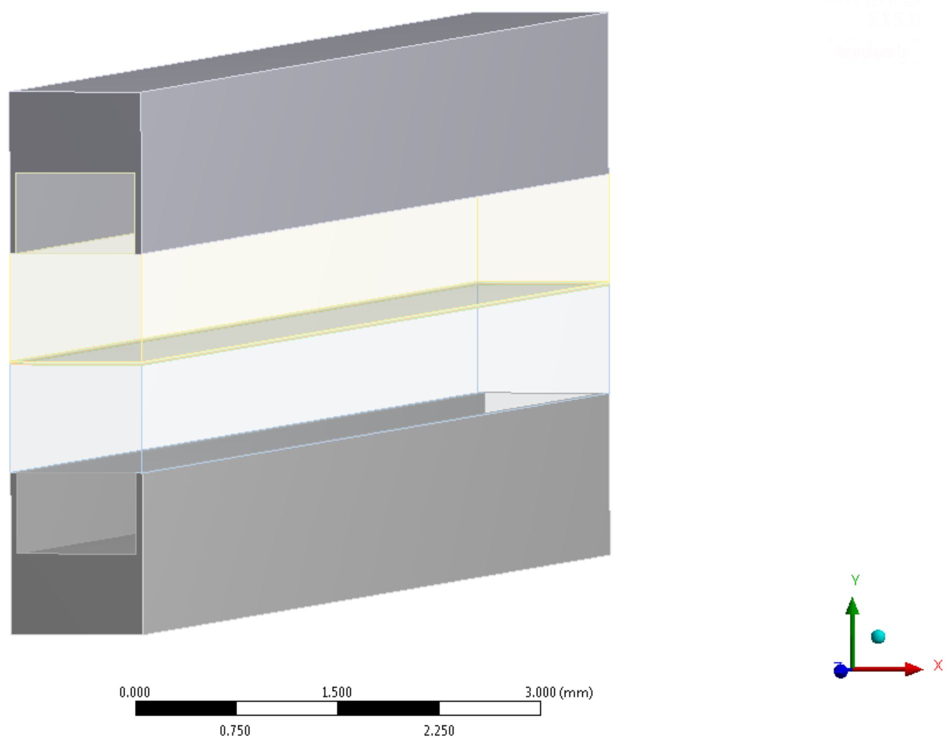

Figure A1: Basic geometry of the flat anode model with scale shown.

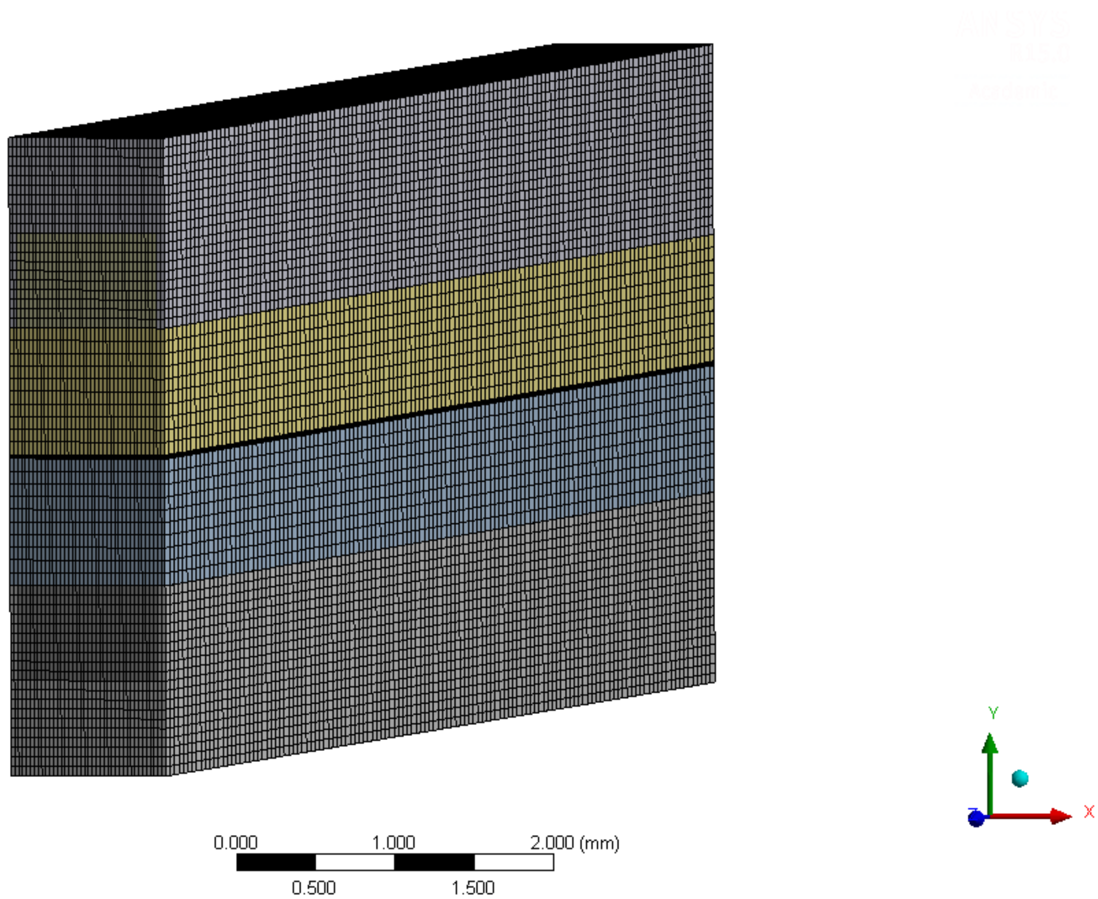

Figure A2: Mesh of the flat anode model with scale shown.

Details of "Mesh"	
Defaults	
Physics Preference	Mechanical
Relevance	0
Sizing	
Use Advanced Size Fun...	Off
Relevance Center	Coarse
Element Size	Default
Initial Size Seed	Active Assembly
Smoothing	Medium
Transition	Fast
Span Angle Center	Coarse
Minimum Edge Length	8.e-003 mm
Inflation	
Use Automatic Inflation	None
Inflation Option	Smooth Transition
Transition Ratio	0.272
Maximum Layers	5
Growth Rate	1.2
Inflation Algorithm	Pre
View Advanced Options	No
Patch Conforming Options	
Triangle Surface Mesher	Program Controlled
Patch Independent Options	
Topology Checking	Yes
Advanced	
Number of CPUs for Pa...	Program Controlled
Shape Checking	Standard Mechanical
Element Midside Nodes	Program Controlled
Straight Sided Elements	No
Number of Retries	Default (4)
Extra Retries For Assem...	Yes
Rigid Body Behavior	Dimensionally Reduced
Mesh Morphing	Disabled
Defeaturing	
Pinch Tolerance	Please Define
Generate Pinch on Ref...	No
Automatic Mesh Based...	On
Defeaturing Tolerance	Default
Statistics	
Nodes	1368133
Elements	330000
Mesh Metric	None

Figure A3: Mesh details of the flat anode model

A2: Fluent Iterations of Flat Anode Model

Below are the first 50 iterations of calculations for the flat anode model calculated with a porosity of 0.75 at a discharge voltage of 2.70 V.

iter continuity x-velocity y-velocity z-velocity energy h2 o2 h2o
uds-0 uds-1 uds-3 time/iter
V_cell = 2.700000 (V) ... V_open = 2.800000 (V)
I_anode = 0.001267 (A/cm^2) ... I_cathode = 0.001267 (A/cm^2) ... dI_mea = 0.000000 (A/cm^2) ... dI_stk = 0.000000 (A/cm^2)
1 1.0000e+00 0.0000e+00 5.4823e-07 3.9781e+03 6.8597e-07 5.4212e-05
0.0000e+00 0.0000e+00 7.5734e-11 3.5795e-01 0.0000e+00 0:25:07 199
V_cell = 2.700000 (V) ... V_open = 2.800000 (V)
I_anode = 0.000387 (A/cm^2) ... I_cathode = 0.000287 (A/cm^2) ... dI_mea = 0.000099 (A/cm^2) ... dI_stk = 0.000099 (A/cm^2)
2 1.0000e+00 3.9564e-04 5.1026e-03 1.5750e-01 5.0499e-07 3.3703e-05 1.5897e-05
0.0000e+00 8.6420e-11 5.0302e-02 0.0000e+00 0:25:16 198
V_cell = 2.700000 (V) ... V_open = 2.800000 (V)
I_anode = 0.000144 (A/cm^2) ... I_cathode = 0.000172 (A/cm^2) ... dI_mea = -0.000028 (A/cm^2) ... dI_stk = -0.000028 (A/cm^2)
3 3.9506e-01 5.7009e-04 6.9556e-03 1.2618e-01 2.1428e-07 0.0000e+00 3.7788e-06
0.0000e+00 2.8495e-11 1.5849e-02 0.0000e+00 0:24:43 197
V_cell = 2.700000 (V) ... V_open = 2.800000 (V)
I_anode = 0.000119 (A/cm^2) ... I_cathode = 0.000122 (A/cm^2) ... dI_mea = -0.000003 (A/cm^2) ... dI_stk = -0.000003 (A/cm^2)
4 1.6477e-01 2.7596e-04 2.7144e-03 7.3743e-02 2.3005e-08 0.0000e+00 2.2698e-06
0.0000e+00 1.1334e-11 4.9230e-03 0.0000e+00 0:24:54 196
V_cell = 2.700000 (V) ... V_open = 2.800000 (V)
I_anode = 0.000110 (A/cm^2) ... I_cathode = 0.000105 (A/cm^2) ... dI_mea = 0.000005 (A/cm^2) ... dI_stk = 0.000005 (A/cm^2)
5 1.0000e+00 2.4224e-04 3.0127e-01 3.1221e-02 1.2054e-08 0.0000e+00 1.4419e-06
0.0000e+00 3.6755e-12 1.5078e-03 0.0000e+00 0:24:22 195
V_cell = 2.700000 (V) ... V_open = 2.800000 (V)
I_anode = 0.000105 (A/cm^2) ... I_cathode = 0.000105 (A/cm^2) ... dI_mea = -0.000000 (A/cm^2) ... dI_stk = -0.000000 (A/cm^2)
6 6.0379e-01 9.5524e-04 7.1252e-02 3.5153e-02 5.7162e-09 1.9726e-08 1.2550e-06
1.0599e-02 1.1660e-12 4.5720e-04 7.8175e-02 0:23:55 194
V_cell = 2.700000 (V) ... V_open = 2.800000 (V)

I_anode = 0.000104 (A/cm^2) ... I_cathode = 0.000103 (A/cm^2) ... dI_mea = 0.000001 (A/cm^2) ... dI_stk = 0.000001 (A/cm^2)
7 3.0264e-01 6.0867e-04 2.4606e-02 3.1159e-02 5.1447e-09 1.2095e-08 1.1706e-06 1.1843e-02 4.0710e-13 1.1047e-04 6.4625e-02 0:23:32 193
V_cell = 2.700000 (V) ... V_open = 2.800000 (V)
I_anode = 0.000103 (A/cm^2) ... I_cathode = 0.000101 (A/cm^2) ... dI_mea = 0.000002 (A/cm^2) ... dI_stk = 0.000002 (A/cm^2)
8 1.0918e-01 6.1784e-04 1.2970e-02 2.3196e-02 4.3862e-09 1.1183e-08 9.9096e-07 2.5175e-02 2.9390e-13 3.5637e-05 5.4565e-02 0:23:51 192
V_cell = 2.700000 (V) ... V_open = 2.800000 (V)
I_anode = 0.000102 (A/cm^2) ... I_cathode = 0.000096 (A/cm^2) ... dI_mea = 0.000006 (A/cm^2) ... dI_stk = 0.000006 (A/cm^2)
9 8.2118e-01 5.0056e-04 2.6905e-01 2.7169e-02 9.3359e-09 1.3313e-08 2.8216e-06 3.0848e-02 1.9431e-13 2.7837e-05 4.6813e-02 0:22:48 191
V_cell = 2.700000 (V) ... V_open = 2.800000 (V)
I_anode = 0.000099 (A/cm^2) ... I_cathode = 0.000098 (A/cm^2) ... dI_mea = 0.000001 (A/cm^2) ... dI_stk = 0.000001 (A/cm^2)
10 5.6546e-01 6.7876e-04 6.5301e-02 1.8044e-02 7.3697e-09 1.2981e-08 1.8628e-06 9.0413e-03 9.6663e-14 2.1871e-05 4.0666e-02 0:21:57 190
V_cell = 2.700000 (V) ... V_open = 2.800000 (V)
I_anode = 0.000098 (A/cm^2) ... I_cathode = 0.000097 (A/cm^2) ... dI_mea = 0.000001 (A/cm^2) ... dI_stk = 0.000001 (A/cm^2)
11 2.7100e-01 5.3321e-04 2.4491e-02 1.6232e-02 5.7354e-09 1.1330e-08 9.6937e-07 1.4775e-02 9.5192e-14 2.5891e-05 3.5682e-02 0:21:53 189
V_cell = 2.700000 (V) ... V_open = 2.800000 (V)
I_anode = 0.000098 (A/cm^2) ... I_cathode = 0.000095 (A/cm^2) ... dI_mea = 0.000003 (A/cm^2) ... dI_stk = 0.000003 (A/cm^2)
iter continuity x-velocity y-velocity z-velocity energy h2 o2 h2o uds-0 uds-1 uds-3 time/iter
12 1.0619e-01 5.6685e-04 1.3771e-02 1.6143e-02 8.0219e-09 1.0970e-08 2.5502e-06 8.6549e-03 1.7034e-13 3.5846e-05 3.1656e-02 0:21:48 188
V_cell = 2.700000 (V) ... V_open = 2.800000 (V)
I_anode = 0.000096 (A/cm^2) ... I_cathode = 0.000091 (A/cm^2) ... dI_mea = 0.000005 (A/cm^2) ... dI_stk = 0.000005 (A/cm^2)
13 2.1562e-01 4.3953e-04 9.3957e-02 2.7888e-02 6.2775e-09 1.0976e-08 3.0044e-06 7.5774e-03 1.6213e-13 3.0231e-05 2.8169e-02 0:22:20 187
V_cell = 2.700000 (V) ... V_open = 2.800000 (V)
I_anode = 0.000093 (A/cm^2) ... I_cathode = 0.000092 (A/cm^2) ... dI_mea = 0.000001 (A/cm^2) ... dI_stk = 0.000001 (A/cm^2)
14 1.9031e-01 2.9923e-04 2.3140e-02 2.3078e-02 6.5566e-09 1.1140e-08 1.4724e-06 1.2746e-02 1.0301e-13 1.5567e-05 2.5229e-02 0:21:29 186
V_cell = 2.700000 (V) ... V_open = 2.800000 (V)
I_anode = 0.000093 (A/cm^2) ... I_cathode = 0.000092 (A/cm^2) ... dI_mea = 0.000001

(A/cm^2) ... dI_stk = 0.000001 (A/cm^2)
15 9.1820e-02 3.1898e-04 1.0222e-02 2.0569e-02 5.0133e-09 1.1224e-08 1.6616e-06 9.7429e-03 6.9233e-14 1.6696e-05 2.2708e-02 0:20:48 185
V_cell = 2.700000 (V) ... V_open = 2.800000 (V)
I_anode = 0.000092 (A/cm^2) ... I_cathode = 0.000090 (A/cm^2) ... dI_mea = 0.000002 (A/cm^2) ... dI_stk = 0.000002 (A/cm^2)
16 4.2203e-02 3.1302e-04 7.4098e-03 2.2379e-02 4.4414e-09 1.1053e-08 1.3307e-06 8.6968e-03 7.6902e-14 2.0879e-05 2.0527e-02 0:20:51 184
V_cell = 2.700000 (V) ... V_open = 2.800000 (V)
I_anode = 0.000091 (A/cm^2) ... I_cathode = 0.000090 (A/cm^2) ... dI_mea = 0.000002 (A/cm^2) ... dI_stk = 0.000002 (A/cm^2)
reversed flow in 2 faces on pressure-outlet 42.
17 2.3050e-02 3.1500e-04 6.2450e-03 2.4875e-02 3.4351e-09 1.9507e-08 9.6578e-07 1.0977e-02 7.2133e-14 2.2208e-05 1.8624e-02 0:20:51 183
V_cell = 2.700000 (V) ... V_open = 2.800000 (V)
I_anode = 0.000091 (A/cm^2) ... I_cathode = 0.000090 (A/cm^2) ... dI_mea = 0.000001 (A/cm^2) ... dI_stk = 0.000001 (A/cm^2)
reversed flow in 2 faces on pressure-outlet 42.
18 1.6483e-02 2.4548e-04 4.8920e-03 2.4065e-02 2.8743e-09 2.2378e-08 7.7739e-07 1.2329e-02 5.9317e-14 2.1037e-05 1.6952e-02 0:20:50 182
V_cell = 2.700000 (V) ... V_open = 2.800000 (V)
I_anode = 0.000090 (A/cm^2) ... I_cathode = 0.000091 (A/cm^2) ... dI_mea = -0.000000 (A/cm^2) ... dI_stk = -0.000000 (A/cm^2)
19 1.3556e-02 1.8929e-04 3.7431e-03 2.0808e-02 2.5363e-09 1.2839e-08 6.7941e-07 1.2082e-02 5.6315e-14 2.2232e-05 1.5474e-02 0:20:12 181
V_cell = 2.700000 (V) ... V_open = 2.800000 (V)
I_anode = 0.000091 (A/cm^2) ... I_cathode = 0.000092 (A/cm^2) ... dI_mea = -0.000001 (A/cm^2) ... dI_stk = -0.000001 (A/cm^2)
20 1.0663e-02 1.7864e-04 3.5890e-03 1.9499e-02 2.0745e-09 1.1282e-08 6.6655e-07 1.0266e-02 5.1566e-14 2.1489e-05 1.4160e-02 0:19:40 180
V_cell = 2.700000 (V) ... V_open = 2.800000 (V)
I_anode = 0.000091 (A/cm^2) ... I_cathode = 0.000093 (A/cm^2) ... dI_mea = -0.000001 (A/cm^2) ... dI_stk = -0.000001 (A/cm^2)
21 8.7541e-03 1.7401e-04 3.2918e-03 1.7821e-02 1.6188e-09 1.1137e-08 6.5925e-07 9.1756e-03 5.6310e-14 1.9917e-05 1.2988e-02 0:19:49 179
V_cell = 2.700000 (V) ... V_open = 2.800000 (V)
I_anode = 0.000092 (A/cm^2) ... I_cathode = 0.000093 (A/cm^2) ... dI_mea = -0.000001 (A/cm^2) ... dI_stk = -0.000001 (A/cm^2)
22 7.4558e-03 1.6981e-04 3.0257e-03 1.6311e-02 1.3334e-09 1.1081e-08 6.6378e-07 7.3474e-03 4.7242e-14 1.5120e-05 1.1936e-02 0:19:20 178
V_cell = 2.700000 (V) ... V_open = 2.800000 (V)
I_anode = 0.000093 (A/cm^2) ... I_cathode = 0.000093 (A/cm^2) ... dI_mea = -0.000001 (A/cm^2) ... dI_stk = -0.000001 (A/cm^2)

```
  iter  continuity  x-velocity  y-velocity  z-velocity     energy         h2         o2        h2o
uds-0      uds-1      uds-3     time/iter
   23  7.0405e-03  1.5427e-04  2.4997e-03  1.2877e-02  1.1349e-09  1.1015e-08  6.6636e-07
6.2710e-03  3.9220e-14  1.2916e-05  1.0989e-02  0:18:55  177
      V_cell  = 2.700000 (V)      ... V_open    = 2.800000 (V)
      I_anode = 0.000093 (A/cm^2) ... I_cathode = 0.000094 (A/cm^2) ... dI_mea = -0.000001
(A/cm^2) ... dI_stk = -0.000001 (A/cm^2)
   24  6.2221e-03  1.4135e-04  2.3090e-03  1.0446e-02  1.0857e-09  1.1037e-08  6.7576e-07
4.7238e-03  3.2485e-14  8.9254e-06  1.0134e-02  0:18:34  176
      V_cell  = 2.700000 (V)      ... V_open    = 2.800000 (V)
      I_anode = 0.000093 (A/cm^2) ... I_cathode = 0.000094 (A/cm^2) ... dI_mea = -0.000000
(A/cm^2) ... dI_stk = -0.000000 (A/cm^2)
   25  5.9381e-03  1.3030e-04  1.8486e-03  8.1449e-03  8.8916e-10  1.0970e-08  6.6059e-07
4.1632e-03  2.4951e-14  7.2656e-06  9.3595e-03  0:18:16  175
      V_cell  = 2.700000 (V)      ... V_open    = 2.800000 (V)
      I_anode = 0.000093 (A/cm^2) ... I_cathode = 0.000094 (A/cm^2) ... dI_mea = -0.000000
(A/cm^2) ... dI_stk = -0.000000 (A/cm^2)
   26  5.3657e-03  1.1926e-04  1.6868e-03  6.4770e-03  8.8623e-10  1.1005e-08  6.4517e-07
3.2366e-03  2.1365e-14  4.8796e-06  8.6556e-03  0:18:01  174
      V_cell  = 2.700000 (V)      ... V_open    = 2.800000 (V)
      I_anode = 0.000094 (A/cm^2) ... I_cathode = 0.000094 (A/cm^2) ... dI_mea = -0.000000
(A/cm^2) ... dI_stk = -0.000000 (A/cm^2)
   27  4.8887e-03  1.0964e-04  1.4242e-03  5.2573e-03  6.9365e-10  1.0999e-08  6.4389e-07
2.7926e-03  1.5170e-14  3.5810e-06  8.0144e-03  0:17:13  173
      V_cell  = 2.700000 (V)      ... V_open    = 2.800000 (V)
      I_anode = 0.000094 (A/cm^2) ... I_cathode = 0.000094 (A/cm^2) ... dI_mea = -0.000000
(A/cm^2) ... dI_stk = -0.000000 (A/cm^2)
   28  4.4128e-03  1.0052e-04  1.2657e-03  4.3615e-03  5.8501e-10  1.0989e-08  6.4404e-07
2.5338e-03  1.2908e-14  2.7164e-06  7.4289e-03  0:16:33  172
      V_cell  = 2.700000 (V)      ... V_open    = 2.800000 (V)
      I_anode = 0.000094 (A/cm^2) ... I_cathode = 0.000094 (A/cm^2) ... dI_mea = -0.000000
(A/cm^2) ... dI_stk = -0.000000 (A/cm^2)
   29  3.9968e-03  9.2702e-05  1.1659e-03  3.7643e-03  5.0316e-10  1.0998e-08  6.4469e-07
2.3116e-03  1.1929e-14  2.0722e-06  6.8932e-03  0:16:35  171
      V_cell  = 2.700000 (V)      ... V_open    = 2.800000 (V)
      I_anode = 0.000094 (A/cm^2) ... I_cathode = 0.000094 (A/cm^2) ... dI_mea = -0.000000
(A/cm^2) ... dI_stk = -0.000000 (A/cm^2)
   30  3.6697e-03  8.6758e-05  1.0701e-03  3.2818e-03  4.5336e-10  1.0984e-08  6.4500e-07
2.1141e-03  1.1084e-14  1.5394e-06  6.4020e-03  0:16:02  170
      V_cell  = 2.700000 (V)      ... V_open    = 2.800000 (V)
      I_anode = 0.000094 (A/cm^2) ... I_cathode = 0.000094 (A/cm^2) ... dI_mea = -0.000000
(A/cm^2) ... dI_stk = -0.000000 (A/cm^2)
   31  3.3896e-03  8.1975e-05  9.7811e-04  2.9102e-03  3.9762e-10  1.0981e-08  6.4149e-07
1.9470e-03  9.7270e-15  1.0604e-06  5.9510e-03  0:15:34  169
```

V_cell = 2.700000 (V) ... V_open = 2.800000 (V)
I_anode = 0.000094 (A/cm^2) ... I_cathode = 0.000094 (A/cm^2) ... dI_mea = -0.000000 (A/cm^2) ... dI_stk = -0.000000 (A/cm^2)
32 3.1614e-03 7.7864e-05 8.8921e-04 2.5582e-03 3.7362e-10 1.1020e-08 6.0785e-07 1.9627e-03 8.6757e-15 7.2713e-07 5.5360e-03 0:15:44 168
V_cell = 2.700000 (V) ... V_open = 2.800000 (V)
I_anode = 0.000094 (A/cm^2) ... I_cathode = 0.000094 (A/cm^2) ... dI_mea = -0.000000 (A/cm^2) ... dI_stk = -0.000000 (A/cm^2)
33 2.9803e-03 7.4344e-05 8.2577e-04 2.2914e-03 3.8507e-10 1.1031e-08 6.3505e-07 1.8176e-03 8.0233e-15 5.5160e-07 5.1537e-03 0:15:18 167
V_cell = 2.700000 (V) ... V_open = 2.800000 (V)
I_anode = 0.000094 (A/cm^2) ... I_cathode = 0.000094 (A/cm^2) ... dI_mea = -0.000000 (A/cm^2) ... dI_stk = -0.000000 (A/cm^2)
iter continuity x-velocity y-velocity z-velocity energy h2 o2 h2o uds-0 uds-1 uds-3 time/iter
34 2.8055e-03 7.1033e-05 7.7590e-04 2.0840e-03 3.1533e-10 1.1024e-08 6.0357e-07 1.8615e-03 7.7036e-15 4.0514e-07 4.8010e-03 0:14:56 166
V_cell = 2.700000 (V) ... V_open = 2.800000 (V)
I_anode = 0.000094 (A/cm^2) ... I_cathode = 0.000094 (A/cm^2) ... dI_mea = 0.000000 (A/cm^2) ... dI_stk = 0.000000 (A/cm^2)
35 2.6391e-03 6.7916e-05 7.3399e-04 1.8979e-03 3.6771e-10 1.1044e-08 6.3692e-07 1.7228e-03 7.3327e-15 3.4328e-07 4.4752e-03 0:14:37 165
V_cell = 2.700000 (V) ... V_open = 2.800000 (V)
I_anode = 0.000094 (A/cm^2) ... I_cathode = 0.000094 (A/cm^2) ... dI_mea = 0.000000 (A/cm^2) ... dI_stk = 0.000000 (A/cm^2)
36 2.4631e-03 6.5096e-05 6.9438e-04 1.7460e-03 2.8925e-10 1.1080e-08 6.4048e-07 1.6340e-03 6.9861e-15 3.0839e-07 4.1739e-03 0:14:22 164
V_cell = 2.700000 (V) ... V_open = 2.800000 (V)
I_anode = 0.000094 (A/cm^2) ... I_cathode = 0.000094 (A/cm^2) ... dI_mea = 0.000000 (A/cm^2) ... dI_stk = 0.000000 (A/cm^2)
37 2.2915e-03 6.2521e-05 6.5150e-04 1.6256e-03 2.7928e-10 1.1049e-08 6.3908e-07 1.5304e-03 7.0076e-15 2.9787e-07 3.8949e-03 0:14:08 163
V_cell = 2.700000 (V) ... V_open = 2.800000 (V)
I_anode = 0.000094 (A/cm^2) ... I_cathode = 0.000094 (A/cm^2) ... dI_mea = 0.000000 (A/cm^2) ... dI_stk = 0.000000 (A/cm^2)
38 2.1308e-03 5.9973e-05 6.0824e-04 1.5187e-03 2.4235e-10 1.1044e-08 6.4305e-07 1.4387e-03 7.0064e-15 2.9619e-07 3.6363e-03 0:13:24 162
V_cell = 2.700000 (V) ... V_open = 2.800000 (V)
I_anode = 0.000094 (A/cm^2) ... I_cathode = 0.000094 (A/cm^2) ... dI_mea = 0.000000 (A/cm^2) ... dI_stk = 0.000000 (A/cm^2)
39 1.9693e-03 5.7974e-05 5.7346e-04 1.4469e-03 2.6112e-10 1.1106e-08 6.1501e-07 1.4560e-03 7.1453e-15 3.0468e-07 3.3964e-03 0:13:20 161
V_cell = 2.700000 (V) ... V_open = 2.800000 (V)

I_anode = 0.000094 (A/cm^2) ... I_cathode = 0.000094 (A/cm^2) ... dI_mea = 0.000000 (A/cm^2) ... dI_stk = 0.000000 (A/cm^2)
40 1.8049e-03 5.6312e-05 5.4268e-04 1.3986e-03 3.3342e-10 1.1107e-08 6.4945e-07 1.3188e-03 6.8388e-15 2.9045e-07 3.1737e-03 0:13:16 160
V_cell = 2.700000 (V) ... V_open = 2.800000 (V)
I_anode = 0.000094 (A/cm^2) ... I_cathode = 0.000094 (A/cm^2) ... dI_mea = 0.000000 (A/cm^2) ... dI_stk = 0.000000 (A/cm^2)
41 1.6982e-03 5.4415e-05 5.0876e-04 1.3407e-03 2.8340e-10 1.1111e-08 6.1511e-07 1.3114e-03 6.8774e-15 2.8352e-07 2.9667e-03 0:13:12 159
V_cell = 2.700000 (V) ... V_open = 2.800000 (V)
I_anode = 0.000094 (A/cm^2) ... I_cathode = 0.000094 (A/cm^2) ... dI_mea = 0.000000 (A/cm^2) ... dI_stk = 0.000000 (A/cm^2)
42 1.6052e-03 5.2970e-05 4.8014e-04 1.2906e-03 2.7771e-10 1.1105e-08 6.5307e-07 1.1991e-03 7.1140e-15 2.9971e-07 2.7742e-03 0:13:08 158
V_cell = 2.700000 (V) ... V_open = 2.800000 (V)
I_anode = 0.000094 (A/cm^2) ... I_cathode = 0.000094 (A/cm^2) ... dI_mea = 0.000000 (A/cm^2) ... dI_stk = 0.000000 (A/cm^2)
43 1.5131e-03 5.2406e-05 4.6272e-04 1.2471e-03 2.1358e-10 1.1070e-08 6.5600e-07 1.0997e-03 6.9646e-15 2.9997e-07 2.5951e-03 0:12:32 157
V_cell = 2.700000 (V) ... V_open = 2.800000 (V)
I_anode = 0.000094 (A/cm^2) ... I_cathode = 0.000094 (A/cm^2) ... dI_mea = 0.000000 (A/cm^2) ... dI_stk = 0.000000 (A/cm^2)
44 1.4574e-03 5.1271e-05 4.4171e-04 1.2023e-03 2.2870e-10 1.1039e-08 6.1947e-07 1.1502e-03 7.9967e-15 4.2539e-07 2.4283e-03 0:12:34 156
V_cell = 2.700000 (V) ... V_open = 2.800000 (V)
I_anode = 0.000094 (A/cm^2) ... I_cathode = 0.000094 (A/cm^2) ... dI_mea = 0.000000 (A/cm^2) ... dI_stk = 0.000000 (A/cm^2)
iter continuity x-velocity y-velocity z-velocity energy h2 o2 h2o uds-0 uds-1 uds-3 time/iter
45 1.3901e-03 5.0612e-05 4.3410e-04 1.2078e-03 2.9833e-10 1.1027e-08 6.6978e-07 1.0058e-03 7.2870e-15 3.7232e-07 2.2729e-03 0:12:34 155
V_cell = 2.700000 (V) ... V_open = 2.800000 (V)
I_anode = 0.000094 (A/cm^2) ... I_cathode = 0.000094 (A/cm^2) ... dI_mea = 0.000000 (A/cm^2) ... dI_stk = 0.000000 (A/cm^2)
46 1.3249e-03 4.8352e-05 4.0279e-04 1.1625e-03 3.1186e-10 1.1003e-08 6.2229e-07 9.9144e-04 6.8935e-15 3.3556e-07 2.1281e-03 0:12:33 154
V_cell = 2.700000 (V) ... V_open = 2.800000 (V)
I_anode = 0.000094 (A/cm^2) ... I_cathode = 0.000094 (A/cm^2) ... dI_mea = 0.000000 (A/cm^2) ... dI_stk = 0.000000 (A/cm^2)
47 1.2540e-03 4.6657e-05 3.7814e-04 1.1216e-03 2.3506e-10 1.1007e-08 6.6405e-07 8.9084e-04 7.1109e-15 3.2919e-07 1.9929e-03 0:12:32 153
V_cell = 2.700000 (V) ... V_open = 2.800000 (V)
I_anode = 0.000094 (A/cm^2) ... I_cathode = 0.000094 (A/cm^2) ... dI_mea = -0.000000 (A/cm^2) ... dI_stk = -0.000000 (A/cm^2)

48 1.1815e-03 4.5163e-05 3.6467e-04 1.0908e-03 1.9004e-10 1.0950e-08 6.5907e-07 8.2415e-04 7.0811e-15 3.5685e-07 1.8668e-03 0:12:29 152

V_cell = 2.700000 (V) ... V_open = 2.800000 (V)

I_anode = 0.000094 (A/cm^2) ... I_cathode = 0.000094 (A/cm^2) ... dI_mea = -0.000000 (A/cm^2) ... dI_stk = -0.000000 (A/cm^2)

49 1.1115e-03 4.4018e-05 3.4990e-04 1.0863e-03 2.2296e-10 1.0917e-08 6.2793e-07 8.3824e-04 6.9368e-15 3.6538e-07 1.7491e-03 0:12:27 151

V_cell = 2.700000 (V) ... V_open = 2.800000 (V)

I_anode = 0.000094 (A/cm^2) ... I_cathode = 0.000094 (A/cm^2) ... dI_mea = -0.000000 (A/cm^2) ... dI_stk = -0.000000 (A/cm^2)

50 1.0449e-03 4.2517e-05 3.3283e-04 1.0639e-03 2.3181e-10 1.0868e-08 6.5090e-07 7.5145e-04 6.9380e-15 3.6366e-07 1.6391e-03 0:12:23 150

V_cell = 2.700000 (V) ... V_open = 2.800000 (V)

I_anode = 0.000094 (A/cm^2) ... I_cathode = 0.000094 (A/cm^2) ... dI_mea = -0.000000 (A/cm^2) ... dI_stk = -0.000000 (A/cm^2)

A3: Mesh of the Long Dendrite Anode Model

Details of "Mesh"	
Defaults	
Physics Preference	Mechanical
Relevance	0
Sizing	
Use Advanced Size Fun...	Off
Relevance Center	Coarse
Element Size	Default
Initial Size Seed	Active Assembly
Smoothing	Medium
Transition	Fast
Span Angle Center	Coarse
Minimum Edge Length	4.5e-003 mm
Inflation	
Use Automatic Inflation	None
Inflation Option	Smooth Transition
Transition Ratio	0.272
Maximum Layers	5
Growth Rate	1.2
Inflation Algorithm	Pre
View Advanced Options	No
Patch Conforming Options	
Triangle Surface Mesher	Program Controlled
Patch Independent Options	
Topology Checking	Yes
Advanced	
Number of CPUs for Pa...	Program Controlled
Shape Checking	Standard Mechanical
Element Midside Nodes	Program Controlled
Straight Sided Elements	No
Number of Retries	Default (4)
Extra Retries For Assem...	Yes
Rigid Body Behavior	Dimensionally Reduced
Mesh Morphing	Disabled
Defeaturing	
Pinch Tolerance	Please Define
Generate Pinch on Ref...	No
Automatic Mesh Based...	On
Defeaturing Tolera...	Default
Statistics	
Nodes	1228783
Elements	296700
Mesh Metric	None

Figure A4: Mesh details of the long-dendrite anode model

A4: Fluent Iterations of Long Dendrite Anode Model

Below are the first 50 iterations of calculations for the long dendrite anode model calculated with a porosity of 0.75 at a discharge voltage of 2.725 V.

```
iter  continuity  x-velocity  y-velocity  z-velocity     energy        h2         o2        h2o
uds-0      uds-1      uds-3     time/iter
       V_cell  = 2.725000 (V)      ... V_open    = 2.800000 (V)
       I_anode = 0.000534 (A/cm^2) ... I_cathode = 0.000534 (A/cm^2) ... dI_mea = 0.000000
(A/cm^2) ... dI_stk = 0.000000 (A/cm^2)
     1  1.0000e+00  0.0000e+00  4.9369e-06  2.1999e-01  3.6701e-06  2.0202e-04  1.1493e-05
0.0000e+00  2.1412e-11  5.1425e-01  0.0000e+00  0:19:29  149
       V_cell  = 2.725000 (V)      ... V_open    = 2.800000 (V)
       I_anode = 0.000099 (A/cm^2) ... I_cathode = 0.000127 (A/cm^2) ... dI_mea = -0.000028
(A/cm^2) ... dI_stk = -0.000028 (A/cm^2)
     2  6.1516e-01  1.8741e-03  3.7252e-03  3.4320e-02  6.5616e-06  5.7504e-04  2.9578e-05
0.0000e+00  2.8808e-11  7.1665e-02  0.0000e+00  0:19:55  148
       V_cell  = 2.725000 (V)      ... V_open    = 2.800000 (V)
       I_anode = 0.000015 (A/cm^2) ... I_cathode = 0.000072 (A/cm^2) ... dI_mea = -0.000057
(A/cm^2) ... dI_stk = -0.000057 (A/cm^2)
     3  5.6064e-01  6.0018e-04  3.2680e-03  7.3847e-03  5.2025e-06  4.3113e-04  1.9135e-05
0.0000e+00  7.2672e-12  1.4849e-02  0.0000e+00  0:20:14  147
       V_cell  = 2.725000 (V)      ... V_open    = 2.800000 (V)
       I_anode = 0.000020 (A/cm^2) ... I_cathode = 0.000026 (A/cm^2) ... dI_mea = -0.000006
(A/cm^2) ... dI_stk = -0.000006 (A/cm^2)
     4  4.0053e-01  2.4364e-04  9.1727e-04  3.3871e-03  2.9863e-06  3.1298e-04  2.4396e-05
0.0000e+00  3.7270e-12  5.7860e-03  0.0000e+00  0:20:27  146
       V_cell  = 2.725000 (V)      ... V_open    = 2.800000 (V)
       I_anode = 0.000020 (A/cm^2) ... I_cathode = 0.000019 (A/cm^2) ... dI_mea = 0.000000
(A/cm^2) ... dI_stk = 0.000000 (A/cm^2)
 reversed flow in 2 faces on pressure-outlet 104.
     5  2.5975e-01  1.2824e-04  4.4397e-04  2.3066e-03  1.7654e-06  2.0204e-04  1.0747e-05
0.0000e+00  1.6656e-12  3.3395e-03  0.0000e+00  0:20:36  145
       V_cell  = 2.725000 (V)      ... V_open    = 2.800000 (V)
       I_anode = 0.000017 (A/cm^2) ... I_cathode = 0.000018 (A/cm^2) ... dI_mea = -0.000001
(A/cm^2) ... dI_stk = -0.000001 (A/cm^2)
     6  2.0607e-01  7.9788e-05  3.1090e-04  1.8651e-03  1.1682e-06  1.7733e-04  8.9553e-06
8.1955e-02  7.4629e-13  2.1268e-03  8.8284e-02  0:20:41  144
       V_cell  = 2.725000 (V)      ... V_open    = 2.800000 (V)
```

I_anode = 0.000016 (A/cm^2) ... I_cathode = 0.000017 (A/cm^2) ... dI_mea = -0.000001 (A/cm^2) ... dI_stk = -0.000001 (A/cm^2)

7 1.5576e-01 5.9362e-05 2.3247e-04 1.4816e-03 8.1475e-07 1.7148e-04 7.5275e-06 8.7720e-02 3.4861e-13 1.3464e-03 7.3011e-02 0:20:15 143

V_cell = 2.725000 (V) ... V_open = 2.800000 (V)

I_anode = 0.000015 (A/cm^2) ... I_cathode = 0.000016 (A/cm^2) ... dI_mea = -0.000001 (A/cm^2) ... dI_stk = -0.000001 (A/cm^2)

8 1.2726e-01 4.8889e-05 2.1904e-04 1.1514e-03 6.1968e-07 1.7009e-04 7.2517e-06 1.0378e-01 1.7542e-13 8.5235e-04 6.1664e-02 0:20:21 142

V_cell = 2.725000 (V) ... V_open = 2.800000 (V)

I_anode = 0.000015 (A/cm^2) ... I_cathode = 0.000015 (A/cm^2) ... dI_mea = -0.000001 (A/cm^2) ... dI_stk = -0.000001 (A/cm^2)

9 1.0342e-01 4.1340e-05 2.0557e-04 9.0079e-04 5.3248e-07 1.6799e-04 6.9661e-06 1.1904e-01 9.3580e-14 5.4214e-04 5.2915e-02 0:19:55 141

V_cell = 2.725000 (V) ... V_open = 2.800000 (V)

I_anode = 0.000014 (A/cm^2) ... I_cathode = 0.000015 (A/cm^2) ... dI_mea = -0.000001 (A/cm^2) ... dI_stk = -0.000001 (A/cm^2)

10 8.7388e-02 3.1612e-05 1.6175e-04 7.0724e-04 4.5267e-07 1.6301e-04 6.6879e-06 1.4746e-01 5.4735e-14 3.4573e-04 4.5975e-02 0:20:02 140

V_cell = 2.725000 (V) ... V_open = 2.800000 (V)

I_anode = 0.000014 (A/cm^2) ... I_cathode = 0.000015 (A/cm^2) ... dI_mea = -0.000001 (A/cm^2) ... dI_stk = -0.000001 (A/cm^2)

11 7.2468e-02 2.4086e-05 1.3084e-04 5.6466e-04 3.3850e-07 1.6362e-04 6.3781e-06 1.9101e-01 3.6163e-14 2.1393e-04 4.0347e-02 0:19:37 139

V_cell = 2.725000 (V) ... V_open = 2.800000 (V)

I_anode = 0.000014 (A/cm^2) ... I_cathode = 0.000014 (A/cm^2) ... dI_mea = -0.000000 (A/cm^2) ... dI_stk = -0.000000 (A/cm^2)

iter continuity x-velocity y-velocity z-velocity energy h2 o2 h2o uds-0 uds-1 uds-3 time/iter

12 5.9312e-02 1.9035e-05 1.1456e-04 4.6429e-04 2.8354e-07 1.6250e-04 6.2041e-06 2.5049e-01 1.7704e-14 1.4326e-04 3.5794e-02 0:18:48 138

V_cell = 2.725000 (V) ... V_open = 2.800000 (V)

I_anode = 0.000014 (A/cm^2) ... I_cathode = 0.000014 (A/cm^2) ... dI_mea = -0.000000 (A/cm^2) ... dI_stk = -0.000000 (A/cm^2)

13 4.9053e-02 1.6455e-05 8.9920e-05 3.8764e-04 2.5193e-07 1.6103e-04 6.0985e-06 3.4978e-01 1.2922e-14 1.0938e-04 3.1861e-02 0:18:08 137

V_cell = 2.725000 (V) ... V_open = 2.800000 (V)

I_anode = 0.000014 (A/cm^2) ... I_cathode = 0.000014 (A/cm^2) ... dI_mea = -0.000000 (A/cm^2) ... dI_stk = -0.000000 (A/cm^2)

14 4.0806e-02 1.4250e-05 7.3397e-05 3.2516e-04 2.1237e-07 1.6006e-04 5.9932e-06 5.1904e-01 1.2998e-14 9.4152e-05 2.8538e-02 0:18:01 136

V_cell = 2.725000 (V) ... V_open = 2.800000 (V)

I_anode = 0.000013 (A/cm^2) ... I_cathode = 0.000014 (A/cm^2) ... dI_mea = -0.000000 (A/cm^2) ... dI_stk = -0.000000 (A/cm^2)

15 3.4135e-02 1.1823e-05 6.5622e-05 2.7597e-04 1.9031e-07 1.5945e-04 5.9056e-06 8.1720e-01 1.1507e-14 8.6204e-05 2.5689e-02 0:17:28 135

V_cell = 2.725000 (V) ... V_open = 2.800000 (V)

I_anode = 0.000013 (A/cm^2) ... I_cathode = 0.000014 (A/cm^2) ... dI_mea = -0.000000 (A/cm^2) ... dI_stk = -0.000000 (A/cm^2)

16 2.8830e-02 9.6251e-06 5.3832e-05 2.3876e-04 1.6828e-07 1.5887e-04 5.8413e-06 1.3115e+00 1.0287e-14 8.1683e-05 2.3222e-02 0:17:00 134

V_cell = 2.725000 (V) ... V_open = 2.800000 (V)

I_anode = 0.000013 (A/cm^2) ... I_cathode = 0.000014 (A/cm^2) ... dI_mea = -0.000000 (A/cm^2) ... dI_stk = -0.000000 (A/cm^2)

17 2.4521e-02 7.6485e-06 4.5315e-05 2.0729e-04 1.4907e-07 1.5787e-04 5.8079e-06 2.2081e+00 1.0276e-14 7.8411e-05 2.1070e-02 0:16:36 133

V_cell = 2.725000 (V) ... V_open = 2.800000 (V)

I_anode = 0.000013 (A/cm^2) ... I_cathode = 0.000013 (A/cm^2) ... dI_mea = -0.000000 (A/cm^2) ... dI_stk = -0.000000 (A/cm^2)

18 2.1106e-02 6.2162e-06 3.0683e-05 1.8040e-04 1.2486e-07 1.5708e-04 5.8262e-06 3.6220e+00 9.7984e-15 7.6156e-05 1.9179e-02 0:16:15 132

V_cell = 2.725000 (V) ... V_open = 2.800000 (V)

I_anode = 0.000013 (A/cm^2) ... I_cathode = 0.000013 (A/cm^2) ... dI_mea = -0.000000 (A/cm^2) ... dI_stk = -0.000000 (A/cm^2)

19 1.8174e-02 5.1728e-06 3.0171e-05 1.5730e-04 1.1167e-07 1.5649e-04 5.7916e-06 4.8901e+00 8.6669e-15 7.4136e-05 1.7508e-02 0:15:58 131

V_cell = 2.725000 (V) ... V_open = 2.800000 (V)

I_anode = 0.000013 (A/cm^2) ... I_cathode = 0.000013 (A/cm^2) ... dI_mea = -0.000000 (A/cm^2) ... dI_stk = -0.000000 (A/cm^2)

20 1.5645e-02 4.3187e-06 2.7098e-05 1.3837e-04 9.9076e-08 1.5568e-04 5.7620e-06 5.5536e+00 9.0299e-15 7.2380e-05 1.6022e-02 0:15:42 130

V_cell = 2.725000 (V) ... V_open = 2.800000 (V)

I_anode = 0.000013 (A/cm^2) ... I_cathode = 0.000013 (A/cm^2) ... dI_mea = -0.000000 (A/cm^2) ... dI_stk = -0.000000 (A/cm^2)

21 1.3570e-02 3.6411e-06 2.6305e-05 1.2230e-04 8.9919e-08 1.5496e-04 5.7197e-06 5.9752e+00 9.3757e-15 7.0548e-05 1.4696e-02 0:15:29 129

V_cell = 2.725000 (V) ... V_open = 2.800000 (V)

I_anode = 0.000013 (A/cm^2) ... I_cathode = 0.000013 (A/cm^2) ... dI_mea = -0.000000 (A/cm^2) ... dI_stk = -0.000000 (A/cm^2)

22 1.1830e-02 3.0331e-06 1.9160e-05 1.0776e-04 7.5853e-08 1.5442e-04 5.7071e-06 6.1326e+00 9.4480e-15 6.9189e-05 1.3506e-02 0:15:16 128

V_cell = 2.725000 (V) ... V_open = 2.800000 (V)

I_anode = 0.000013 (A/cm^2) ... I_cathode = 0.000013 (A/cm^2) ... dI_mea = -0.000000 (A/cm^2) ... dI_stk = -0.000000 (A/cm^2)

iter continuity x-velocity y-velocity z-velocity energy h2 o2 h2o uds-0 uds-1 uds-3 time/iter

23 1.0386e-02 2.5338e-06 2.0045e-05 9.4571e-05 6.9882e-08 1.5399e-04 5.6856e-06 6.3413e+00 8.9240e-15 6.8146e-05 1.2435e-02 0:15:05 127

V_cell = 2.725000 (V)   ... V_open   = 2.800000 (V)
I_anode = 0.000013 (A/cm^2) ... I_cathode = 0.000013 (A/cm^2) ... dI_mea = -0.000000 (A/cm^2) ... dI_stk = -0.000000 (A/cm^2)
24 9.1067e-03 2.2416e-06 1.3827e-05 8.2339e-05 6.7805e-08 1.5477e-04 5.6263e-06 6.4204e+00 1.0315e-14 6.6292e-05 1.1468e-02 0:14:55 126
V_cell = 2.725000 (V)   ... V_open   = 2.800000 (V)
I_anode = 0.000013 (A/cm^2) ... I_cathode = 0.000013 (A/cm^2) ... dI_mea = -0.000000 (A/cm^2) ... dI_stk = -0.000000 (A/cm^2)
25 7.9690e-03 2.0355e-06 1.8605e-05 7.2629e-05 7.2708e-08 1.5373e-04 5.6362e-06 6.5756e+00 9.8874e-15 6.5523e-05 1.0592e-02 0:14:45 125
V_cell = 2.725000 (V)   ... V_open   = 2.800000 (V)
I_anode = 0.000013 (A/cm^2) ... I_cathode = 0.000013 (A/cm^2) ... dI_mea = 0.000000 (A/cm^2) ... dI_stk = 0.000000 (A/cm^2)
26 6.9766e-03 1.8825e-06 1.0559e-05 6.3324e-05 6.0126e-08 1.5441e-04 5.6178e-06 6.6192e+00 1.0150e-14 6.3843e-05 9.7951e-03 0:14:36 124
V_cell = 2.725000 (V)   ... V_open   = 2.800000 (V)
I_anode = 0.000013 (A/cm^2) ... I_cathode = 0.000013 (A/cm^2) ... dI_mea = -0.000000 (A/cm^2) ... dI_stk = -0.000000 (A/cm^2)
27 6.0349e-03 1.7267e-06 1.4888e-05 5.6892e-05 6.0966e-08 1.5351e-04 5.6369e-06 6.7246e+00 9.6839e-15 6.3292e-05 9.0696e-03 0:14:27 123
V_cell = 2.725000 (V)   ... V_open   = 2.800000 (V)
I_anode = 0.000013 (A/cm^2) ... I_cathode = 0.000013 (A/cm^2) ... dI_mea = 0.000000 (A/cm^2) ... dI_stk = 0.000000 (A/cm^2)
28 5.2364e-03 1.5305e-06 9.3870e-06 5.0576e-05 4.9424e-08 1.5384e-04 5.5983e-06 6.7320e+00 1.0045e-14 6.1740e-05 8.4072e-03 0:14:19 122
V_cell = 2.725000 (V)   ... V_open   = 2.800000 (V)
I_anode = 0.000013 (A/cm^2) ... I_cathode = 0.000013 (A/cm^2) ... dI_mea = -0.000000 (A/cm^2) ... dI_stk = -0.000000 (A/cm^2)
29 4.5366e-03 1.3147e-06 1.2615e-05 4.5560e-05 5.1668e-08 1.5325e-04 5.6284e-06 6.7886e+00 9.8204e-15 6.1284e-05 7.8010e-03 0:14:11 121
V_cell = 2.725000 (V)   ... V_open   = 2.800000 (V)
I_anode = 0.000013 (A/cm^2) ... I_cathode = 0.000013 (A/cm^2) ... dI_mea = 0.000000 (A/cm^2) ... dI_stk = 0.000000 (A/cm^2)
30 3.9579e-03 1.0842e-06 8.1223e-06 4.0330e-05 4.5922e-08 1.5375e-04 5.6011e-06 6.7681e+00 9.9791e-15 5.9829e-05 7.2453e-03 0:14:03 120
V_cell = 2.725000 (V)   ... V_open   = 2.800000 (V)
I_anode = 0.000013 (A/cm^2) ... I_cathode = 0.000013 (A/cm^2) ... dI_mea = -0.000000 (A/cm^2) ... dI_stk = -0.000000 (A/cm^2)
31 3.4354e-03 9.2079e-07 1.0764e-05 3.6565e-05 4.7554e-08 1.5310e-04 5.6250e-06 6.7826e+00 9.7894e-15 5.9492e-05 6.7349e-03 0:13:32 119
V_cell = 2.725000 (V)   ... V_open   = 2.800000 (V)
I_anode = 0.000013 (A/cm^2) ... I_cathode = 0.000013 (A/cm^2) ... dI_mea = 0.000000 (A/cm^2) ... dI_stk = 0.000000 (A/cm^2)
32 3.0206e-03 8.0625e-07 7.4770e-06 3.2807e-05 4.2633e-08 1.5357e-04 5.5980e-06

6.7288e+00 9.9461e-15 5.8095e-05 6.2653e-03 0:13:29 118
V_cell = 2.725000 (V) ... V_open = 2.800000 (V)
I_anode = 0.000013 (A/cm^2) ... I_cathode = 0.000013 (A/cm^2) ... dI_mea = -0.000000 (A/cm^2) ... dI_stk = -0.000000 (A/cm^2)
33 2.6291e-03 7.1186e-07 9.2050e-06 2.9501e-05 4.4652e-08 1.5287e-04 5.6155e-06 6.7048e+00 9.6428e-15 5.7812e-05 5.8327e-03 0:13:26 117
V_cell = 2.725000 (V) ... V_open = 2.800000 (V)
I_anode = 0.000013 (A/cm^2) ... I_cathode = 0.000013 (A/cm^2) ... dI_mea = 0.000000 (A/cm^2) ... dI_stk = 0.000000 (A/cm^2)
iter continuity x-velocity y-velocity z-velocity energy h2 o2 h2o uds-0 uds-1 uds-3 time/iter
34 2.3249e-03 6.2240e-07 6.7715e-06 2.6286e-05 3.8255e-08 1.5332e-04 5.5887e-06 6.6265e+00 9.8245e-15 5.6456e-05 5.4336e-03 0:13:21 116
V_cell = 2.725000 (V) ... V_open = 2.800000 (V)
I_anode = 0.000013 (A/cm^2) ... I_cathode = 0.000013 (A/cm^2) ... dI_mea = -0.000000 (A/cm^2) ... dI_stk = -0.000000 (A/cm^2)
35 2.0448e-03 5.5300e-07 8.1568e-06 2.3854e-05 3.8328e-08 1.5288e-04 5.6265e-06 6.5700e+00 9.3731e-15 5.6318e-05 5.0649e-03 0:13:17 115
V_cell = 2.725000 (V) ... V_open = 2.800000 (V)
I_anode = 0.000013 (A/cm^2) ... I_cathode = 0.000013 (A/cm^2) ... dI_mea = 0.000000 (A/cm^2) ... dI_stk = 0.000000 (A/cm^2)
36 1.8273e-03 4.9673e-07 6.7775e-06 2.1518e-05 3.8441e-08 1.5346e-04 5.5998e-06 6.4641e+00 9.7354e-15 5.4968e-05 4.7239e-03 0:13:11 114
V_cell = 2.725000 (V) ... V_open = 2.800000 (V)
I_anode = 0.000013 (A/cm^2) ... I_cathode = 0.000013 (A/cm^2) ... dI_mea = -0.000000 (A/cm^2) ... dI_stk = -0.000000 (A/cm^2)
37 1.6309e-03 4.4251e-07 7.1795e-06 1.9384e-05 3.7531e-08 1.5289e-04 5.6314e-06 6.3803e+00 9.1567e-15 5.4839e-05 4.4082e-03 0:13:06 113
V_cell = 2.725000 (V) ... V_open = 2.800000 (V)
I_anode = 0.000013 (A/cm^2) ... I_cathode = 0.000013 (A/cm^2) ... dI_mea = 0.000000 (A/cm^2) ... dI_stk = 0.000000 (A/cm^2)
38 1.4797e-03 3.9899e-07 6.1221e-06 1.7454e-05 3.5427e-08 1.5342e-04 5.6014e-06 6.2570e+00 9.6438e-15 5.3547e-05 4.1155e-03 0:13:00 112
V_cell = 2.725000 (V) ... V_open = 2.800000 (V)
I_anode = 0.000013 (A/cm^2) ... I_cathode = 0.000013 (A/cm^2) ... dI_mea = -0.000000 (A/cm^2) ... dI_stk = -0.000000 (A/cm^2)
39 1.3365e-03 3.6854e-07 6.9061e-06 1.5954e-05 3.6182e-08 1.5283e-04 5.6303e-06 6.1484e+00 9.2852e-15 5.3478e-05 3.8441e-03 0:12:54 111
V_cell = 2.725000 (V) ... V_open = 2.800000 (V)
I_anode = 0.000013 (A/cm^2) ... I_cathode = 0.000013 (A/cm^2) ... dI_mea = 0.000000 (A/cm^2) ... dI_stk = 0.000000 (A/cm^2)
40 1.2171e-03 3.4485e-07 6.2494e-06 1.4578e-05 3.4722e-08 1.5337e-04 5.6035e-06 6.0092e+00 9.6373e-15 5.2221e-05 3.5920e-03 0:12:47 110
V_cell = 2.725000 (V) ... V_open = 2.800000 (V)

I_anode = 0.000013 (A/cm^2) ... I_cathode = 0.000013 (A/cm^2) ... dI_mea = -0.000000 (A/cm^2) ... dI_stk = -0.000000 (A/cm^2)
41 1.1117e-03 3.1669e-07 6.5479e-06 1.3229e-05 3.4344e-08 1.5279e-04 5.6312e-06 5.8794e+00 9.2616e-15 5.2176e-05 3.3578e-03 0:12:41 109
V_cell = 2.725000 (V) ... V_open = 2.800000 (V)
I_anode = 0.000013 (A/cm^2) ... I_cathode = 0.000013 (A/cm^2) ... dI_mea = 0.000000 (A/cm^2) ... dI_stk = 0.000000 (A/cm^2)
42 1.0353e-03 2.9484e-07 5.9249e-06 1.2062e-05 3.2911e-08 1.5336e-04 5.6055e-06 5.7306e+00 9.5108e-15 5.0951e-05 3.1399e-03 0:12:34 108
V_cell = 2.725000 (V) ... V_open = 2.800000 (V)
I_anode = 0.000013 (A/cm^2) ... I_cathode = 0.000013 (A/cm^2) ... dI_mea = -0.000000 (A/cm^2) ... dI_stk = -0.000000 (A/cm^2)
43 9.5991e-04 2.7672e-07 6.2697e-06 1.1070e-05 3.3409e-08 1.5281e-04 5.6363e-06 5.5866e+00 9.1994e-15 5.0960e-05 2.9372e-03 0:12:06 107
V_cell = 2.725000 (V) ... V_open = 2.800000 (V)
I_anode = 0.000013 (A/cm^2) ... I_cathode = 0.000013 (A/cm^2) ... dI_mea = 0.000000 (A/cm^2) ... dI_stk = 0.000000 (A/cm^2)
44 8.9399e-04 2.6548e-07 6.0031e-06 1.0257e-05 3.2670e-08 1.5333e-04 5.6067e-06 5.4279e+00 9.4534e-15 4.9752e-05 2.7485e-03 0:12:04 106
V_cell = 2.725000 (V) ... V_open = 2.800000 (V)
I_anode = 0.000013 (A/cm^2) ... I_cathode = 0.000013 (A/cm^2) ... dI_mea = -0.000000 (A/cm^2) ... dI_stk = -0.000000 (A/cm^2)
iter continuity x-velocity y-velocity z-velocity energy h2 o2 h2o uds-0 uds-1 uds-3 time/iter
45 8.3587e-04 2.5023e-07 6.0134e-06 9.3472e-06 3.3296e-08 1.5269e-04 5.6291e-06 5.2708e+00 9.0648e-15 4.9770e-05 2.5726e-03 0:12:01 105
V_cell = 2.725000 (V) ... V_open = 2.800000 (V)
I_anode = 0.000013 (A/cm^2) ... I_cathode = 0.000013 (A/cm^2) ... dI_mea = 0.000000 (A/cm^2) ... dI_stk = 0.000000 (A/cm^2)
46 7.8684e-04 2.3872e-07 5.6954e-06 8.6484e-06 3.0280e-08 1.5319e-04 5.6002e-06 5.1101e+00 9.4061e-15 4.8586e-05 2.4086e-03 0:11:57 104
V_cell = 2.725000 (V) ... V_open = 2.800000 (V)
I_anode = 0.000013 (A/cm^2) ... I_cathode = 0.000013 (A/cm^2) ... dI_mea = -0.000000 (A/cm^2) ... dI_stk = -0.000000 (A/cm^2)
47 7.4547e-04 2.3076e-07 6.0674e-06 7.9781e-06 2.9964e-08 1.5278e-04 5.6401e-06 4.9453e+00 9.0806e-15 4.8666e-05 2.2557e-03 0:11:52 103
V_cell = 2.725000 (V) ... V_open = 2.800000 (V)
I_anode = 0.000013 (A/cm^2) ... I_cathode = 0.000013 (A/cm^2) ... dI_mea = 0.000000 (A/cm^2) ... dI_stk = 0.000000 (A/cm^2)
48 7.0566e-04 2.2397e-07 5.9132e-06 7.4766e-06 3.1427e-08 1.5330e-04 5.6094e-06 4.7791e+00 9.3703e-15 4.7492e-05 2.1130e-03 0:11:47 102
V_cell = 2.725000 (V) ... V_open = 2.800000 (V)
I_anode = 0.000013 (A/cm^2) ... I_cathode = 0.000013 (A/cm^2) ... dI_mea = -0.000000 (A/cm^2) ... dI_stk = -0.000000 (A/cm^2)

49 6.7417e-04 2.1250e-07 5.8282e-06 6.8277e-06 3.0688e-08 1.5277e-04 5.6399e-06 4.6097e+00 8.9467e-15 4.7572e-05 1.9797e-03 0:11:21 101

V_cell = 2.725000 (V) ... V_open = 2.800000 (V)

I_anode = 0.000013 (A/cm^2) ... I_cathode = 0.000013 (A/cm^2) ... dI_mea = 0.000000 (A/cm^2) ... dI_stk = 0.000000 (A/cm^2)

50 6.4318e-04 2.0557e-07 5.6123e-06 6.3905e-06 3.0083e-08 1.5331e-04 5.6109e-06 4.4451e+00 9.2765e-15 4.6418e-05 1.8552e-03 0:11:20 100

V_cell = 2.725000 (V) ... V_open = 2.800000 (V)

I_anode = 0.000013 (A/cm^2) ... I_cathode = 0.000013 (A/cm^2) ... dI_mea = -0.000000 (A/cm^2) ... dI_stk = -0.000000 (A/cm^2)

A5: Mesh of the Small Dendrite Anode Model

Details of "Mesh"

Defaults	
Physics Preference	Mechanical
Relevance	0
Sizing	
Use Advanced Size Fun...	Off
Relevance Center	Coarse
Element Size	Default
Initial Size Seed	Active Assembly
Smoothing	Medium
Transition	Fast
Span Angle Center	Coarse
Minimum Edge Length	4.e-003 mm
Inflation	
Use Automatic Inflation	None
Inflation Option	Smooth Transition
Transition Ratio	0.272
Maximum Layers	5
Growth Rate	1.2
Inflation Algorithm	Pre
View Advanced Options	No
Patch Conforming Options	
Triangle Surface Mesher	Program Controlled
Patch Independent Options	
Topology Checking	Yes
Advanced	
Number of CPUs for Pa...	Program Controlled
Shape Checking	Standard Mechanical
Element Midside Nodes	Program Controlled
Straight Sided Elements	No
Number of Retries	Default (4)
Extra Retries For Assem...	Yes
Rigid Body Behavior	Dimensionally Reduced
Mesh Morphing	Disabled
Defeaturing	
Pinch Tolerance	Please Define
Generate Pinch on Ref...	No
Automatic Mesh Based...	On
Defeaturing Tolerance	Default
Statistics	
Nodes	1228783
Elements	296700
Mesh Metric	None

Figure A5: Mesh details of the small dendrite anode model

A6: Fluent Iterations of Small Dendrite Anode Model

Below are the first 50 iterations of calculations for the small dendrite anode model calculated with a porosity of 0.75 at a discharge voltage of 2.60 V.

```
iter  continuity  x-velocity  y-velocity  z-velocity     energy        h2        o2       h2o
uds-0      uds-1      uds-3    time/iter
       V_cell  = 2.600000 (V)      ... V_open    = 2.800000 (V)
       I_anode = 0.010134 (A/cm^2) ... I_cathode = 0.010134 (A/cm^2) ... dI_mea = 0.000000
(A/cm^2) ... dI_stk = 0.000000 (A/cm^2)
     1  1.0000e+00  0.0000e+00  4.9369e-06  2.1999e-01  3.7008e-06  2.0550e-04  1.1444e-05
0.0000e+00  4.4781e-10  1.2922e-01  0.0000e+00  0:21:23  149
       V_cell  = 2.600000 (V)      ... V_open    = 2.800000 (V)
       I_anode = 0.002934 (A/cm^2) ... I_cathode = 0.004160 (A/cm^2) ... dI_mea = -0.001226
(A/cm^2) ... dI_stk = -0.001226 (A/cm^2)
     2  6.1885e-01  1.8750e-03  3.6890e-03  3.4311e-02  6.5899e-06  5.8584e-04  2.9591e-05
0.0000e+00  5.3328e-10  2.7228e-02  0.0000e+00  0:21:26  148
       V_cell  = 2.600000 (V)      ... V_open    = 2.800000 (V)
       I_anode = 0.000788 (A/cm^2) ... I_cathode = 0.001919 (A/cm^2) ... dI_mea = -0.001130
(A/cm^2) ... dI_stk = -0.001130 (A/cm^2)
     3  5.7183e-01  5.8999e-04  3.2941e-03  7.4122e-03  5.1706e-06  4.4162e-04  1.9990e-05
0.0000e+00  1.4661e-10  6.5297e-03  0.0000e+00  0:21:56  147
       V_cell  = 2.600000 (V)      ... V_open    = 2.800000 (V)
       I_anode = 0.000863 (A/cm^2) ... I_cathode = 0.000877 (A/cm^2) ... dI_mea = -0.000014
(A/cm^2) ... dI_stk = -0.000014 (A/cm^2)
     4  4.0720e-01  2.3525e-04  9.7622e-04  3.3972e-03  3.0524e-06  3.2553e-04  2.4193e-05
0.0000e+00  8.1985e-11  1.4933e-03  0.0000e+00  0:21:19  146
       V_cell  = 2.600000 (V)      ... V_open    = 2.800000 (V)
       I_anode = 0.000792 (A/cm^2) ... I_cathode = 0.000839 (A/cm^2) ... dI_mea = -0.000046
(A/cm^2) ... dI_stk = -0.000046 (A/cm^2)
 reversed flow in 2 faces on pressure-outlet 47.
     5  2.6466e-01  1.2065e-04  4.8766e-04  2.3049e-03  1.8056e-06  2.0548e-04  1.0624e-05
0.0000e+00  3.8557e-11  8.5721e-04  0.0000e+00  0:21:17  145
       V_cell  = 2.600000 (V)      ... V_open    = 2.800000 (V)
       I_anode = 0.000840 (A/cm^2) ... I_cathode = 0.000821 (A/cm^2) ... dI_mea = 0.000019
(A/cm^2) ... dI_stk = 0.000019 (A/cm^2)
     6  2.1031e-01  7.3529e-05  2.8378e-04  1.8677e-03  1.1837e-06  1.8032e-04  8.6765e-06
3.1538e-01  1.6925e-11  4.2697e-04  7.7621e-02  0:21:14  144
       V_cell  = 2.600000 (V)      ... V_open    = 2.800000 (V)
```

I_anode = 0.000798 (A/cm^2) ... I_cathode = 0.000834 (A/cm^2) ... dI_mea = -0.000036 (A/cm^2) ... dI_stk = -0.000036 (A/cm^2)
7 1.5824e-01 5.4304e-05 2.0622e-04 1.4845e-03 8.1195e-07 1.7268e-04 7.5240e-06 2.4869e-01 7.5596e-12 3.4568e-04 6.4165e-02 0:21:09 143
V_cell = 2.600000 (V)   ... V_open   = 2.800000 (V)
I_anode = 0.000776 (A/cm^2) ... I_cathode = 0.000818 (A/cm^2) ... dI_mea = -0.000042 (A/cm^2) ... dI_stk = -0.000042 (A/cm^2)
8 1.2879e-01 4.4778e-05 2.0502e-04 1.1533e-03 6.1793e-07 1.7037e-04 7.2449e-06 1.1749e-01 3.9532e-12 2.6980e-04 5.4175e-02 0:20:36 142
V_cell = 2.600000 (V)   ... V_open   = 2.800000 (V)
I_anode = 0.000769 (A/cm^2) ... I_cathode = 0.000800 (A/cm^2) ... dI_mea = -0.000031 (A/cm^2) ... dI_stk = -0.000031 (A/cm^2)
9 1.0391e-01 3.7916e-05 1.8781e-04 9.0297e-04 5.2692e-07 1.6832e-04 6.8940e-06 5.2368e-02 2.1939e-12 2.1677e-04 4.6478e-02 0:20:35 141
V_cell = 2.600000 (V)   ... V_open   = 2.800000 (V)
I_anode = 0.000761 (A/cm^2) ... I_cathode = 0.000787 (A/cm^2) ... dI_mea = -0.000026 (A/cm^2) ... dI_stk = -0.000026 (A/cm^2)
10 8.7866e-02 2.8849e-05 1.5549e-04 7.0535e-04 4.2610e-07 1.6509e-04 6.7042e-06 3.6438e-02 1.6522e-12 2.1919e-04 4.0375e-02 0:20:33 140
V_cell = 2.600000 (V)   ... V_open   = 2.800000 (V)
I_anode = 0.000742 (A/cm^2) ... I_cathode = 0.000775 (A/cm^2) ... dI_mea = -0.000033 (A/cm^2) ... dI_stk = -0.000033 (A/cm^2)
11 7.2603e-02 2.1847e-05 1.2600e-04 5.6509e-04 3.2875e-07 1.6528e-04 6.4799e-06 3.0788e-02 1.4345e-12 1.7874e-04 3.5426e-02 0:20:02 139
V_cell = 2.600000 (V)   ... V_open   = 2.800000 (V)
I_anode = 0.000743 (A/cm^2) ... I_cathode = 0.000761 (A/cm^2) ... dI_mea = -0.000018 (A/cm^2) ... dI_stk = -0.000018 (A/cm^2)
iter continuity x-velocity y-velocity z-velocity   energy   h2   o2   h2o   uds-0   uds-1   uds-3   time/iter
12 5.9546e-02 1.7188e-05 1.0445e-04 4.6416e-04 2.8938e-07 1.6392e-04 6.2273e-06 2.7737e-02 9.3267e-13 1.3683e-04 3.1430e-02 0:20:03 138
V_cell = 2.600000 (V)   ... V_open   = 2.800000 (V)
I_anode = 0.000740 (A/cm^2) ... I_cathode = 0.000754 (A/cm^2) ... dI_mea = -0.000014 (A/cm^2) ... dI_stk = -0.000014 (A/cm^2)
13 4.9089e-02 1.4947e-05 8.8155e-05 3.8761e-04 2.4674e-07 1.6280e-04 6.1271e-06 2.5975e-02 7.9064e-13 1.0686e-04 2.7968e-02 0:20:02 137
V_cell = 2.600000 (V)   ... V_open   = 2.800000 (V)
I_anode = 0.000738 (A/cm^2) ... I_cathode = 0.000749 (A/cm^2) ... dI_mea = -0.000012 (A/cm^2) ... dI_stk = -0.000012 (A/cm^2)
14 4.0861e-02 1.2994e-05 7.3940e-05 3.2499e-04 2.0966e-07 1.6205e-04 6.0510e-06 2.4646e-02 6.2661e-13 9.2244e-05 2.5048e-02 0:19:32 136
V_cell = 2.600000 (V)   ... V_open   = 2.800000 (V)
I_anode = 0.000733 (A/cm^2) ... I_cathode = 0.000745 (A/cm^2) ... dI_mea = -0.000012 (A/cm^2) ... dI_stk = -0.000012 (A/cm^2)

15 3.4227e-02 1.0786e-05 6.0345e-05 2.7496e-04 1.9325e-07 1.6101e-04 5.9583e-06 1.7382e-02 5.3725e-13 7.2565e-05 2.2545e-02 0:19:34 135
V_cell = 2.600000 (V) ... V_open = 2.800000 (V)
I_anode = 0.000732 (A/cm^2) ... I_cathode = 0.000740 (A/cm^2) ... dI_mea = -0.000008 (A/cm^2) ... dI_stk = -0.000008 (A/cm^2)
16 2.8876e-02 8.7882e-06 5.2917e-05 2.3834e-04 1.6676e-07 1.6011e-04 5.9220e-06 9.4892e-03 4.0135e-13 5.7205e-05 2.0379e-02 0:19:33 134
V_cell = 2.600000 (V) ... V_open = 2.800000 (V)
I_anode = 0.000731 (A/cm^2) ... I_cathode = 0.000737 (A/cm^2) ... dI_mea = -0.000006 (A/cm^2) ... dI_stk = -0.000006 (A/cm^2)
17 2.4622e-02 6.9455e-06 3.9922e-05 2.0706e-04 1.4500e-07 1.5926e-04 5.9134e-06 6.6872e-03 4.0087e-13 5.7820e-05 1.8490e-02 0:19:04 133
V_cell = 2.600000 (V) ... V_open = 2.800000 (V)
I_anode = 0.000725 (A/cm^2) ... I_cathode = 0.000735 (A/cm^2) ... dI_mea = -0.000009 (A/cm^2) ... dI_stk = -0.000009 (A/cm^2)
18 2.1072e-02 5.6497e-06 4.0416e-05 1.8076e-04 1.3556e-07 1.5837e-04 5.8692e-06 5.0361e-03 5.4203e-13 4.3087e-05 1.6830e-02 0:19:06 132
V_cell = 2.600000 (V) ... V_open = 2.800000 (V)
I_anode = 0.000733 (A/cm^2) ... I_cathode = 0.000731 (A/cm^2) ... dI_mea = 0.000001 (A/cm^2) ... dI_stk = 0.000001 (A/cm^2)
19 1.8279e-02 4.6886e-06 2.6419e-05 1.5732e-04 1.1175e-07 1.5721e-04 5.9050e-06 4.2059e-03 4.7462e-13 3.0095e-05 1.5362e-02 0:19:06 131
V_cell = 2.600000 (V) ... V_open = 2.800000 (V)
I_anode = 0.000727 (A/cm^2) ... I_cathode = 0.000732 (A/cm^2) ... dI_mea = -0.000005 (A/cm^2) ... dI_stk = -0.000005 (A/cm^2)
20 1.5705e-02 3.9116e-06 2.6134e-05 1.3824e-04 1.0152e-07 1.5616e-04 5.8838e-06 3.7051e-03 2.0497e-13 2.1108e-05 1.4058e-02 0:18:38 130
V_cell = 2.600000 (V) ... V_open = 2.800000 (V)
I_anode = 0.000728 (A/cm^2) ... I_cathode = 0.000730 (A/cm^2) ... dI_mea = -0.000003 (A/cm^2) ... dI_stk = -0.000003 (A/cm^2)
21 1.3647e-02 3.2871e-06 2.2974e-05 1.2199e-04 8.9480e-08 1.5533e-04 5.8889e-06 3.8966e-03 1.4821e-13 1.8738e-05 1.2894e-02 0:18:39 129
V_cell = 2.600000 (V) ... V_open = 2.800000 (V)
I_anode = 0.000726 (A/cm^2) ... I_cathode = 0.000729 (A/cm^2) ... dI_mea = -0.000003 (A/cm^2) ... dI_stk = -0.000003 (A/cm^2)
22 1.1912e-02 2.7390e-06 1.9487e-05 1.0758e-04 6.9194e-08 1.5557e-04 5.9713e-06 3.9450e-03 1.4767e-13 1.6502e-05 1.1850e-02 0:18:13 128
V_cell = 2.600000 (V) ... V_open = 2.800000 (V)
I_anode = 0.000726 (A/cm^2) ... I_cathode = 0.000728 (A/cm^2) ... dI_mea = -0.000002 (A/cm^2) ... dI_stk = -0.000002 (A/cm^2)
iter continuity x-velocity y-velocity z-velocity energy h2 o2 h2o uds-0 uds-1 uds-3 time/iter
23 1.0503e-02 2.3017e-06 1.7770e-05 9.4322e-05 6.4484e-08 1.5543e-04 6.0010e-06 3.2748e-03 2.1328e-13 2.1605e-05 1.0910e-02 0:18:17 127

V_cell = 2.600000 (V)   ... V_open   = 2.800000 (V)
I_anode = 0.000722 (A/cm^2) ... I_cathode = 0.000727 (A/cm^2) ... dI_mea = -0.000005 (A/cm^2) ... dI_stk = -0.000005 (A/cm^2)
24 9.2120e-03 2.0388e-06 1.7153e-05 8.2314e-05 6.3677e-08 1.5511e-04 5.9999e-06 2.4756e-03 3.9251e-13 2.5354e-05 1.0061e-02 0:18:17 126
V_cell = 2.600000 (V)   ... V_open   = 2.800000 (V)
I_anode = 0.000729 (A/cm^2) ... I_cathode = 0.000725 (A/cm^2) ... dI_mea = 0.000003 (A/cm^2) ... dI_stk = 0.000003 (A/cm^2)
25 8.1701e-03 1.8485e-06 9.3656e-06 7.1638e-05 5.2112e-08 1.5493e-04 6.0332e-06 1.8485e-03 3.9058e-13 1.5352e-05 9.2919e-03 0:17:51 125
V_cell = 2.600000 (V)   ... V_open   = 2.800000 (V)
I_anode = 0.000724 (A/cm^2) ... I_cathode = 0.000727 (A/cm^2) ... dI_mea = -0.000003 (A/cm^2) ... dI_stk = -0.000003 (A/cm^2)
26 7.1696e-03 1.7214e-06 9.5509e-06 6.3076e-05 5.2260e-08 1.5459e-04 6.0271e-06 1.4082e-03 1.5834e-13 1.1214e-05 8.5931e-03 0:17:53 124
V_cell = 2.600000 (V)   ... V_open   = 2.800000 (V)
I_anode = 0.000723 (A/cm^2) ... I_cathode = 0.000725 (A/cm^2) ... dI_mea = -0.000002 (A/cm^2) ... dI_stk = -0.000002 (A/cm^2)
27 6.2871e-03 1.5782e-06 1.1413e-05 5.6342e-05 4.2760e-08 1.5506e-04 6.0989e-06 1.1875e-03 1.5541e-13 1.1901e-05 7.9564e-03 0:17:28 123
V_cell = 2.600000 (V)   ... V_open   = 2.800000 (V)
I_anode = 0.000726 (A/cm^2) ... I_cathode = 0.000725 (A/cm^2) ... dI_mea = 0.000001 (A/cm^2) ... dI_stk = 0.000001 (A/cm^2)
28 5.4794e-03 1.3947e-06 8.6047e-06 5.0416e-05 3.8848e-08 1.5455e-04 6.0827e-06 1.0302e-03 1.8914e-13 8.3832e-06 7.3752e-03 0:17:31 122
V_cell = 2.600000 (V)   ... V_open   = 2.800000 (V)
I_anode = 0.000724 (A/cm^2) ... I_cathode = 0.000725 (A/cm^2) ... dI_mea = -0.000001 (A/cm^2) ... dI_stk = -0.000001 (A/cm^2)
29 4.8516e-03 1.1823e-06 5.2440e-06 4.4804e-05 3.1674e-08 1.5507e-04 6.1322e-06 9.1204e-04 1.5313e-13 1.1803e-05 6.8433e-03 0:17:32 121
V_cell = 2.600000 (V)   ... V_open   = 2.800000 (V)
I_anode = 0.000722 (A/cm^2) ... I_cathode = 0.000724 (A/cm^2) ... dI_mea = -0.000002 (A/cm^2) ... dI_stk = -0.000002 (A/cm^2)
30 4.2729e-03 9.8612e-07 9.6440e-06 4.0255e-05 5.2399e-08 1.5376e-04 6.0227e-06 8.3375e-04 2.3810e-13 1.4409e-05 6.3557e-03 0:17:07 120
V_cell = 2.600000 (V)   ... V_open   = 2.800000 (V)
I_anode = 0.000726 (A/cm^2) ... I_cathode = 0.000724 (A/cm^2) ... dI_mea = 0.000003 (A/cm^2) ... dI_stk = 0.000003 (A/cm^2)
31 3.8173e-03 8.1540e-07 4.7282e-06 3.6004e-05 3.9735e-08 1.5449e-04 6.1355e-06 7.8070e-04 2.9023e-13 1.3740e-05 5.9079e-03 0:17:09 119
V_cell = 2.600000 (V)   ... V_open   = 2.800000 (V)
I_anode = 0.000722 (A/cm^2) ... I_cathode = 0.000725 (A/cm^2) ... dI_mea = -0.000003 (A/cm^2) ... dI_stk = -0.000003 (A/cm^2)
32 3.3701e-03 7.1217e-07 5.7193e-06 3.2505e-05 2.6944e-08 1.5421e-04 6.1147e-06

7.2791e-04 2.3238e-13 1.0132e-05 5.4960e-03 0:16:45 118
V_cell = 2.600000 (V)   ... V_open   = 2.800000 (V)
I_anode = 0.000725 (A/cm^2) ... I_cathode = 0.000724 (A/cm^2) ... dI_mea = 0.000001 (A/cm^2) ... dI_stk = 0.000001 (A/cm^2)
33 3.0429e-03 6.2955e-07 3.9696e-06 2.8945e-05 2.4709e-08 1.5484e-04 6.1474e-06 6.6412e-04 1.6053e-13 7.9510e-06 5.1164e-03 0:16:48 117
V_cell = 2.600000 (V)   ... V_open   = 2.800000 (V)
I_anode = 0.000723 (A/cm^2) ... I_cathode = 0.000724 (A/cm^2) ... dI_mea = -0.000001 (A/cm^2) ... dI_stk = -0.000001 (A/cm^2)
iter continuity x-velocity y-velocity z-velocity   energy   h2   o2   h2o uds-0   uds-1   uds-3   time/iter
34 2.6977e-03 5.4111e-07 4.6687e-06 2.6021e-05 2.2920e-08 1.5454e-04 6.1527e-06 6.2588e-04 1.0339e-13 4.4380e-06 4.7663e-03 0:16:25 116
V_cell = 2.600000 (V)   ... V_open   = 2.800000 (V)
I_anode = 0.000724 (A/cm^2) ... I_cathode = 0.000723 (A/cm^2) ... dI_mea = 0.000000 (A/cm^2) ... dI_stk = 0.000000 (A/cm^2)
35 2.4509e-03 4.6675e-07 2.8129e-06 2.3305e-05 2.0209e-08 1.5427e-04 6.1466e-06 6.3110e-04 5.3684e-14 2.3508e-06 4.4428e-03 0:16:05 115
V_cell = 2.600000 (V)   ... V_open   = 2.800000 (V)
I_anode = 0.000723 (A/cm^2) ... I_cathode = 0.000724 (A/cm^2) ... dI_mea = -0.000000 (A/cm^2) ... dI_stk = -0.000000 (A/cm^2)
36 2.2271e-03 4.1020e-07 2.0294e-06 2.1006e-05 2.5689e-08 1.5395e-04 6.1150e-06 6.5048e-04 4.1052e-14 3.1132e-06 4.1436e-03 0:15:48 114
V_cell = 2.600000 (V)   ... V_open   = 2.800000 (V)
I_anode = 0.000724 (A/cm^2) ... I_cathode = 0.000724 (A/cm^2) ... dI_mea = 0.000000 (A/cm^2) ... dI_stk = 0.000000 (A/cm^2)
37 2.0522e-03 3.6317e-07 2.6001e-06 1.8898e-05 2.2395e-08 1.5427e-04 6.1581e-06 6.5320e-04 6.1518e-14 4.5252e-06 3.8667e-03 0:15:55 113
V_cell = 2.600000 (V)   ... V_open   = 2.800000 (V)
I_anode = 0.000723 (A/cm^2) ... I_cathode = 0.000724 (A/cm^2) ... dI_mea = -0.000000 (A/cm^2) ... dI_stk = -0.000000 (A/cm^2)
38 1.8913e-03 3.2844e-07 2.4368e-06 1.7063e-05 2.1800e-08 1.5436e-04 6.1443e-06 6.3685e-04 7.5396e-14 4.6996e-06 3.6099e-03 0:15:36 112
V_cell = 2.600000 (V)   ... V_open   = 2.800000 (V)
I_anode = 0.000723 (A/cm^2) ... I_cathode = 0.000723 (A/cm^2) ... dI_mea = -0.000001 (A/cm^2) ... dI_stk = -0.000001 (A/cm^2)
39 1.7672e-03 2.9930e-07 3.3178e-06 1.5527e-05 2.0485e-08 1.5442e-04 6.1662e-06 6.1795e-04 7.9646e-14 4.5174e-06 3.3718e-03 0:15:20 111
V_cell = 2.600000 (V)   ... V_open   = 2.800000 (V)
I_anode = 0.000724 (A/cm^2) ... I_cathode = 0.000723 (A/cm^2) ... dI_mea = 0.000001 (A/cm^2) ... dI_stk = 0.000001 (A/cm^2)
40 1.6403e-03 2.7001e-07 2.0693e-06 1.4174e-05 2.4450e-08 1.5402e-04 6.1152e-06 5.8980e-04 1.1625e-13 7.4552e-06 3.1507e-03 0:15:27 110
V_cell = 2.600000 (V)   ... V_open   = 2.800000 (V)

I_anode = 0.000723 (A/cm^2) ... I_cathode = 0.000723 (A/cm^2) ... dI_mea = 0.000000 (A/cm^2) ... dI_stk = 0.000000 (A/cm^2)
41 1.5475e-03 2.6197e-07 3.7447e-06 1.2881e-05 2.2635e-08 1.5420e-04 6.1435e-06 5.8236e-04 1.3188e-13 6.7407e-06 2.9452e-03 0:15:10 109
V_cell = 2.600000 (V) ... V_open = 2.800000 (V)
I_anode = 0.000724 (A/cm^2) ... I_cathode = 0.000723 (A/cm^2) ... dI_mea = 0.000001 (A/cm^2) ... dI_stk = 0.000001 (A/cm^2)
42 1.4618e-03 2.3913e-07 3.0985e-06 1.1709e-05 1.9742e-08 1.5440e-04 6.1391e-06 5.7558e-04 1.2487e-13 7.1014e-06 2.7541e-03 0:15:15 108
V_cell = 2.600000 (V) ... V_open = 2.800000 (V)
I_anode = 0.000722 (A/cm^2) ... I_cathode = 0.000724 (A/cm^2) ... dI_mea = -0.000002 (A/cm^2) ... dI_stk = -0.000002 (A/cm^2)
43 1.3886e-03 2.1620e-07 3.0129e-06 1.0674e-05 1.8099e-08 1.5434e-04 6.1558e-06 5.8457e-04 1.4647e-13 6.5469e-06 2.5763e-03 0:14:57 107
V_cell = 2.600000 (V) ... V_open = 2.800000 (V)
I_anode = 0.000724 (A/cm^2) ... I_cathode = 0.000723 (A/cm^2) ... dI_mea = 0.000001 (A/cm^2) ... dI_stk = 0.000001 (A/cm^2)
44 1.3017e-03 1.8555e-07 1.1397e-06 9.7625e-06 2.0113e-08 1.5376e-04 6.1097e-06 5.7484e-04 1.0201e-13 5.2346e-06 2.4108e-03 0:15:01 106
V_cell = 2.600000 (V) ... V_open = 2.800000 (V)
I_anode = 0.000724 (A/cm^2) ... I_cathode = 0.000723 (A/cm^2) ... dI_mea = 0.000000 (A/cm^2) ... dI_stk = 0.000000 (A/cm^2)
iter continuity x-velocity y-velocity z-velocity energy h2 o2 h2o uds-0 uds-1 uds-3 time/iter
45 1.2566e-03 1.8363e-07 1.8876e-06 8.8822e-06 1.8989e-08 1.5406e-04 6.1355e-06 5.7734e-04 9.8354e-14 6.0985e-06 2.2565e-03 0:14:42 105
V_cell = 2.600000 (V) ... V_open = 2.800000 (V)
I_anode = 0.000723 (A/cm^2) ... I_cathode = 0.000724 (A/cm^2) ... dI_mea = -0.000000 (A/cm^2) ... dI_stk = -0.000000 (A/cm^2)
46 1.2127e-03 1.8181e-07 2.3843e-06 8.2632e-06 2.2033e-08 1.5396e-04 6.1035e-06 5.5604e-04 9.7839e-14 4.6478e-06 2.1126e-03 0:14:46 104
V_cell = 2.600000 (V) ... V_open = 2.800000 (V)
I_anode = 0.000723 (A/cm^2) ... I_cathode = 0.000723 (A/cm^2) ... dI_mea = -0.000000 (A/cm^2) ... dI_stk = -0.000000 (A/cm^2)
47 1.1732e-03 1.7129e-07 2.5271e-06 7.5545e-06 2.3098e-08 1.5429e-04 6.1625e-06 5.6849e-04 8.2401e-14 4.1854e-06 1.9785e-03 0:14:27 103
V_cell = 2.600000 (V) ... V_open = 2.800000 (V)
I_anode = 0.000724 (A/cm^2) ... I_cathode = 0.000723 (A/cm^2) ... dI_mea = 0.000001 (A/cm^2) ... dI_stk = 0.000001 (A/cm^2)
48 1.1251e-03 1.5769e-07 1.9467e-06 7.0324e-06 2.5910e-08 1.5354e-04 6.0866e-06 5.5982e-04 2.1513e-13 1.6579e-05 1.8533e-03 0:14:31 102
V_cell = 2.600000 (V) ... V_open = 2.800000 (V)
I_anode = 0.000718 (A/cm^2) ... I_cathode = 0.000723 (A/cm^2) ... dI_mea = -0.000005 (A/cm^2) ... dI_stk = -0.000005 (A/cm^2)

49 1.1203e-03 2.0482e-07 5.6642e-06 6.5603e-06 2.1141e-08 1.5417e-04 6.1238e-06 5.6896e-04 5.3968e-13 3.1630e-05 1.7364e-03 0:14:11 101

V_cell = 2.600000 (V)   ... V_open   = 2.800000 (V)

I_anode = 0.000728 (A/cm^2) ... I_cathode = 0.000721 (A/cm^2) ... dI_mea = 0.000007 (A/cm^2) ... dI_stk = 0.000007 (A/cm^2)

50 1.1152e-03 2.0230e-07 6.1304e-06 6.1974e-06 2.4715e-08 1.5524e-04 6.1827e-06 6.2674e-04 7.0196e-13 3.3680e-05 1.6272e-03 0:13:54 100

V_cell = 2.600000 (V)   ... V_open   = 2.800000 (V)

I_anode = 0.000718 (A/cm^2) ... I_cathode = 0.000724 (A/cm^2) ... dI_mea = -0.000007 (A/cm^2) ... dI_stk = -0.000007 (A/cm^2)

A7: ANSYS Fluent – Fuel Cell Module Setup

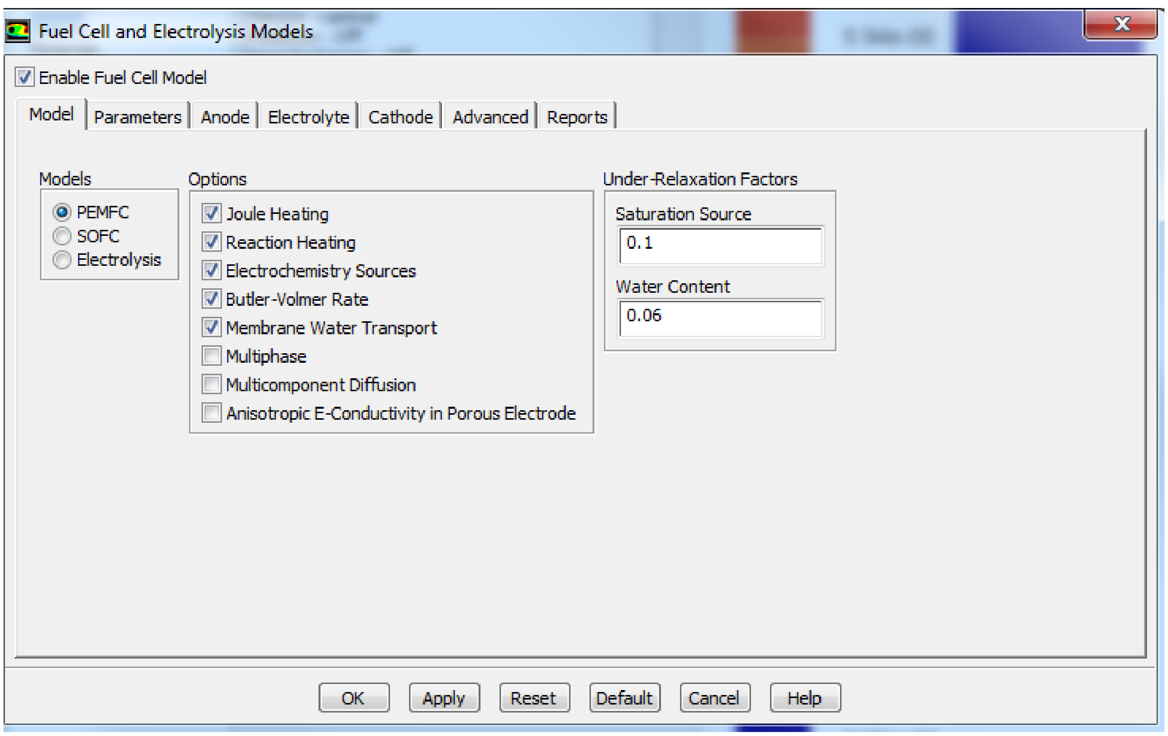

Figure A6: Initial Model Setup Window of Fuel Cell Module within ANSYS Fluent

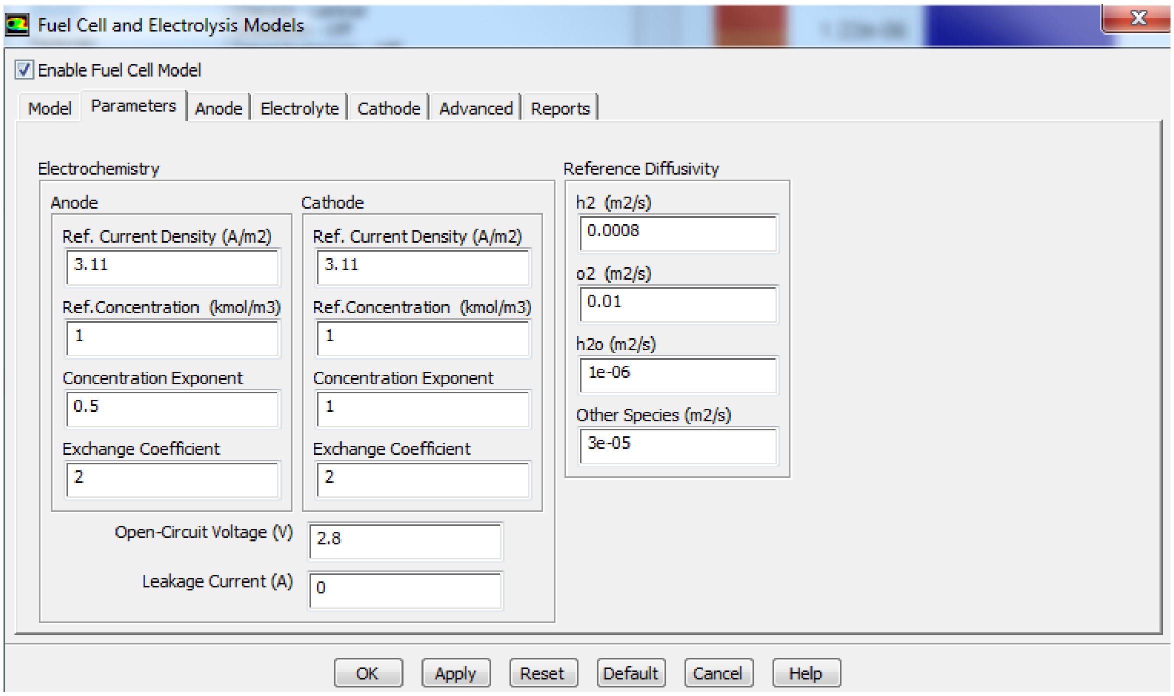

Figure A7: Model Parameter Window of Fuel Cell Module within ANSYS Fluent